



**Evaluation of electromagnetic parameters of materials
for the embedment of WPT coils**

Candidato:
Antonio Virgillito

Relatori:
Prof. Fabio Freschi
Ing. Vincenzo Cirimele

Abstract

Wireless Power Transfer technology (WPT) could represent the future of electric mobility. This technology tries to solve the problems related to the charging time, weight and autonomy of the batteries for electric vehicles (EVs) together with a strong reduction of the emissions in urban areas. WPT, also known as inductive power transfer (IPT), is a technology that allows the charge of the EVs battery thanks to the magnetic coupling between two coils, one placed under the vehicle and one installed at the ground level. One of the main issues related to the integration of the latter coil in the road pavement is related to the effect of the different materials that surround the coil. This thesis focuses on the analysis of the electromagnetic properties of a set of materials used for the embedment of the coils. The electromagnetic characterization of these materials aims to the development of a model for the study of the physical phenomena that arise as a result of the interaction between the coil and the materials adopted for its embedment. This work presents the design and the development of different systems used for the characterization of a set of materials adopted for the road paving. These systems are used for the measurement of the main electromagnetic parameters that are dielectric permittivity, magnetic permeability and electric conductivity.

A Giosuè

Contents

1	INTRODUCTION	5
2	PROBLEM FRAMEWORK	7
2.1	Coil embedding problem	7
2.2	Theory of electromagnetic parameters ϵ, σ, μ	9
2.3	Research in the literature	12
3	DESIGN PROCESS OF THE ADOPTED DEVICE	14
3.1	HIOKI 3532-50 LCR HiTESTER	14
3.2	Test accuracy of HIOKI 3532-50	16
3.3	Measurement of ϵ and σ with only one device	18
3.4	Experimental prototype design	21
3.5	Preliminary measures	30
4	ELECTRIC PARAMETERS MEASUREMENT	38
4.1	Procedure performed in the measurements	39
4.2	Black Catramina	41
4.3	Catramix	46
4.4	Cement 1	50
4.5	Cement 2	54
4.6	Unolastic	58
4.7	Variation of impedance and phase of concretes over time	62
5	MAGNETIC RESULTS	66
5.1	Black Catramina	70
5.2	Catramix	74
5.3	Cement 1	77
5.4	Cement 2	81
5.5	Unolastic	84
6	PEEC MODEL OF WPT	88

Chapter 1

INTRODUCTION

The basis of this study is the analysis of the problems related to the installation of coils for Wireless Power Technology and the electromagnetic problems related to the presence of the materials used as covers for the coils. The coils, once buried, have different electrical characteristics than the case in the air. It was therefore decided to investigate the origin of these issues, trying to understand the effect of the materials in which the coils are buried.

The research in literature of these electrical parameters has not produced many results, therefore the main purpose of this thesis is to create a test setup to measure conductivity σ , relative permittivity ϵ_r and relative permeability μ_r for different frequencies of the applied electromagnetic quantities.

As first step, two devices have been created, one for the measurement of the two electrical parameters σ and ϵ_r and one for the estimation of the magnetic permeability μ_r . Subsequently, for each material analyzed, the trend of the three parameters was obtained in a frequency range from 50 Hz to 500 kHz.

These problems has been encountered in [3] where the coils have been covered with different materials. It has been noticed how some materials are suitable for the purpose of landfill, while others are to be discarded. Once these phenomena are known, this thesis aims to provide the necessary information to model the embeddment condition. Therefore, an analysis of these materials was necessary, in order to obtain the electrical and magnetic parameters i.e. conductivity σ , relative permittivity ϵ_r and relative magnetic permeability μ_r .

The work is divided in 6 chapters. In the first chapter the problems encountered in the work [3] are summarised and subsequently the theory concerning the parameters σ , ϵ_r and μ_r is treated. The second chapter is dedicated both to the operation and setting of the device used for the measurements, i.e. the HIOKI 3532-50 LCR HiTESTER impedance meter, and to the procedure followed for the realization of the two devices for the calculation of the electrical and magnetic parameters and to some preliminary measurements. The next chapter deals with the electrical results obtained from the tested materials, fo-

cusing on both conductivity σ and relative permittivity ϵ_r as a function of frequency. The fourth chapter deals with the trend of magnetic permeability obtained from the tested materials, putting it also in correlation with the frequency. The fifth chapter treats a comparison between the measurements and a model based on a PEEC formulation in order to identify the physical causes of these effects. Finally, in the sixth chapter the electromagnetic parameters previously obtained are summarized in two tables.

Chapter 2

PROBLEM FRAMEWORK

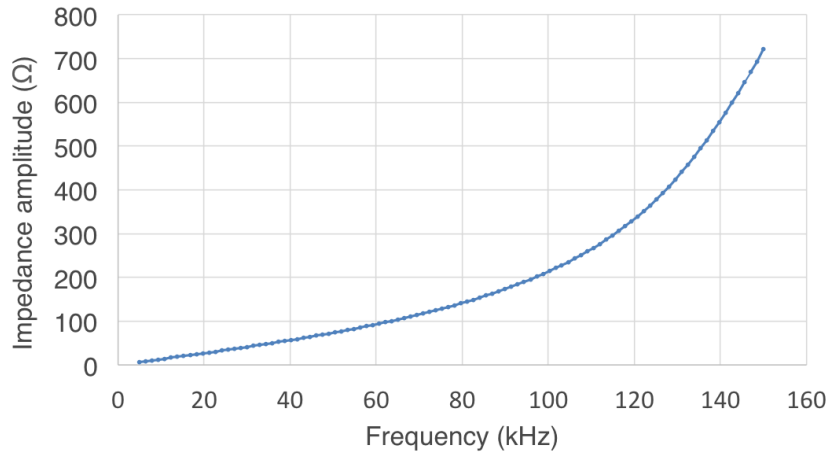
2.1 Coil embedding problem

The first trial of embedding has been done in [3] on the test site with a transmitter having inner dimensions $1.25\text{ m} \times 0.5\text{ m}$ made of 9 turns of litz wire with a diameter of 4 mm. Its values of resistance R and self-inductance L have been preliminarily measured at the frequency of 85 kHz as suggested by the SAEJ2954 [5] on WPT for electric vehicles with an HIOKI 3532-50 LCR HiTESTER. The obtained values have been $R = 303\text{ m}\Omega$ and $L = 211.8\text{ }\mu\text{H}$. The coil has been embedded in a basement of not reinforced concrete following the procedure shown in Figure 2.1. The coil has been covered with a layer of 2 cm of concrete and another layer of 3 cm of cold asphalt.

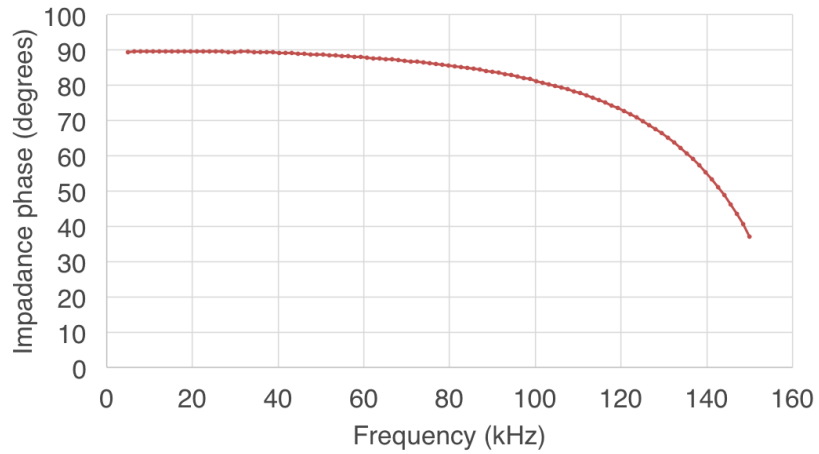


Figure 2.1: Coil embedding with a layer of 2 cm of concrete [3].

A new set of measurements has been carried out after the complete drying of concrete and asphalt. The measurements have been carried out in the frequency range from 5 to 150 kHz. The resulting behaviour of the coil impedance is shown in Figure 2.2.



(a)



(b)

Figure 2.2: Amplitude (a) and phase (b) of the coil impedance in the frequency range 5 to 150 kHz [3].

Conversely to what was expected, the behaviour of the impedance of the embedded coil was far from the one of an inductor. As shown in Figure 2.2a and Figure 2.2b, the amplitude of the impedance is not linear with the frequency and the phase starts to be much lower than 90° above 60 kHz. The interpretation of the measurements with a series R-L model has provided a value of resistance and self-inductance equal to $14.7\ \Omega$ and $293\ \mu\text{H}$ respectively. For this reason, in this work we deal the definition of a procedure for the measurement of electrical parameters in order to classify the different materials used as cover for the coils and then understand which ones can be used and which are to be avoided. The identification of suitable materials for the road pavements will surely

represent a necessary step concerning the future integration in the road infrastructure of WPT.

2.2 Theory of electromagnetic parameters ϵ , σ , μ

The electric permittivity ϵ measures how materials contrast electric field to which they are subject. In other words, permittivity ϵ represents the ability of a material to store an electric field and so permittivity describes the amount of charge needed to generate one unit of electric flux in the material. Moreover, electrical permittivity is a quantity that depends in general on different parameters like the position in the medium, the frequency of the applied field, the temperature or the humidity.

In general electrical permittivity varies according to the direction of the electric field with respect to the medium, so it is represented through a tensor which represents a local description function of the coordinates of the point:

$$\vec{D} = \epsilon \vec{E} \quad (2.1)$$

where permittivity ϵ is a tensor. We can express (2.1) in its components as follow:

$$\begin{bmatrix} D_x \\ D_y \\ D_z \end{bmatrix} = \begin{bmatrix} \epsilon_{xx} & \epsilon_{xy} & \epsilon_{xz} \\ \epsilon_{yx} & \epsilon_{yy} & \epsilon_{yz} \\ \epsilon_{zx} & \epsilon_{zy} & \epsilon_{zz} \end{bmatrix} \begin{bmatrix} E_x \\ E_y \\ E_z \end{bmatrix} \quad (2.2)$$

Only if we consider a linear, homogeneous and isotropic material, all the components of the tensor have the same value and the permittivity can be treated as a scalar. In this case only the definition of permittivity ϵ is simple a constant of proportionality between electric displacement \vec{D} and electric field intensity \vec{E} . According to [6], permittivity is often treated as a complex function of the frequency f of the applied field, because not all materials have an instantaneous response when an electric field is applied. So the response of normal materials to external fields generally depends on the frequency of the field:

$$\epsilon = \epsilon(f) \quad (2.3)$$

Since the response of materials to alternating fields is characterized by a complex permittivity, it is natural to separate its real and imaginary parts:

$$\epsilon(f) = \epsilon'(f) - j\epsilon''(f) \quad (2.4)$$

where:

$$\epsilon' = \left| \frac{\vec{D}}{\vec{E}} \right| \quad (2.5)$$

is the real part of complex permittivity, also called dielectric constant, while the imaginary part of the permittivity ϵ'' also called electric loss factor is defined:

$$\epsilon'' = \frac{\sigma}{\omega} \quad (2.6)$$

where σ is the conductivity of the medium and $\omega = 2\pi f$. The quantity Q called dissipation factor can be introduced from the ratio of components of complex permittivity:

$$Q = \tan \delta = \frac{\epsilon''}{\epsilon'} \quad (2.7)$$

where δ is the loss angle. It is possible to introduce starting from (2.5) the relative dielectric constant:

$$\epsilon_r = \frac{\epsilon'}{\epsilon_0} \quad (2.8)$$

where $1 \leq \epsilon_r \leq \infty$ and $\epsilon_0 = 8.85418 \times 10^{-12} \text{F/m}$ represents vacuum's permittivity. So we can resume (2.4),(2.5),(2.6) and (4.19) in:

$$\epsilon = \epsilon' - j\epsilon'' = \epsilon_0\epsilon_r - j\frac{\sigma}{\omega} \quad (2.9)$$

Thanks to this, materials can be classified according to their imaginary ϵ'' and real ϵ' components ratio:

Medium classification	Perfect dielectric	Good dielectric	General medium	Good conductor	Perfect conductor
ϵ''/ϵ'	0	$\ll 1$	≈ 1	$\gg 1$	∞

Table 2.1: Media classification

It is important to underline that for HF fields or when conductivity σ can be neglected, equation (2.9) is usually written as $\epsilon = \epsilon_r\epsilon_0$, but the latter is an approximation of the form (2.9). Thus materials with high dielectric constant are those in which conduction process is almost entirely ohmic, while for materials with low dielectric constant, conduction is almost entirely by displacement currents.

Electrical resistivity ρ is the characteristic of a material to prevent the flow of electric current. Therefore, a low resistivity ρ indicates a material that allows the flow of electric current. The reciprocal of resistivity ρ is a parameter known as electrical conductivity σ . The simplest way to define resistivity is to assign a single number for the whole object, but this definition depends on the assumption that the electric field \vec{E} and current density \vec{J} are both parallel and constant everywhere in the material. If conductors have a uniform cross section with a uniform flow of electric current, and are made of a uniform single

material, this is a good model. In this case only resistivity ρ can be calculated by the following:

$$\rho = R \frac{S}{l} \quad (2.10)$$

where R is the electrical resistance of the material, l is the length of the specimen and S is the cross-sectional area of the specimen.

For all other cases that have a more complicated geometry, or when the current and electric field vary in different parts of the material, it is necessary to use a more general expression of (2.10) in which the resistivity at a particular point is defined as the ratio of the electric field to the density of the current it creates at that point considered. In these cases, we have to use the most general expression for resistivity or conductivity, that starts from the tensor-vector form of Ohm's law which relates the electric field \vec{E} inside a material to the electric current flow \vec{J} . This equation is valid in all cases, including those mentioned above:

$$\begin{bmatrix} E_x \\ E_y \\ E_z \end{bmatrix} = \begin{bmatrix} \rho_{xx} & \rho_{xy} & \rho_{xz} \\ \rho_{yx} & \rho_{yy} & \rho_{yz} \\ \rho_{zx} & \rho_{zy} & \rho_{zz} \end{bmatrix} \begin{bmatrix} J_x \\ J_y \\ J_z \end{bmatrix} \quad (2.11)$$

where \vec{E} is the electric field vector with components E_x, E_y, E_z , ρ is the resistivity tensor, in general a three by three matrix and \vec{J} is the electric current density vector with components J_x, J_y, J_z .

The conductivity σ is the inverse matrix of resistivity ρ , according to (2.11):

$$\begin{bmatrix} J_x \\ J_y \\ J_z \end{bmatrix} = \begin{bmatrix} \sigma_{xx} & \sigma_{xy} & \sigma_{xz} \\ \sigma_{yx} & \sigma_{yy} & \sigma_{yz} \\ \sigma_{zx} & \sigma_{zy} & \sigma_{zz} \end{bmatrix} \begin{bmatrix} E_x \\ E_y \\ E_z \end{bmatrix} \quad (2.12)$$

However, generally, the individual matrix elements are not always reciprocals, in fact the individual components are not necessarily inverses.

In electromagnetism, magnetic permeability μ expresses the ability of a material to magnetize itself when a magnetic field is applied to it. In particular, it represents how magnetic field \vec{H} influences the organization of magnetic dipoles in a given medium, including dipole migration and magnetic dipole reorientation. Like for the other parameters, the simplest way to define permeability μ is to assign a single number for the whole object. Clearly this definition depends on the assumption that the magnetic field \vec{B} and magnetic field strength \vec{H} are both parallel and constant everywhere in the material. In this case the relation with permeability is:

$$\vec{B} = \mu \vec{H} \quad (2.13)$$

where the permeability μ is a scalar. In general, permeability is not a constant, as it can vary with the position in the medium, the frequency of the field applied, humidity,

temperature, and other parameters. In these cases, equation (2.13) becomes:

$$\begin{bmatrix} H_x \\ H_y \\ H_z \end{bmatrix} = \begin{bmatrix} \mu_{xx} & \mu_{xy} & \mu_{xz} \\ \mu_{yx} & \mu_{yy} & \mu_{yz} \\ \mu_{zx} & \mu_{zy} & \mu_{zz} \end{bmatrix} \begin{bmatrix} B_x \\ B_y \\ B_z \end{bmatrix} \quad (2.14)$$

Like permittivity, it also possible consider the complex permeability [6], and so the permeability μ can be written as:

$$\mu(f) = \mu(f)' - j\mu(f)'' \quad (2.15)$$

where μ' is called relative magnetic permeability and μ'' is called magnetic loss factor.

From magnetic permeability μ' is possible to derive relative permeability μ_r . In fact this latter is the ratio of the real part of permeability of a specific medium to the permeability of vacuum $\mu_0 = 4\pi \times 10^{-7} \text{H/m}$:

$$\mu_r = \frac{\mu'}{\mu_0} \quad (2.16)$$

where $1 \leq \mu_r \leq \infty$.

The ratio of the imaginary to the real part of the complex permeability is called loss tangent:

$$\delta = \tan \left(\frac{\mu''}{\mu'} \right) \quad (2.17)$$

which provides a measure of how much power is lost in a material versus how much is stored. Depending on the relative permeability value, the materials can be classified into 3 classes:

Medium Classification	Diamagnetic medium	Paramagnetic medium	Ferromagnetic medium
μ_r	< 1	> 1	$\gg 1$

Table 2.2: Magnetic medium classification

2.3 Research in the literature

The main purpose of this thesis is to find permittivity, conductivity and magnetic permeability of some materials used as a coil cover. However, during the research phase, few references were found. To the best of author's knowledge, only the work [2] treats the characterization of the relative permittivity ϵ_r of pure bitumen in different grades and wax-modified bitumen (WMB). In [2] is found that the dielectric response of bitumen is strongly temperature and frequency dependent, which is also highly linked to the rheology

of the system. Moreover, there are no remarkable differences in the dielectric constant ϵ' among different grades of bitumen. Regular changes of dielectric loss tangent ($\tan\delta$) among the different grades of bitumen can be observed, which can be a good indicator for the linkage between the dielectric and rheological responses. Regards electrical conductivity, only some standards report ranges of values for cementitious materials that are too high for the purposes of this thesis. This high range is dictated by the variability of this parameter on whether the cement is wet or dry and on its reology. However, all these values represented the starting point during design and simulation phase of the devices useful for measuring permittivity, conductivity and permeability.

Chapter 3

DESIGN PROCESS OF THE ADOPTED DEVICE

In this chapter we will describe the design of the device realized in order to measure the permittivity and the conductivity of the tested materials. First of all, however, we will talk about the electrical impedance meter used to measure the parameters of interest and how it has significantly impacted on the sizing the device itself.

3.1 HIOKI 3532-50 LCR HiTESTER

In order to calculate the conductivity and the permittivity of the tested materials, the HIOKI 3532-50 LCR HiTESTER impedance meter was used. Starting from the voltage \bar{V} which is applied between the terminals of the sample under test, the current \bar{I} which flows through the test sample, the phase angle θ between voltage \bar{V} and current \bar{I} , and the angular frequency ω , the LCR meter can measure the impedance \bar{Z} :

$$\bar{V} = V e^{j(\omega t + \phi_V)} \quad (3.1)$$

$$\bar{I} = I e^{j(\omega t + \phi_I)} \quad (3.2)$$

where V and I are respectively the voltage and current amplitude. The impedance \bar{Z} is defined as the ratio of these quantities:

$$\bar{Z} = \frac{\bar{V}}{\bar{I}} = \frac{V}{I} e^{j(\phi_V - \phi_I)} = Z e^{j\theta} = \bar{Z} = R + jX \quad (3.3)$$

where the magnitude Z represents the ratio of the voltage difference amplitude to the current amplitude, while the argument of the impedance θ gives the phase difference

between voltage and current, while the real part of impedance R is the resistance and the imaginary part X is the reactance. Moreover, it is possible to use the admittance \bar{Y} , which is the reciprocal of the impedance \bar{Z} .

$$\bar{Y} = \frac{1}{\bar{Z}} = G + jB \quad (3.4)$$

Therefore according with [4], LCR meter can calculate the following components by using the calculation equations shown in the table 3.1.

Quantity	Series equivalent circuit mode	Parallel equivalent circuit mode
Z	$Z = \frac{V}{I} = \sqrt{R^2 + X^2}$	
Y	$Y = \frac{1}{Z} = \sqrt{G^2 + B^2}$	
R	$R_s = ESR = Z \cos \theta $	$R_p = \left \frac{1}{Y \cos \theta} \right $
X	$X = Z \sin \theta $	
G		$G = Y \cos \phi $
B		$B = Y \sin \phi $
L	$L_s = \frac{X}{\omega}$	$L_p = \frac{1}{\omega B}$
C	$C_s = \frac{1}{\omega X}$	$C_p = \frac{B}{\omega}$
D	$ D = \left \frac{1}{\tan \theta} \right $	
Q	$ Q = \tan \theta$	

Table 3.1: Testing parameters and calculation equations [4].

where $\phi = \tan^{-1} \left(\frac{B}{G} \right)$, L_s , R_s , C_s are the measured values of L , C , and R in series equivalent circuit mode, while L_p , R_p , C_p are the measured values of L , C , and R in parallel equivalent circuit mode.

3.2 Test accuracy of HIOKI 3532-50

The test accuracy is calculated from a basic accuracy, which is based on the accuracy for impedance Z and phase angle θ , and the following coefficients:

$$\text{Test accuracy} = \text{Basic accuracy} \times C \times D + E \quad (3.5)$$

where:

- C = Test speed coefficient
- D = Cable length coefficient
- E = Temperature coefficient

The basic accuracy is calculated from two values A and B provided in the accuracy coefficient table. These values are dependent on the measurement frequency, the measurement range, and the measurement signal level. There are two formulas to calculate the value of A and B , depending on the measured impedance range:

$$\text{Basic accuracy } Z(\%) \text{ or } \theta(^{\circ}) = \pm \left(A \times \frac{B \times |10 \times Z(\Omega) - \text{Range}(\Omega)|}{\text{Range}(\Omega)} \right) \quad (3.6)$$

$$\text{Basic accuracy } Z(\%) \text{ or } \theta(^{\circ}) = \pm \left(A \times \frac{B \times |\text{Range}(\Omega) - Z(\Omega)| \times 10}{\text{Range}(\Omega)} \right) \quad (3.7)$$

where the impedance of the sample $Z[\Omega]$ is taken to be either the measured value, or the value referred to the conversion table 3.1. The (3.6) is valid for 1 k Ω range or more, while (3.7) is for the 100 Ω range or less. Regarding the test speed coefficient C , the test cable length coefficient D , and the temperature coefficient E we have to refer to the following tables:

Test speed	Fast	Normal	Slow	Slow2
C	5	2	1.5	1

Table 3.2: Test speed coefficient C table [4].

Cable length	0 m	1 m
D	1	[100 kHz max] $1.5 + 0.015 \cdot f(kHz)$
		[100.1 kHz min] $1.5 + 0.3 \cdot f(MHz)$

Table 3.3: Cable length coefficient D table [4].

Temperature	Operating temperature = $T(^{\circ})$
E	$0.1 \times \text{basic accuracy} \times (T(^{\circ}) - 23)$

Table 3.4: Temperature coefficient E table [4].

Finally, after these definitions, the basic accuracy table of the A and B parameters is reported. The following table refers to a voltage range set from 1.001 V to 5.000 V:

	Range	42 Hz to 99.9 Hz	100 Hz to 1 kHz	1.001 kHz to 10 kHz	10.01 kHz to 100 kHz	100.1 kHz to 1 MHz	1.001 MHz to 5 MHz
1 year	100 MΩ	$A = 6.75 \ B = 6$ $A = 6 \ B = 3$	$A = 3.75 \ B = 3$ $A = 3 \ B = 2.25$	$A = 3.75 \ B = 3$ $A = 3 \ B = 2.25$			
	10 MΩ	$A = 1.5 \ B = 0.6$ $A = 3 \ B = 0.45$	$A = 0.75 \ B = 0.3$ $A = 0.45 \ B = 0.15$	$A = 0.75 \ B = 0.3$ $A = 0.45 \ B = 0.15$	$A = 1.8 \ B = 0.75$ $A = 1.8 \ B = 0.75$		
	1 MΩ	$A = 0.75 \ B = 0.15$ $A = 0.6 \ B = 0.3$	$A = 0.3 \ B = 0.075$ $A = 0.3 \ B = 0.03$	$A = 0.3 \ B = 0.075$ $A = 0.3 \ B = 0.03$	$A = 0.75 \ B = 0.12$ $A = 0.75 \ B = 0.12$	$A = 4.8 \ B = 1.5$ $A = 4.8 \ B = 0.75$	
	100 kΩ	$A = 0.6 \ B = 0.015$ $A = 0.45 \ B = 0.03$	$A = 0.225 \ B = 0.015$ $A = 0.12 \ B = 0.015$	$A = 0.3 \ B = 0.015$ $A = 0.15 \ B = 0.015$	$A = 0.45 \ B = 0.06$ $A = 0.3 \ B = 0.045$	$A = 1.5 \ B = 0.45$ $A = 0.75 \ B = 0.45$	
	10 kΩ	$A = 0.6 \ B = 0.015$ $A = 0.45 \ B = 0.015$	$A = 0.225 \ B = 0.015$ $A = 0.12 \ B = 0.015$	$A = 0.225 \ B = 0.015$ $A = 0.12 \ B = 0.015$	$A = 0.375 \ B = 0.03$ $A = 0.15 \ B = 0.03$	$A = 1.05 \ B = 0.075$ $A = 0.3 \ B = 0.03$	
	1 kΩ	$A = 0.6 \ B = 0.015$ $A = 0.45 \ B = 0.015$	$A = 0.225 \ B = 0.015$ $A = 0.12 \ B = 0.015$	$A = 0.225 \ B = 0.015$ $A = 0.12 \ B = 0.015$	$A = 0.375 \ B = 0.03$ $A = 0.15 \ B = 0.03$	$A = 0.75 \ B = 0.075$ $A = 0.3 \ B = 0.03$	
	100 Ω	$A = 0.6 \ B = 0.03$ $A = 0.45 \ B = 0.015$	$A = 0.225 \ B = 0.03$ $A = 0.12 \ B = 0.015$	$A = 0.225 \ B = 0.03$ $A = 0.12 \ B = 0.015$	$A = 0.375 \ B = 0.03$ $A = 0.15 \ B = 0.03$	$A = 0.75 \ B = 0.075$ $A = 0.3 \ B = 0.03$	
	10 Ω	$A = 0.75 \ B = 0.06$ $A = 0.525 \ B = 0.3$	$A = 0.375 \ B = 0.06$ $A = 0.225 \ B = 0.03$	$A = 0.375 \ B = 0.06$ $A = 0.225 \ B = 0.03$	$A = 0.375 \ B = 0.06$ $A = 0.3 \ B = 0.03$	$A = 1.05 \ B = 0.15$ $A = 0.6 \ B = 0.075$	
	1 Ω	$A = 1.2 \ B = 0.75$ $A = 3 \ B = 0.3$	$A = 0.75 \ B = 0.6$ $A = 0.45 \ B = 0.3$	$A = 0.75 \ B = 0.6$ $A = 0.45 \ B = 0.3$	$A = 0.75 \ B = 0.6$ $A = 0.45 \ B = 0.3$	$A = 2.1 \ B = 1.5$ $A = 1.2 \ B = 1.5$	
	100 mΩ	$A = 7.5 \ B = 6$ $A = 5.25 \ B = 3$	$A = 6 \ B = 3$ $A = 3.75 \ B = 1.5$	$A = 6 \ B = 3$ $A = 3.75 \ B = 1.5$	$A = 6 \ B = 3$ $A = 3.75 \ B = 1.5$		

Table 3.5: Basic accuracy table [4].

From Basic accuracy coefficient table 3.5, for each cell, upper values of A and B refer to the Z accuracy while the others values refer to the θ accuracy.

3.3 Measurement of ϵ and σ with only one device

As first step, we tried to realize a device that allow to measure permittivity and conductivity. For this reason, we opt for the realization of a capacitor, in which insert as dielectric the material we want to know permittivity and conductivity. In fact, from the structure of a real capacitor, it is possible to calculate ϵ and σ of the dielectric with a single measure. The generic structure of a real capacitor with plane and parallel faces is that showed in Figure 3.1:

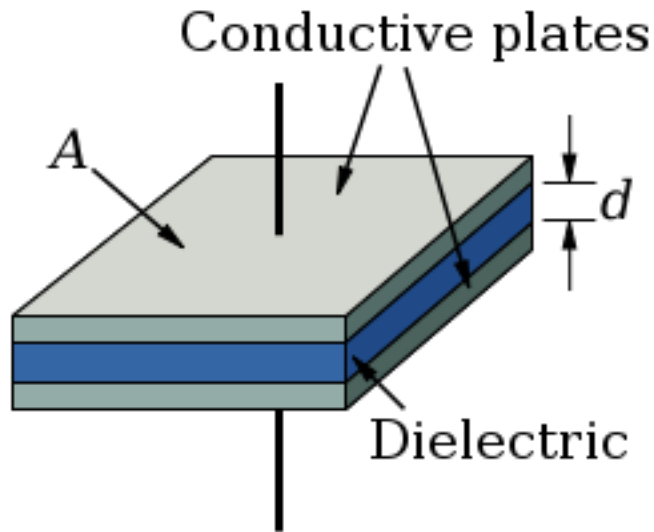


Figure 3.1: Parallel plate capacitor.

where A is the section of the conductive plates and d is the distance between the plates. In Figure 3.2 it is possible to see the commonly adopted equivalent circuit of a real capacitor:

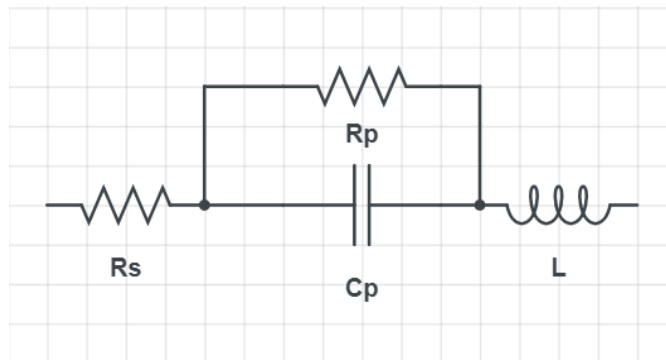


Figure 3.2: Equivalent circuit of a real capacitor.

where L is the inductance of the rheophores, sometimes referred as ESL (equivalent series inductance), R_s is the resistance of the rheophores, R_p is the resistance of the dielectric between the two armatures and C_p is the capacitor's capacity. The equivalent impedance is given by:

$$\bar{Z} = R_s + j\omega L + \frac{R_p}{1 + j\omega C_p R_p} \quad (3.8)$$

From (3.8) it is possible to neglect two of the four quantities that appear in the equivalent

circuit. In particular, it is possible to neglect both the series resistance R_s , being this generally very small, and the series inductance L because this has a significant impact on the total impedance calculation only in the vicinity of the resonant frequency of the model itself. In fact if we increase frequency, the impedance amplitude has the typical trend of an RLC resonant circuits. Depending on the amplitude value and impedance phase, it is possible to understand whether the series inductance should be considered or not in the overall impedance. Generally a small capacitor has an higher resonance frequency with respect to a big capacitor. For these reasons we can consider the simplified model of a real capacitor, which coincides with a parallel RC model, given by the parallel between R_p and C_p :

$$\bar{Z} = \frac{R_p}{1 + j\omega C_p R_p} \quad (3.9)$$

From these, it is possible to calculate permittivity ϵ and conductivity σ . From the capacity C_p it is possible to extrapolate the relative permittivity value of the dielectric, while from the resistance R_p it is possible to calculate the conductivity of the dielectric:

$$C_p = \epsilon \frac{A}{d} \quad (3.10)$$

$$R_p = \frac{1}{\sigma} \frac{d}{A} \quad (3.11)$$

According to (3.9), we can easily calculate the permittivity and conductivity, so if we insert as a dielectric an unknown material, it is possible to calculate two parameters with a single impedance measurement.

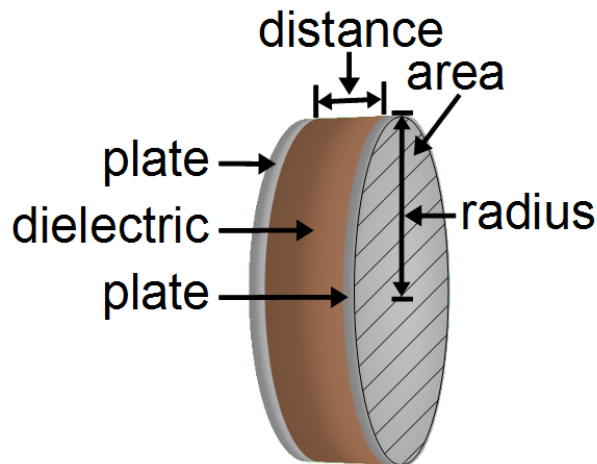


Figure 3.3: Parallel plate capacitor with circular plates.

Therefore it was initially decided to create a sort of condenser with flat and parallel with circular faces, like the one in Figure 3.3. In this case, permittivity ϵ and conductivity σ of the dielectric can easily be calculated with the equations (3.10), (3.11). With this solution, however, some problems arose during the project.

Air inclusions should be avoided and thus, it is necessary to insert spacers in order to adjust the two electrodes until they are parallel to each other and ensure that also the test material is fully contacted on both sides for an accurate measurement. In case of soft material samples the pressure of the electrodes may deform the material sample which can influence the measured parameters. In these cases it is advisable to insert a circular gasket that prevents the material from coming out. However the insertion of this gasket could influence the measurement itself. Like spacers, the gasket should be with low permittivity and dielectric losses in order to not influence the dielectric properties. In case of rigid material samples, the surface of the test material must be flat at all points. When the surface of the test material is not flat, an air gap between the electrode and the solid test material causes measurement errors. Thus, the filling was not guaranteed to be the same for all the materials given the different chemical-physical characteristics because some tested materials have a cement nature and the others a bituminous nature. Besides, in a circular capacitor, the measurement is influenced by stray capacitances due to the presence of strong edge effects on the conductors, whose modeling is rather complex. Environmental changes can influence the measurement results, especially when measuring small signals. To ensure an accurate measurement also for small signals it is necessary to increase the test voltage if possible and ensure that the cabling is shielded. Another problem is the realization of the device how it has been presented because of the absence of machinery predisposed to the cutting of steel to realize the conductive circular plates and the difficulty in obtaining a single device useful both for very fluid mixture of mortar and for more viscous bituminous materials. These reasons led us to exclude this structure and opt for a different geometry.

3.4 Experimental prototype design

The prototype actually created is similar to a cylinder inside which the two metal electrodes are placed, as shown in Figure 3.4:

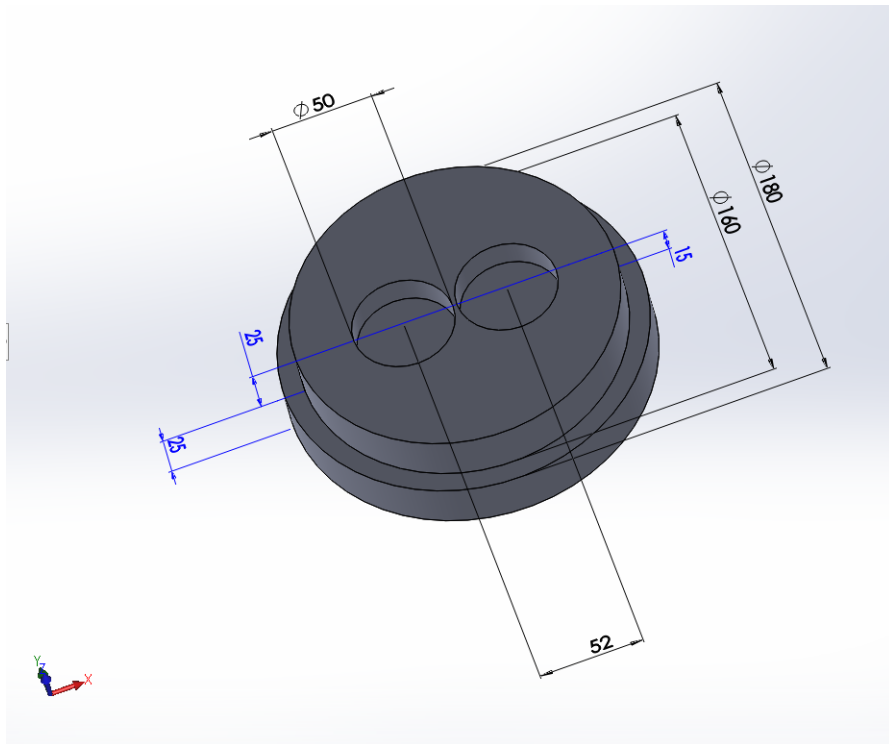


Figure 3.4: Base of the realized capacitor

The two holes are used for the insertion of two cylindrical electrodes, in order to guarantee their stability and the desired spacing between them. These holes have a diameter of 50 mm and a depth of 15 mm. The lower diameter of the base is 160 mm and the height is 25 mm, while the other diameter is 180 mm and has an height of 25 mm. In Figure 3.7, the set composed of base and electrodes is shown. It is possible to notice how the electrodes with a length of 200 mm go inside the two holes and that the distance between the two electrodes is 2 mm.

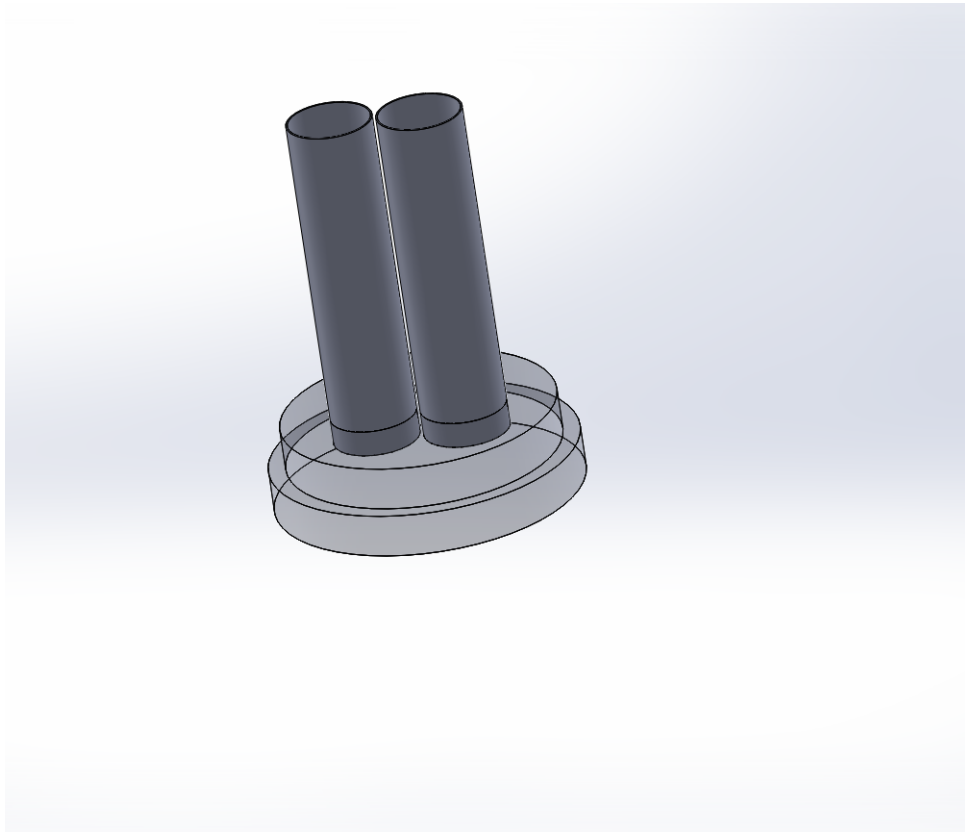


Figure 3.5: Assembly of the base and electrodes

During the sizing process the FEMM software was used. FEMM is a 2D simulation software for electromagnetic problems based on the Finite elements method, in which we have implemented the 2D design of Figure 3.4:

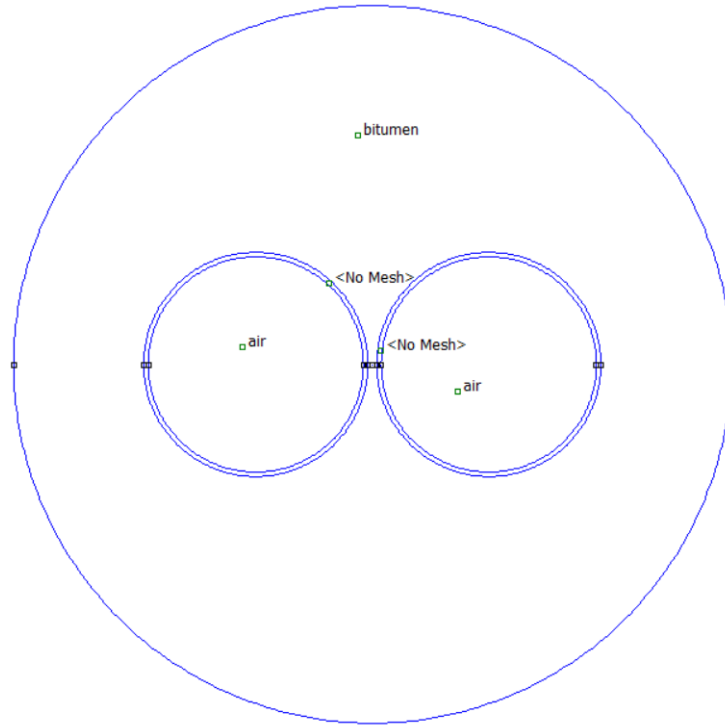


Figure 3.6: FEMM device design

Once the system geometry is known, FEMM is used to calculate the equivalent impedance and therefore consequently we can calculate the accuracy of measurement thanks to table 3.5. We vary both the diameter of the electrodes and the distance between them thus the sizing process was done in order to have the best basic accuracy of the LCR meter. Therefore, different geometric values were modified and simulated before realizing the final structure. In particular, having fixed the external diameter of the prototype at 160 mm, the diameter of the electrodes and their distance to each other has been changed. The diameters of the studied conductors were: 20 mm-30 mm-40 mm-50 mm. The distance between the two electrodes depends on the choice of the electrodes diameter. This distance has been gradually increased, always starting from the initial condition of distance between the electrodes of 2 mm, until the external diameter of 160 mm is reached. For example, if the electrodes have a diameter of 50 mm, the equivalent impedance has been calculated when the electrodes are at a distance d of 2 mm, 14 mm, 26 mm, 38 mm and 50 mm from each other. In Figure 3.7 we can see the prototype drawing with 50 mm electrodes and distance between the electrodes of 50 mm:

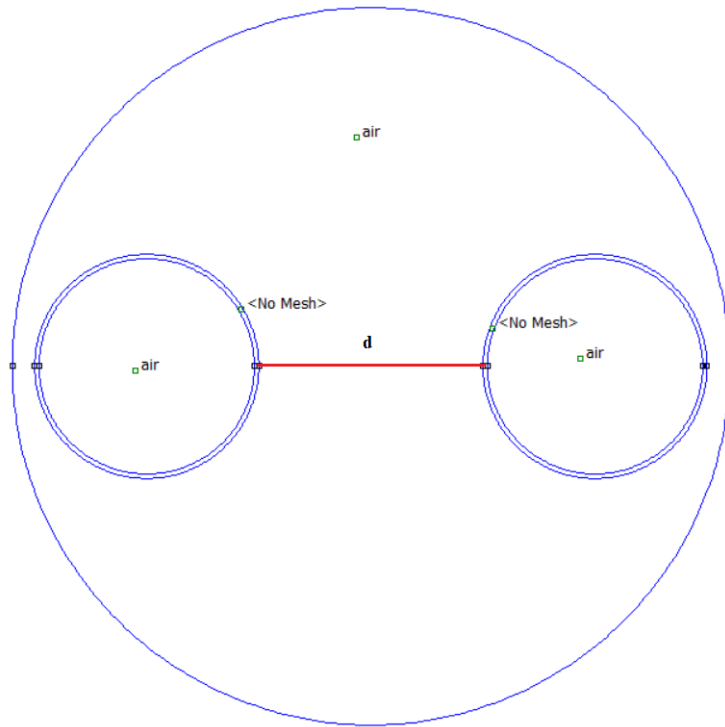


Figure 3.7: Prototype with electrodes of 50 mm and distance from these of 50 mm

Calculating the equivalent impedance in FEMM, however, requires setting parameters during simulation, such as permittivity, conductivity, frequency and depth:

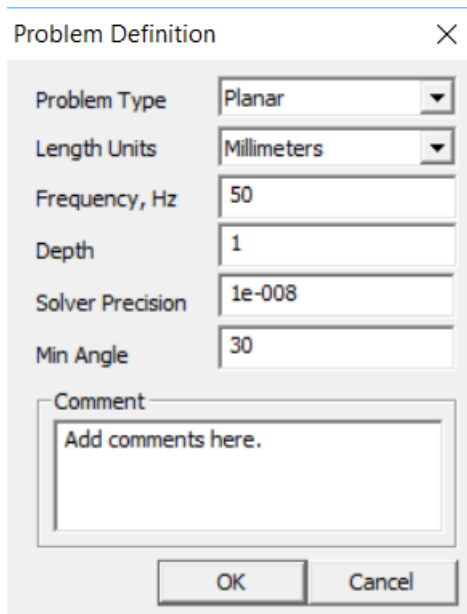


Figure 3.8: Problem definition

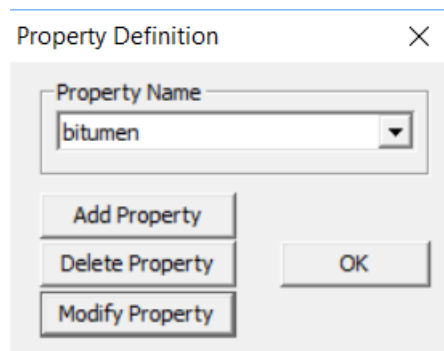


Figure 3.9: FEMM Property Definition window

In the window of Figure 3.8 we can set also frequency according with table 3.5. In Figure 3.9 two custom materials called bitumen and air have been added, whose electrical characteristics are summarized in Figure 3.10:

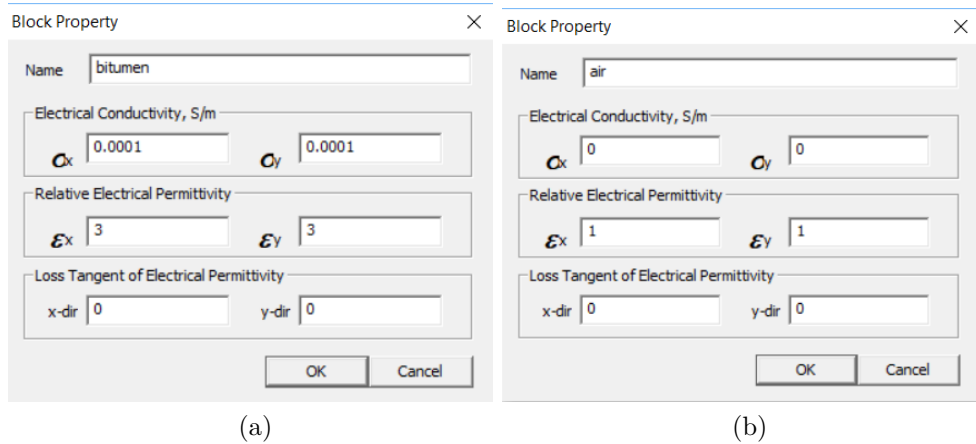


Figure 3.10: Bitumen (a) and air (b) electrical characteristics

Clearly the conductivity of the bitumen material has been varied in a range, so as to try to take into account the variability of this parameter. The value chosen comes out from [1], in which the resistivity of cement-like materials is reported. Typical values fall within the range $1000 \Omega\text{m}$ - $30\,000\,000 \Omega\text{m}$.

The same can be done for relative permittivity. In this case, instead, the value of 3 was chosen according to the study [2] in which it is calculated for a particular type of bituminous mixture.

It is also possible to set the voltage value of the two conductors. In Figure 3.11 we see that these have been set to have a potential difference of 5 V consistent with the table 3.5 of the LCR meter used:

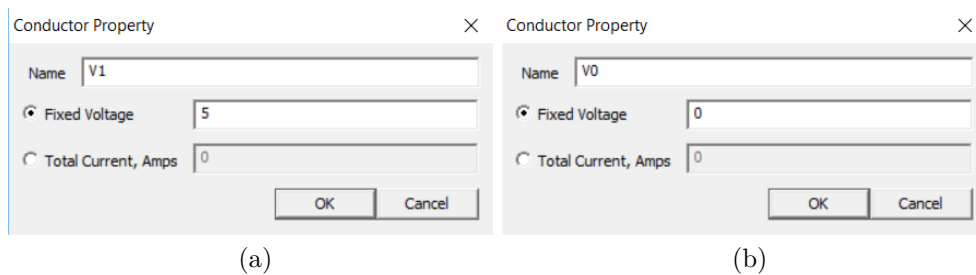


Figure 3.11: Electrode at 5(V) (a) and electrode at 0(V) (b)

Once the dimensions of the device were calculated, FEMM was also used for another purpose. In fact with this new geometry design, it is no longer possible to use relations (3.10) and (3.11) to calculate permittivity and conductivity because the device in Figure 3.7 is not a parallel plate capacitor. Therefore we can interpret the equivalent impedance

as (3.9) where:

$$C_p = \epsilon_0 \epsilon_r k_C \quad (3.12)$$

$$R_p = \frac{1}{\sigma} k_R \quad (3.13)$$

where k_C and k_R are called respectively capacitive form factor and resistive form factor. For a capacitor with flat and parallel faces k_C and k_R are simply:

$$\begin{aligned} k_C &= \frac{A}{d} \\ k_R &= \frac{d}{A} \end{aligned} \quad (3.14)$$

In this case, the electric field \vec{E} inside the armatures is uniform, and the vector has orthogonal direction among the plates, and towards direct from the positive to the negative one. However, for a generic capacitor like the model used in this work, we don't know a priori which is the electric field direction, so equations (3.10),(3.11) can't be used. However, the strength of the introduction of form factors is in the fact that these depend exclusively on the geometry of the device and do not depend on the permittivity and conductivity, on the frequency, on the electric field \vec{E} intensity or direction, on the depth setted. As depth, thus, we have chosen the value of 1 mm in order to have a reference. It is clear that by modifying this value the two form factors change. It is possible to write relationships both between a calculated form factor with a depth of 1 mm and the same form factor calculated for any depth value:

$$\begin{aligned} k_C &= l \cdot k_{C_{1\text{mm}}} \\ k_R &= \frac{k_{R_{1\text{mm}}}}{l} \end{aligned} \quad (3.15)$$

where $k_{C_{1\text{mm}}}$ and $k_{R_{1\text{mm}}}$ are the form factors referred to a depth of 1 mm, l is the desired depth misured in mm, and $k_{C_{1\text{mm}}}$ and $k_{R_{1\text{mm}}}$ are the form factors referred to a l depth also in mm.

It is also possible to write the relationships between the two form factors k_C and k_R :

$$\frac{k_C}{k_{C_{1\text{mm}}}} = \frac{k_{R_{1\text{mm}}}}{k_R} = l \quad (3.16)$$

Tables 3.6, 3.7, 3.8 and 3.9 summarize the analyzed cases, highlighting the basic accuracy values:

Distance d	k_C (m)	k_R (1/m)	C (F)	R (Ω)	$ Z $ (Ω)	$\angle Z$ ($^\circ$)	Test Accuracy $ Z $ (%)	Test Accuracy $\angle Z$ ($^\circ$)
2 mm	1.6055	0.6228	4.2647×10^{-11}	6.2285×10^3	6.2285×10^3	-0.0048	± 1.6629	± 1.2952
14 mm	0.5677	1.7614	1.5080×10^{-11}	1.7614×10^4	1.7614×10^4	-0.0048	± 1.4987	± 1.1590
26 mm	0.3975	2.5154	1.0560×10^{-11}	2.5154×10^4	2.5154×10^4	-0.0048	± 1.5509	± 1.2634
38 mm	0.3144	3.1806	8.3513×10^{-12}	3.1806×10^4	3.1806×10^4	-0.0048	± 1.5264	± 1.2144
50 mm	0.2620	3.8170	6.9590×10^{-12}	3.8170×10^4	3.8170×10^4	-0.0048	± 1.5742	± 1.3102

Table 3.6: Test accuracy table, with 50 (mm) diameters and 200 (mm) length of electrodes, $\sigma = 0.0001$ S/m and $f = 50$ (Hz)

Distance d	k_C (m)	k_R (1/m)	C (F)	R (Ω)	$ Z $ (Ω)	$\angle Z$ ($^\circ$)	Test Accuracy $ Z $ (%)	Test Accuracy $\angle Z$ ($^\circ$)
2 mm	1.6055	0.6228	4.2647×10^{-11}	6.2285×10^3	4.7821×10^3	-39.8445	± 3.5675	± 1.1060
14 mm	0.5677	1.7614	1.5080×10^{-11}	1.7614×10^4	1.3524×10^4	-39.8446	± 4.4367	± 2.4305
26 mm	0.3975	2.5154	1.0560×10^{-11}	2.5154×10^4	1.9313×10^4	-39.8446	± 5.1336	± 3.1273
38 mm	0.3144	3.1806	8.3513×10^{-12}	3.1806×10^4	2.4421×10^4	-39.8446	± 5.7484	± 3.7421
50 mm	0.2620	3.8170	6.9590×10^{-12}	3.8170×10^4	2.9306×10^4	-39.8446	± 6.3365	± 4.3303

Table 3.7: Test accuracy table, with 50 (mm) diameters and 200 (mm) length of electrodes, $\sigma = 0.0001$ (S/m) and $f = 500$ (kHz)

Distance d	k_C (m)	k_R (1/m)	C (F)	R (Ω)	$ Z $ (Ω)	$\angle Z$ ($^\circ$)	Test Accuracy $ Z $ (%)	Test Accuracy $\angle Z$ ($^\circ$)
2 mm	1.6055	0.6228	4.2647×10^{-11}	1.8686×10^7	7.4639×10^3	-89.9771	± 4.1056	± 1.3212
14 mm	0.5677	1.7614	1.5080×10^{-11}	5.2844×10^7	2.1108×10^4	-89.9771	± 5.3496	± 3.3434
26 mm	0.3975	2.5154	1.0560×10^{-11}	7.5463×10^7	3.0143×10^4	-89.9771	± 6.4372	± 4.4310
38 mm	0.3144	3.1806	8.3513×10^{-12}	9.5420×10^7	3.8115×10^4	-89.9771	± 7.3968	± 5.3906
50 mm	0.2620	3.8170	6.9590×10^{-12}	1.1451×10^8	4.5741×10^4	-89.9771	± 8.3148	± 6.3085

Table 3.8: Test accuracy table, with 50 (mm) diameters and 200 (mm) length of electrodes, $\sigma = 3.3333 \times 10^{-8}$ (S/m) and $f = 500$ (kHz)

Distance d	k_C (m)	k_R (1/m)	C (F)	R (Ω)	$ Z $ (Ω)	$\angle Z$ ($^\circ$)	Test Accuracy $ Z $ (%)	Test Accuracy $\angle Z$ ($^\circ$)
2 mm	1.6055	0.6228	4.2647×10^{-11}	1.8686×10^7	1.8126×10^7	-14.0550	± 28.4962	± 20.6823
14 mm	0.5677	1.7614	1.5080×10^{-11}	5.2844×10^7	5.1262×10^7	-14.0550	± 77.2279	± 45.0482
26 mm	0.3975	2.5154	1.0560×10^{-11}	7.5463×10^7	7.3204×10^7	-14.0550	± 109.4979	± 61.1832
38 mm	0.3144	3.1806	8.3513×10^{-12}	9.5420×10^7	9.2564×10^7	-14.0550	± 137.9695	± 75.4190
50 mm	0.2620	3.8170	6.9590×10^{-12}	1.1451×10^8	1.1108×10^8	-14.0550	---	---

Table 3.9: Test accuracy table, with 50 (mm) diameters and 200 (mm) length of electrodes, $\sigma = 3.3333 \times 10^{-8}$ (S/m) and $f = 50$ (Hz)

It can be noted that in the table 3.9 the last test accuracy values are not defined because the A and B parameters are not defined, according to the table 3.5. According to the four tables 3.6, 3.7, 3.8, 3.9 it is clear that the best constructive choice in terms of accuracy is that given by having a distance d equal to 2 mm between the two electrodes. Furthermore, the choice of electrodes with a diameter of 50 mm is the best among the various options in terms of diameter. So for the final system the choice is given by having 50 mm diameter electrodes placed at a mutual distance d of 2 mm.

3.5 Preliminary measures

In Figure 3.12 it is shown the final system realized:



Figure 3.12: Real prototype with electrodes of 200 mm and distance $d = 2$ mm

An air measurement of the electrodes placed at a relative distance of 2 mm was carried out. This has served us to understand what is the difference in the capacitance form factor calculated on FEMM and the one measured by the impedance meter. The capacitive form factor calculated with FEMM in this first test is related with electrodes of 200 mm placed each other at a distance of 2 mm. Therefore the form factor k_C is intended as the capacitive

form factor of only the system in Figure 3.13:



Figure 3.13: Air measure of real system

Subsequently, the form factor was calculated differently according to the test in order to reduce errors. So for this first test on FEMM the electrodes have been inserted inside an external boundary surface that represents the distance at which the electric field E generated by the electrodes can be considered almost zero:

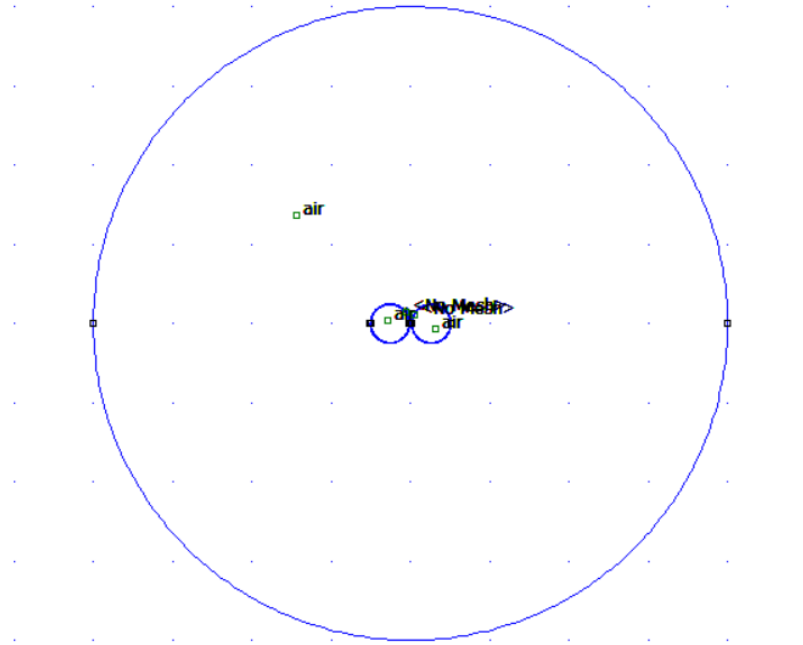


Figure 3.14: FEMM: preliminary test in air only without prototype

This surface has been inserted considering that at a distance equal to 5 times the equivalent radius of the prototype, it is possible to neglect the effect of the electrodes in the surrounding environment. Table 3.10 shows the differences between what is found in simulation with FEMM and what the real measure indicates to us:

f (Hz)	$k_{C,FEMM}$ (m)	$k_{C,measured}$ (m)	C_{FEMM} (F)	$C_{measured}$ (F)	error (%)
50	2.2304	2.3002	1.9749×10^{-11}	2.0367×10^{-11}	3.1293
55600	2.2304	2.3392	1.9749×10^{-11}	2.0712×10^{-11}	4.8762
111200	2.2304	1.0219	1.9749×10^{-11}	9.0479×10^{-12}	54.1855
166700	2.2304	1.9537	1.9749×10^{-11}	1.7299×10^{-11}	12.4057
222200	2.2304	2.2728	1.9749×10^{-11}	2.0124×10^{-11}	1.8988
277800	2.2304	2.3088	1.9749×10^{-11}	2.0443×10^{-11}	3.5141
333400	2.2304	2.3226	1.9749×10^{-11}	2.0565×10^{-11}	4.1319
388900	2.2304	2.3236	1.9749×10^{-11}	2.0574×10^{-11}	4.1774
444400	2.2304	2.3258	1.9749×10^{-11}	2.0594×10^{-11}	4.2787
500000	2.2304	2.3284	1.9749×10^{-11}	2.0617×10^{-11}	4.3952

Table 3.10: Capacitive form factor error

It is important to underline that the major error in the table is due to the fact that the impedance meter at the 100 kHz frequency changes the hardware setup to perform the measurement and around that frequency the measurement has a big error.

After this first test, a second one was done. The base of the system in Figure 3.12 is made of a particular resin, whose electrical characteristics have been obtained in order to have a precise estimation of the electrical parameters of the materials. So the second test was done by inserting the two electrodes in the resin base, setting the frequency in the range 50 Hz – 500 kHz. The procedure is similar to the previous one, in fact it is possible to calculate the relative permittivity of the resin known both the capacitive form factor relative to the air and the capacitive form factor referred to the only resin. Both were calculated in the same way as the previous test using FEMM. It must also be considered that the electrode portion in the air is no longer 200 mm, but almost 185 mm, because 15 mm of the electrode are inserted into the resin. So the system made of electrodes and base of resin can be considered as the parallel of two capacitances, one in air and one in resin. With a digital caliber, therefore, the depth of the holes in the resin base used was measured, and for the difference with the height of the electrodes, the portion of these in

air was also calculated:

$$h_{electrode} = h_{resin} + h_{air} \quad (3.17)$$

where $h_{resin} = 15.9$ mm, $h_{electrode} = 200$ mm, $h_{air} = 184.1$ mm, and we can easily calculate both capacitive form factors thanks to equation (3.15) as :

$$\begin{aligned} k_{C_{resin}} &= h_{resin} \cdot k_{C_{1mm}} \\ k_{C_{air}} &= h_{air} \cdot k_{C_{1mm}} \\ k_{R_{resin}} &= \frac{k_{R_{1mm}}}{h_{resin}} \\ k_{R_{air}} &= \frac{k_{R_{1mm}}}{h_{air}} \end{aligned} \quad (3.18)$$

Subsequently we can find the capacitance associated to the part in the resin as the difference between measured capacitance and air capacitance. In formulas:

$$C_{resin} = C_p - C_{air} \quad (3.19)$$

where C_p represent the value obtained by the LCR meter. Air capacity is calculated as follow:

$$C_{air} = k_{C_{air}} \cdot \epsilon_0 = h_{air} \cdot k_{C_{1mm}} \cdot \epsilon_0 \quad (3.20)$$

where $k_{C_{1mm}} = 0.0112$ m/mm and $h_{air} = 184.1$ mm. Finally we can calculate resin relative permittivity as:

$$\begin{aligned} \epsilon_{r,resin} &= \frac{C_{resin}}{\epsilon_0 \cdot k_{C_{resin}}} \\ k_{C_{resin}} &= h_{resin} \cdot k_{C_{1mm}} \end{aligned} \quad (3.21)$$

where $k_{C_{resin}} = 0.1701$ m. The value of relative permittivity of resin was obtained as the mean value of the array of 100 elements, due to the number of the frequencies setted in the impedance meter. The obtained value is $\epsilon_{r,resin} = 3.41$.

After this test another one was made, in order to verify the accuracy of the prototype realized. During this test, we put water of known electric properties inside a plastic container together with the two electrodes. The electrical characteristics of the tested water are $\sigma = 301$ μ S/cm and $\epsilon_r = 63$. In Figure 3.15 we can see the experiment:

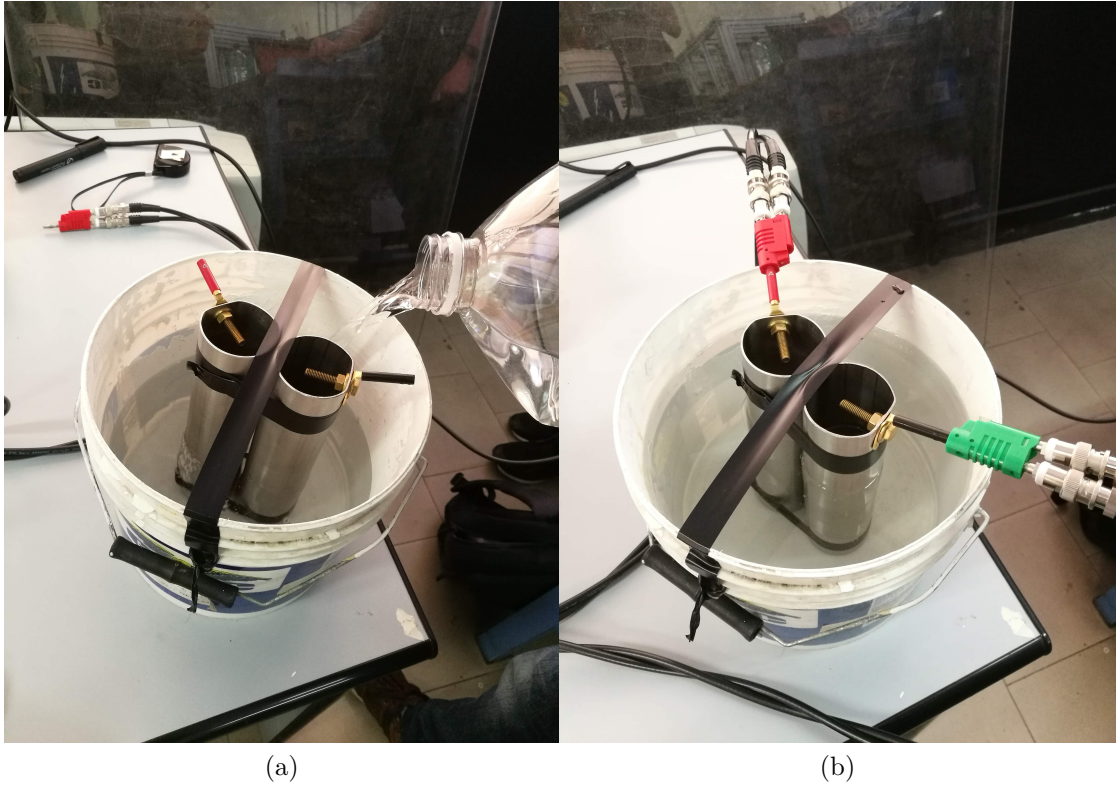


Figure 3.15: Filling the container (a). Measurement of water from known properties (b).

In table 3.11 we summarized the characteristics of the water in question, highlighting the measured quantities and the error made in estimating these parameters:

f (Hz)	Measured permittivity	Expected permittivity	Permittivity error (%)	Measured conductivity ($\mu\text{S}/\text{cm}$)	Real conductivity ($\mu\text{S}/\text{cm}$)	Conductivity error (%)
50	2.3690×10^6	63	99.9973	230.0360	301	30.8491
55600	76.9701	63	37.1889	324.0655	301	7.1175
111200	76.9701	63	18.1501	324.4589	301	7.2301
166700	69.0738	63	8.7932	324.5788	301	7.2644
222200	66.9088	63	5.8420	324.6988	301	7.2987
277800	66.2096	63	4.8476	324.9218	301	7.3623
333400	65.8318	63	4.3016	325.2312	301	7.4505
388900	65.6319	63	4.0100	325.5584	301	7.5435
444400	65.4590	63	3.7565	326.0245	301	7.6757
500000	65.4145	63	3.6911	326.5440	301	7.8225

Table 3.11: Expected and measured water characteristics

This test also confirms the effectiveness of the system implemented and its accuracy in measurements.

Once these tests were carried out in order to verify the accuracy of the system made in this way, we proceeded to test the materials of our interest. In fact, in the following chapter, the main results of these measures will be summarized.

Chapter 4

ELECTRIC PARAMETERS MEASUREMENT

After these preliminary measurements, in the following chapter we will analyze the measurements of some materials used in the covering phase of the coils.

We must also remember that the frequency range has been chosen between 50 Hz and 500 kHz. We chose to take 100 frequency values in logarithmic way, in order to have more values in low frequency with respect to the high frequency. The impedance meter has been set to provide the measurement of the module $|Z|$ and phase θ of the impedance, and of the capacity C_p and resistance R_p according with the parallel RC model of a capacitor real. Furthermore, the calculation table 3.5 was imported from the impedenzimeter manual and through this the error of the impedenzimeter was calculated for each impedance value, according to the equations (3.6) and (3.7). Once accuracy test has been calculated, it has been decided to calculate conductivity σ and relative permittivity ϵ_r only for those values for which the global test accuracy is less than 10 %.

To understand what is meant by global test accuracy we report an example of the manual [4]. Suppose we want to measure the basic accuracy of a capacitor with a known capacity of 160 nF. The measurement conditions are: test frequency = 1 kHz, signal level = 1 V, and speed = SLOW2. The impedance module of the measure is $Z = 1.0144 \text{ k}\Omega$, while the phase is $\theta = -78.69^\circ$ so the test range is 10 k Ω . From Basic Accuracy Coefficient Table (0.501 V to 1.000 V), basic Z accuracy coefficients are $A = 0.08$, $B = 0.01$. Inserting these in the calculation expression yields 3.6 and 3.7 we obtain:

$$Z_{accuracy} = \pm 0.08\% \quad (4.1)$$

Similarly for θ basic accuracy coefficients $A = 0.05$, $B = 0.005$, and thus:

$$\theta_{accuracy} = \pm 0.05^\circ \quad (4.2)$$

From the basic accuracy, find ranges that each of Z and θ can take:

$$Z_{min} = 1.0144 \text{ k}\Omega \cdot (1 - 0.08/100) = 1.0136 \text{ k}\Omega \quad (4.3)$$

$$Z_{max} = 1.0144 \text{ k}\Omega \cdot (1 + 0.08/100) = 1.0152 \text{ k}\Omega \quad (4.4)$$

$$\theta_{min} = 78.69^\circ - 0.05^\circ = 78.64^\circ \quad (4.5)$$

$$\theta_{max} = 78.69^\circ + 0.05^\circ = 78.74^\circ \quad (4.6)$$

From the ranges of Z and θ , determine ranges of C_s can take as follow:

$$C_{s,min} = \frac{1}{Z_{max} \cdot \omega \cdot \sin(\theta_{max})} = 159.85 \text{ nF} \quad (4.7)$$

$$C_{s,max} = \frac{1}{Z_{min} \cdot \omega \cdot \sin(\theta_{min})} = 160.15 \text{ nF} \quad (4.8)$$

where $\omega = 2 \cdot \pi \cdot f$ and f is frequency in Hz. So the error with respect to the real value of capacitance is $\pm 0.09\%$. Hence the accuracy of C_s is 0.009. This logic was also carried out in our tests.

4.1 Procedure performed in the measurements

The procedure followed to calculate the relative permittivity ϵ_r and conductivity σ of the various materials is now described. First of all, we thought of interpreting the capacity C_p that comes out of the measurement with the impedance meter. This is given by the contribution of 3 capacities in parallel. In fact, in the various measurements we are dealing with an air capacity C_{air} , linked to the portion of the electrodes that interface with the latter, a capacity linked exclusively to the material $C_{material}$ used in the measurement, and finally to a capacity of the resin base C_{resin} , linked to the portion in the electrodes inserted in the two holes of the base itself. The total capacity C_p measured therefore represents the equivalent capacity of these three individual capacities, which, as they arise, must be interpreted as three capacities in parallel. Therefore the capacity measured with the impedance meter is equal to:

$$C_p = C_{air} + C_{material} + C_{resin} \quad (4.9)$$

For each of these capacitors, we need to calculate the two capacitive and resistive form factors, in order to extrapolate from the equivalent capacity C_p the only one concerning the material under test. As a result, measurements of the various lengths h have been carried out so as to calculate the form factors according to the equation (3.15).

It is possible to easily calculate the capacities in air C_{air} and in the resin C_{resin} thanks to the preliminary measures, which allowed both to evaluate in advance the error made during the measurement, and the relative permittivity ϵ_r of the resin. So you notice these two capacities, the capacity tied to the material $C_{material}$ is calculated by difference:

$$C_{material} = C_p - C_{air} - C_{resin} \quad (4.10)$$

The same reasoning has been followed for the conductivity σ , however, the discourse is the same and therefore the equivalent resistance R_p provided by the impedance meter must be interpreted as a parallel of three capacities:

$$\frac{1}{R_p} = \frac{1}{R_{air}} + \frac{1}{R_{material}} + \frac{1}{R_{resin}} \quad (4.11)$$

However, in this case it is possible to ignore the resistances in air and in resin, and therefore associate the resistance measured R_p to the only resistance in the material $R_{material}$. This is for a very simple reason, concerning the high resistivity ρ of both air ($1.3 \times 10^{16} - 3.3 \times 10^{16} \Omega\text{m}$) and resin ($5.5 \times 10^7 \Omega\text{m}$).

Therefore, since the three resistances in parallel do not make a big mistake in neglecting the latter and therefore the equation (4.11) becomes:

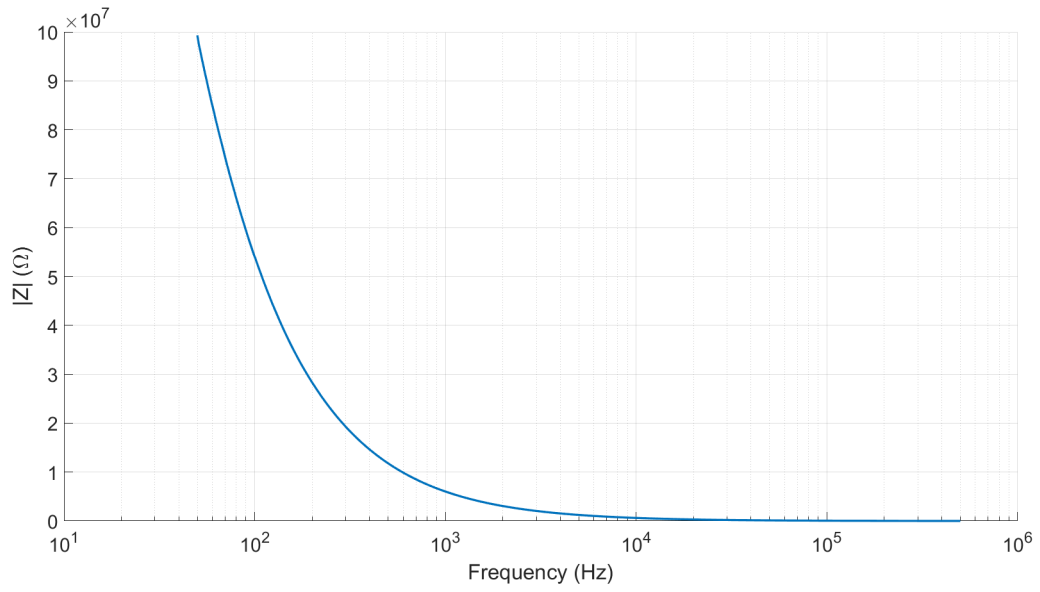
$$\frac{1}{R_p} = \frac{1}{R_{material}} \quad (4.12)$$

and so:

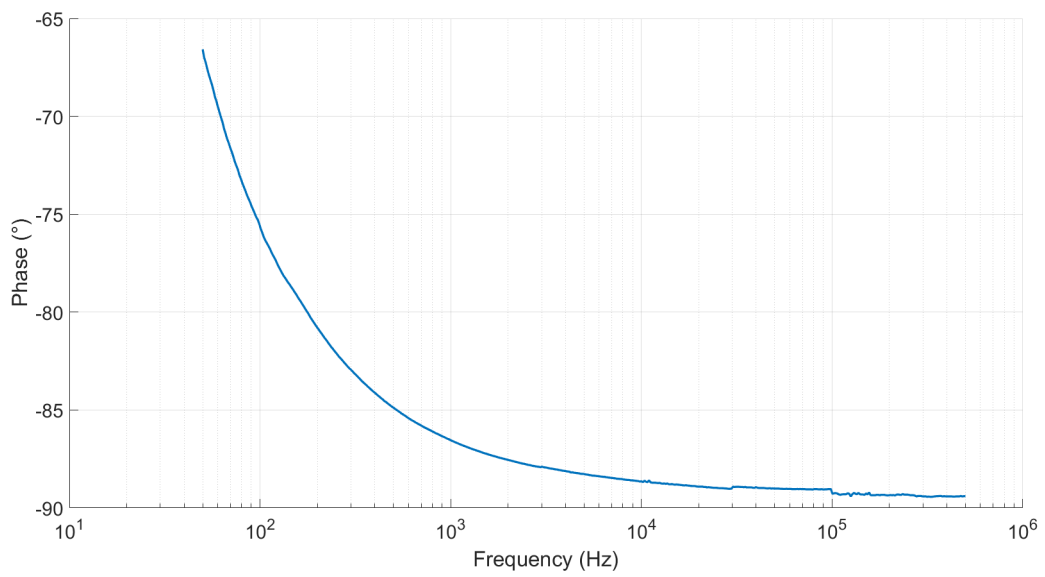
$$R_{material} = R_p \quad (4.13)$$

4.2 Black Catramina

In this section of the chapter, we will report and analyze the main results of the material called Black Catramine. First of all, we report the graphs related to the module of the impedance $|Z|$, the phase of the impedance θ , the capacity C_p and resistance R_p measured by the impedance meter:

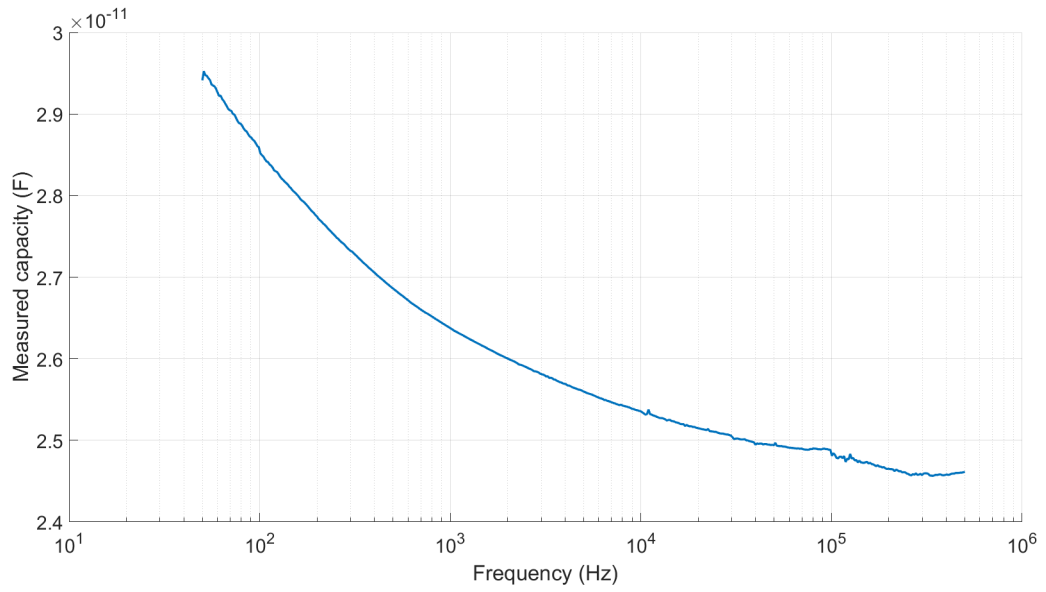


(a)

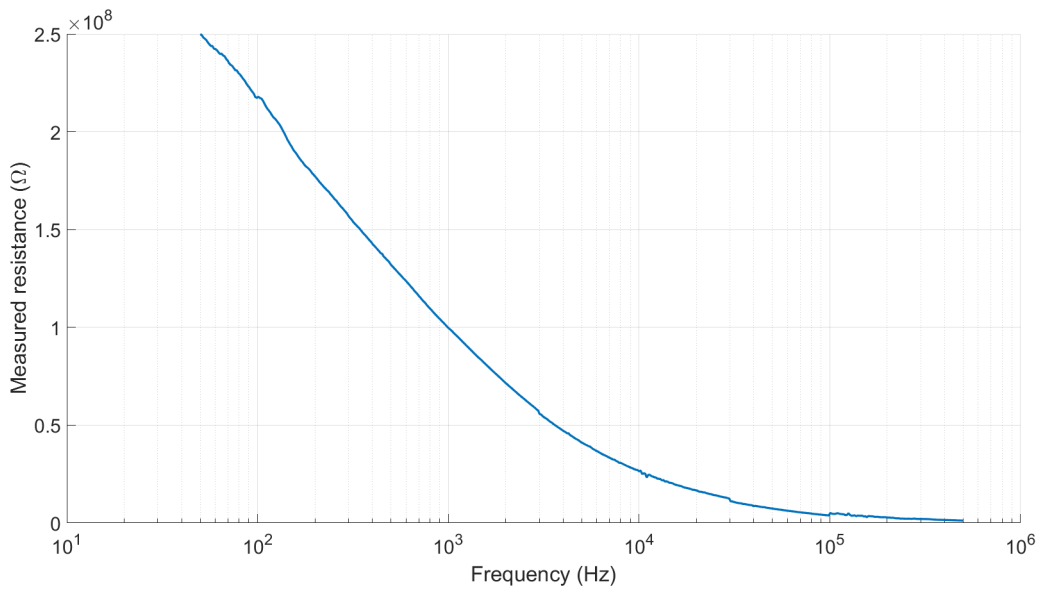


(b)

Figure 4.1: Impedance $|Z|$ (Ω) of the prototype with Black Catramina (a). Phase θ ($^\circ$) of the prototype with Black Catramina (b).



(a)



(b)

Figure 4.2: Measured capacity C_p (F) (a). Measured resistance R_p (Ω) (b).

The latter graphs are calculated automatically by the impedance meter, according to the following formula:

$$\bar{Y} = \frac{1}{\bar{Z}} = \bar{Y}_{R_p} + \bar{Y}_{C_p} = \frac{1}{R_p} + j\omega C_p \quad (4.14)$$

From this equation, note the impedance module $|Z|$ and the phase θ , we can easily calculate the parameters R_p and C_p according to the following formulas:

$$\bar{Z} = |Z|(\cos(\theta) + j \sin(\theta)) \quad (4.15)$$

$$\bar{Y} = \bar{Z}^{-1} \quad (4.16)$$

$$R_p = \frac{1}{\text{Re}\{\bar{Z}\}} \quad (4.17)$$

$$C_p = \frac{1}{\omega \text{Im}\{\bar{Z}\}} \quad (4.18)$$

Note the two electrical parameters C_p and R_p , we can now calculate both the relative permittivity ϵ_r and the conductivity σ of the Black Catramina. To do this we must calculate the three capacitive form factors, and the three resistive form factors. These are calculated using the equation (3.15), measuring the distances relative to the air, the material and the resin of the electrodes mentioned in the previous section. Here are the measured distances and the respective form factors:

- Length electrodes in air $h_{air} = 175$ mm
- Length electrodes in Black Catramina $h_{catramina} = 9.7$ mm
- Length electrodes in resin $h_{resin} = 15.3$ mm

Remember that the capacitive form factor $k_{C,1\text{mm}} = 0.0112$ m/mm, and therefore we can calculate the 6 form factors:

- $k_{C_{air}} = 1.96$ m
- $k_{C_{catramina}} = 0.1086$ m
- $k_{C_{resin}} = 0.1714$ m
- $k_{R_{air}} = 0.512$ m⁻¹
- $k_{R_{catramina}} = 9.242$ m⁻¹
- $k_{R_{resin}} = 5.858$ m⁻¹

Note the form factors we can use the equations (4.10) and (4.13) in order to calculate the relative permittivity and conductivity of the Black Catramina:

$$\epsilon_r = \frac{C_{catramina}}{\epsilon_0 \cdot k_{C_{catramina}}} \quad (4.19)$$

$$\sigma = \frac{k_{R_{catramina}}}{R_{catramina}} = \frac{k_{R_{catramina}}}{R_p} \quad (4.20)$$

The following are the two graphs relating to the trend in relative permittivity ϵ_r and conductivity σ according to frequency:

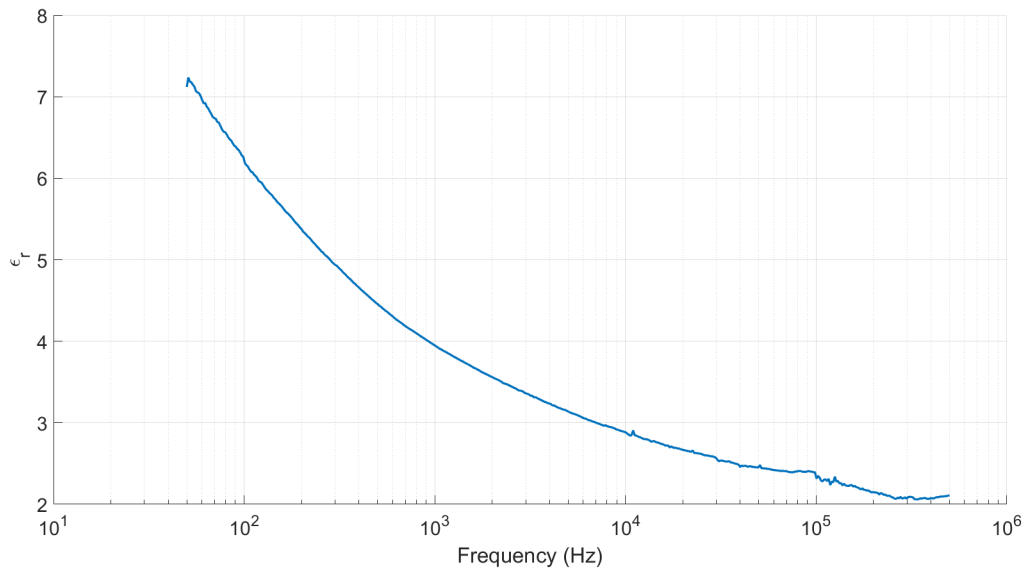


Figure 4.3: Relative permittivity ϵ_r .

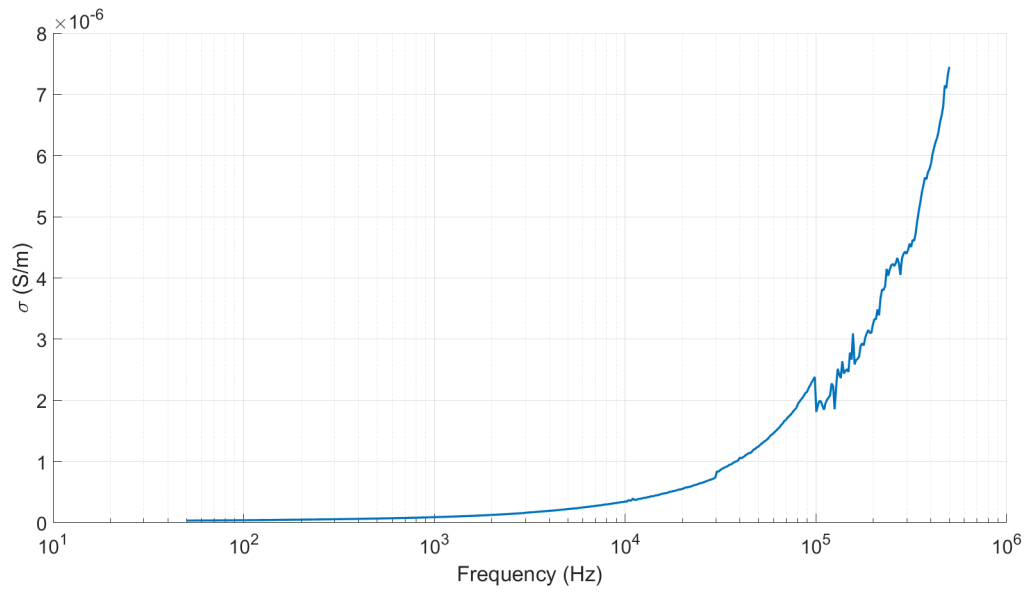
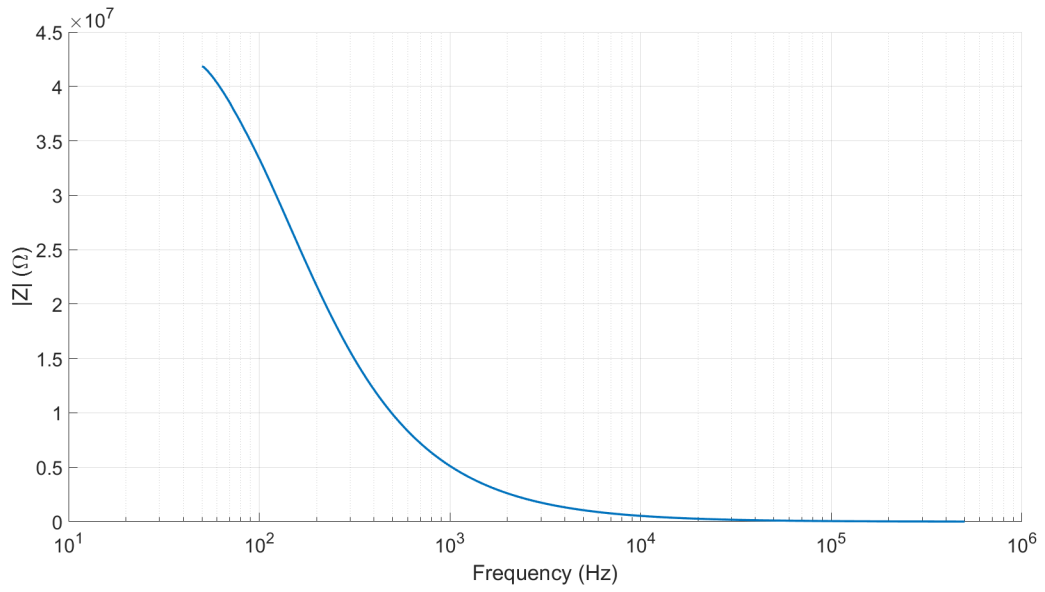


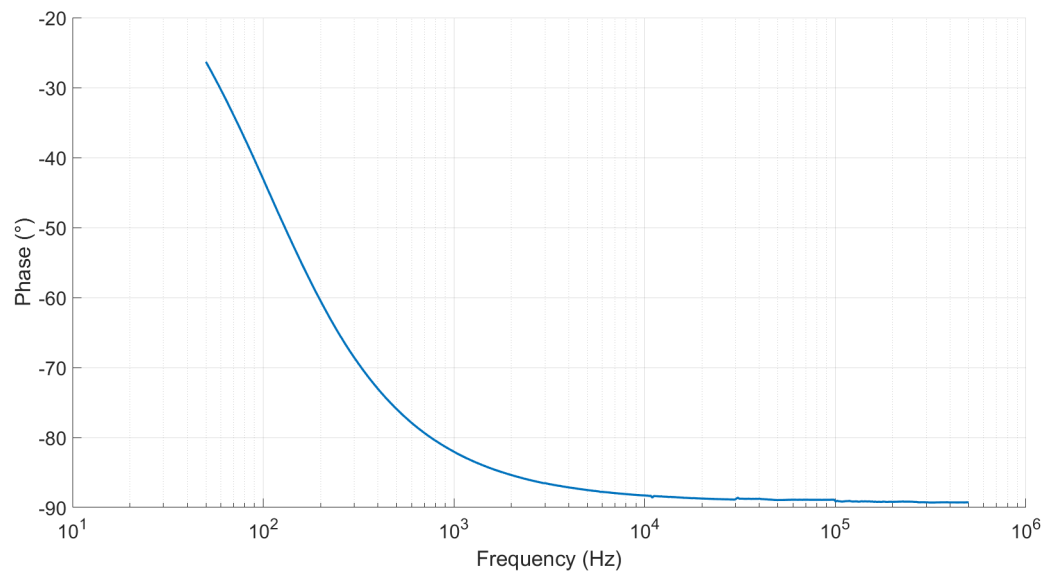
Figure 4.4: Conductivity σ (S/m).

4.3 Catramix

In this section of the chapter, we will report and analyze the main results of the material called Black Catramine. The following graphs are related as usual to the module of the impedance $|Z|$, the phase of the impedance θ , the capacity C_p and resistance R_p measured:

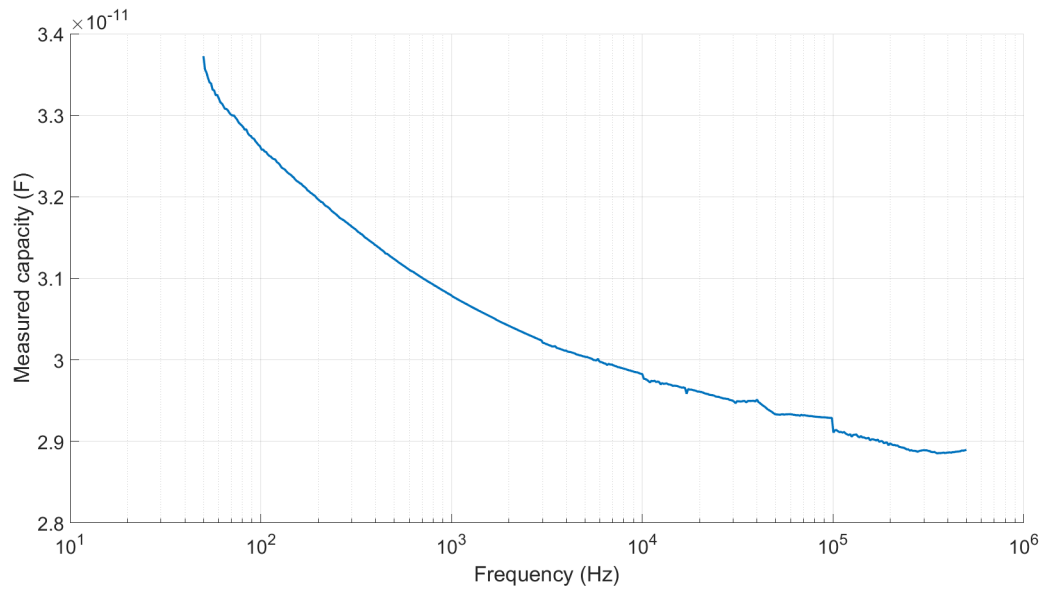


(a)

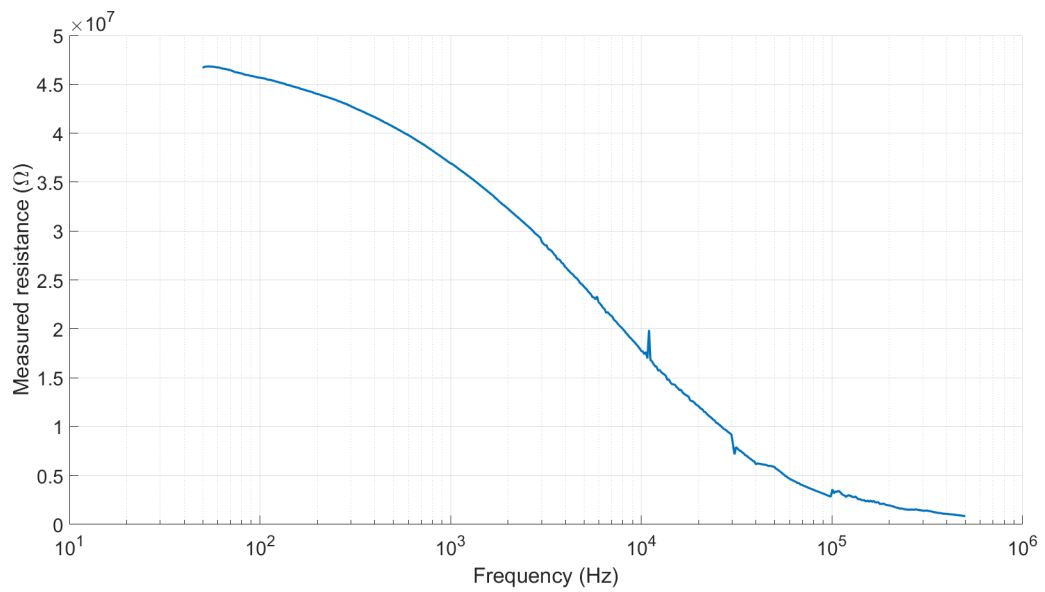


(b)

Figure 4.5: Impedance $|Z|$ (Ω) of the prototype with Catramix (a). Phase θ ($^\circ$) of the prototype with Catramix (b).



(a)



(b)

Figure 4.6: Measured capacity C_p (F) (a). Measured resistance R_p (Ω) (b).

In order to calculate relative permittivity ϵ_r and conductivity σ , we now report the measured distances and the respective form factors:

- Length electrodes in air $h_{air} = 174$ mm

- Length electrodes in Catramix $h_{catramix} = 9 \text{ mm}$
- Length electrodes in resin $h_{resin} = 17 \text{ mm}$

therefore:

- $k_{C_{air}} = 1.9488 \text{ m}$
- $k_{C_{catramix}} = 0.1004 \text{ m}$
- $k_{C_{resin}} = 0.1897 \text{ m}$
- $k_{R_{air}} = 0.5131 \text{ m}^{-1}$
- $k_{R_{catramix}} = 9.9601 \text{ m}^{-1}$
- $k_{R_{resin}} = 5.2714 \text{ m}^{-1}$

The relative permittivity and the conductivity of the Catramix are calculated with the equations (4.19), 4.20, that we can resume in the following graphs:

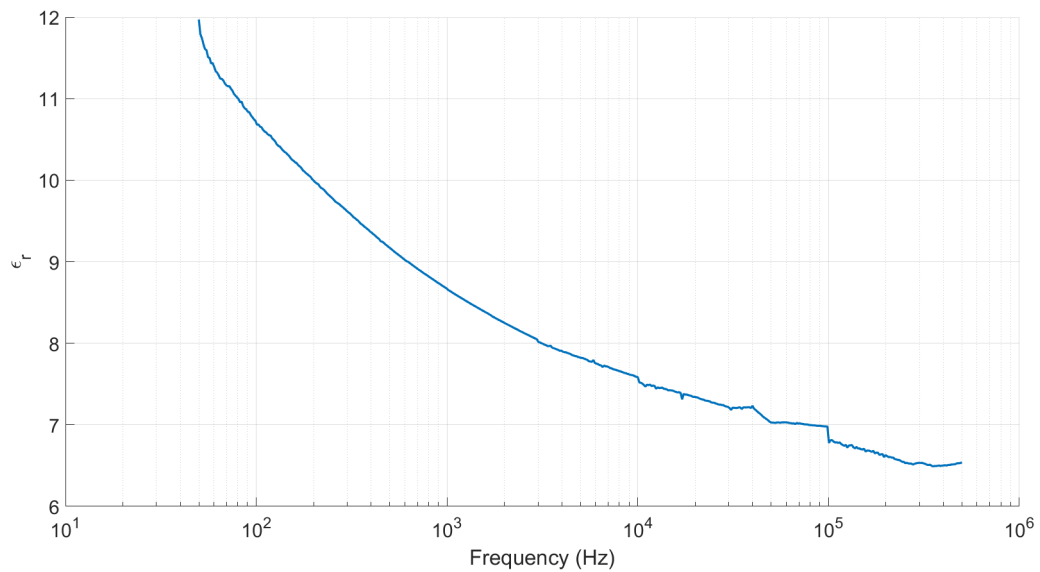


Figure 4.7: Relative permittivity ϵ_r .

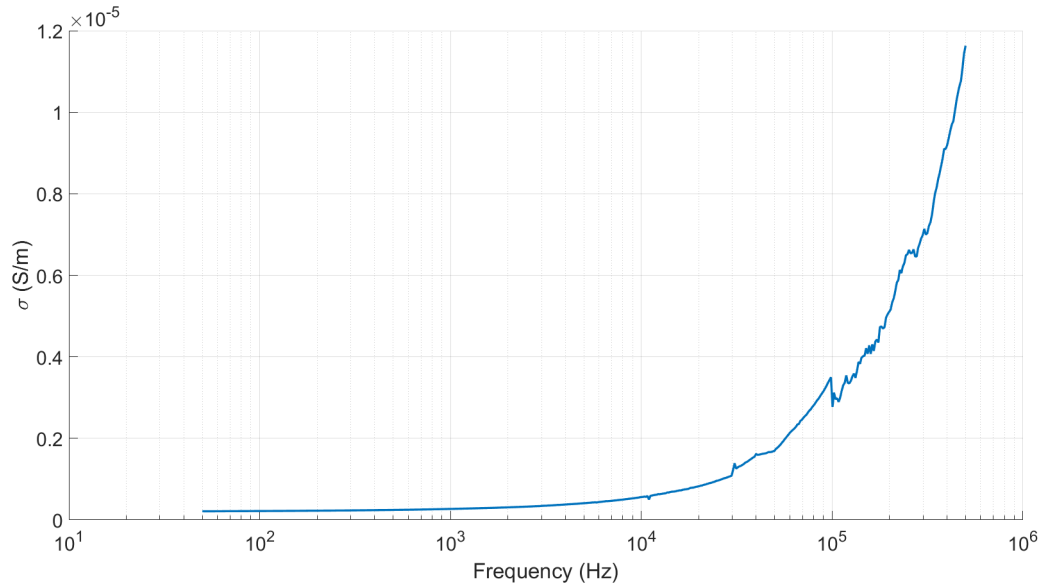
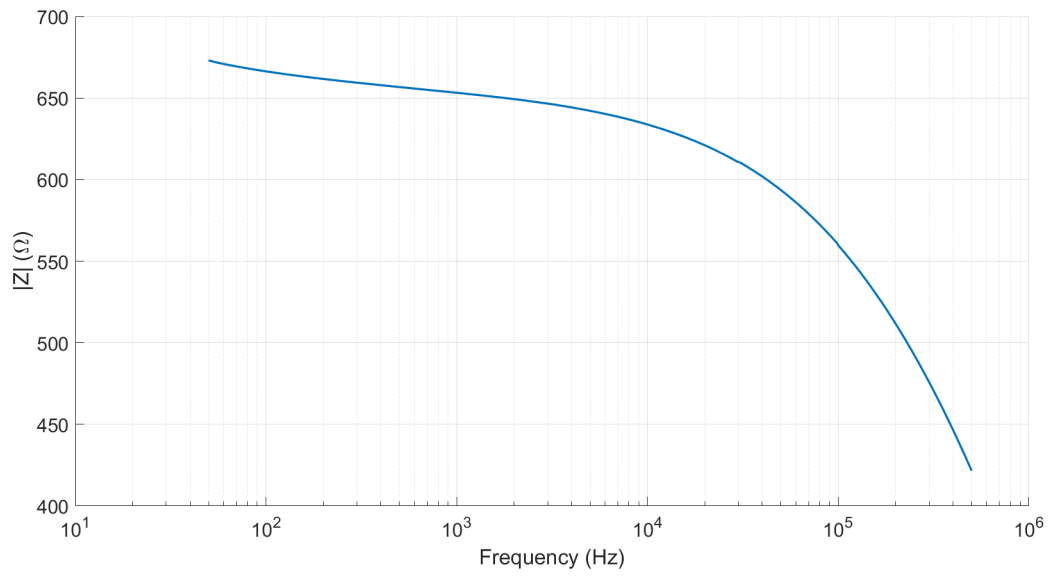


Figure 4.8: Conductivity σ (S/m).

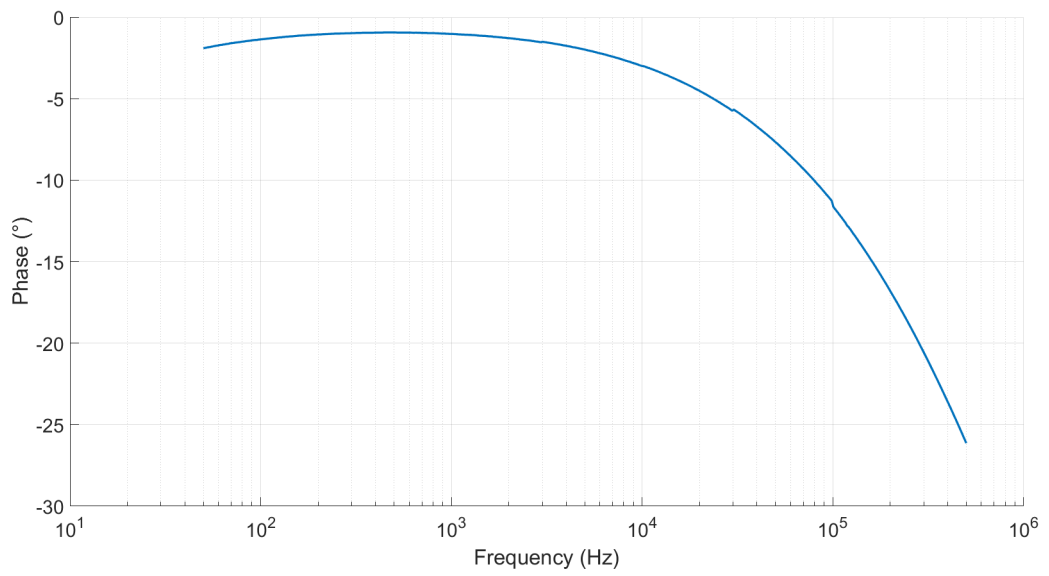
The values from which the error committed is less than 10% are shown in red. From these values a mean value has been made in order to calculate a single one value both of permittivity and of conductivity. The values obtained are respectively $\epsilon_{catramix} = 7.51$ and $\sigma = 1.976 \times 10^{-6}$ (S/m).

4.4 Cement 1

In this section of the chapter, we will report and analyze the main results of the cement material called Cement 1, which is a type of quick-drying cement. The following graphs are related as usual to the module of the impedance $|Z|$, the phase of the impedance θ , the capacity C_p and resistance R_p measured:

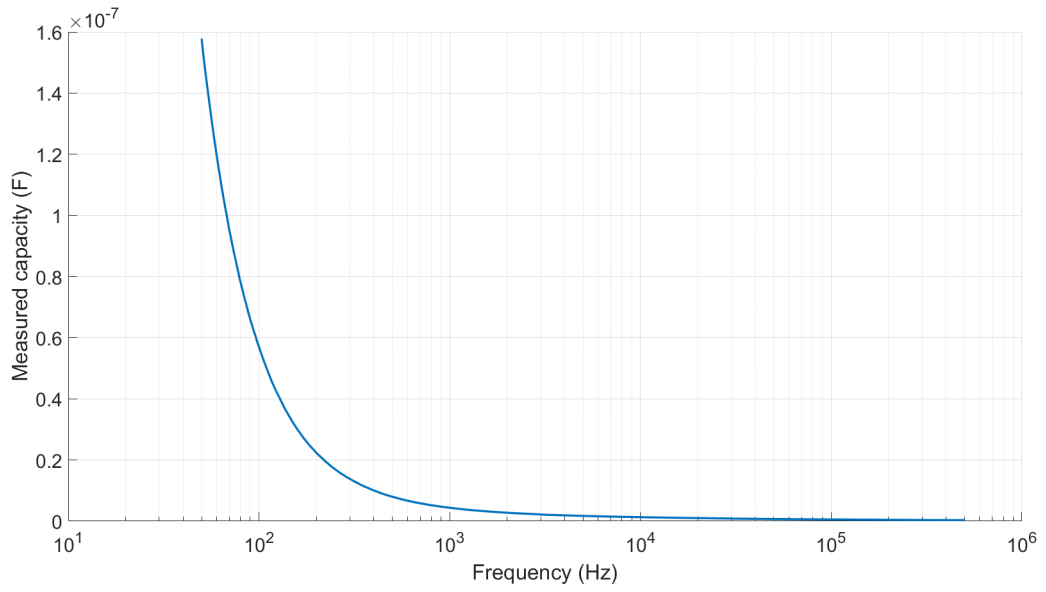


(a)

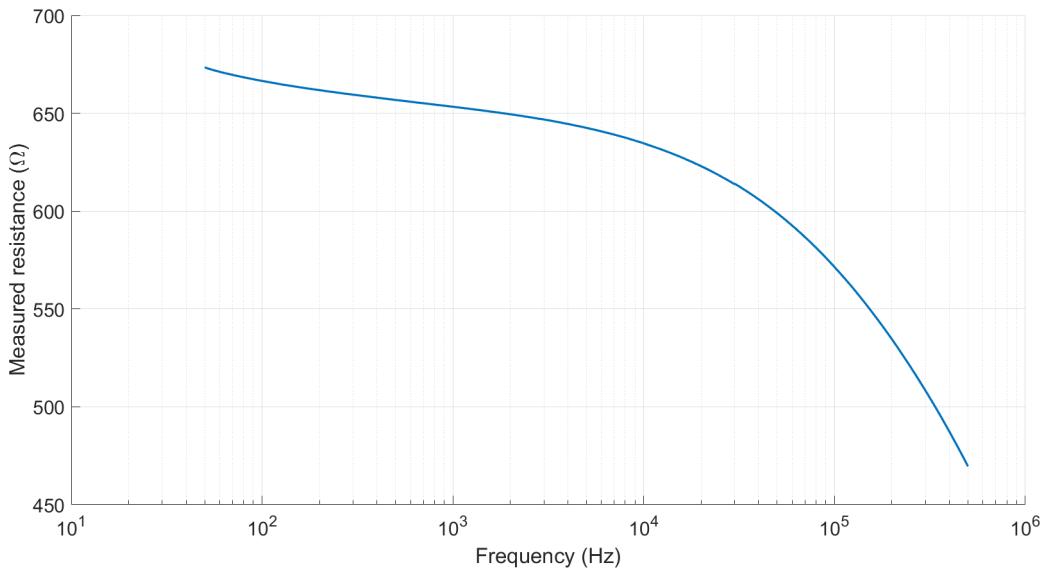


(b)

Figure 4.9: Impedance $|Z|$ (Ω) of the prototype with Cement 1 (a). Phase θ (°) of the prototype with Cement 1 (b).



(a)



(b)

Figure 4.10: Measured capacity C_p (F) (a). Measured resistance R_p (Ω) (b).

In order to calculate relative permittivity ϵ_r and conductivity σ , we now report the measured distances and the respective form factors:

- Length electrodes in air $h_{air} = 43.04$ mm

- Length electrodes in Cement 1 $h_{Cement1} = 141.07$ mm
- Length electrodes in resin $h_{resin} = 15.9$ mm

therefore:

- $k_{C_{air}} = 0.4802$ m
- $k_{C_{Cement1}} = 1.5739$ m
- $k_{C_{resin}} = 0.1774$ m
- $k_{R_{air}} = 2.0825$ m⁻¹
- $k_{R_{Cement1}} = 0.6354$ m⁻¹
- $k_{R_{resin}} = 5.6370$ m⁻¹

The relative permittivity and the conductivity of the Cement 1 are calculated with the equations (4.19), (4.20), that we can resume in the following graphs:

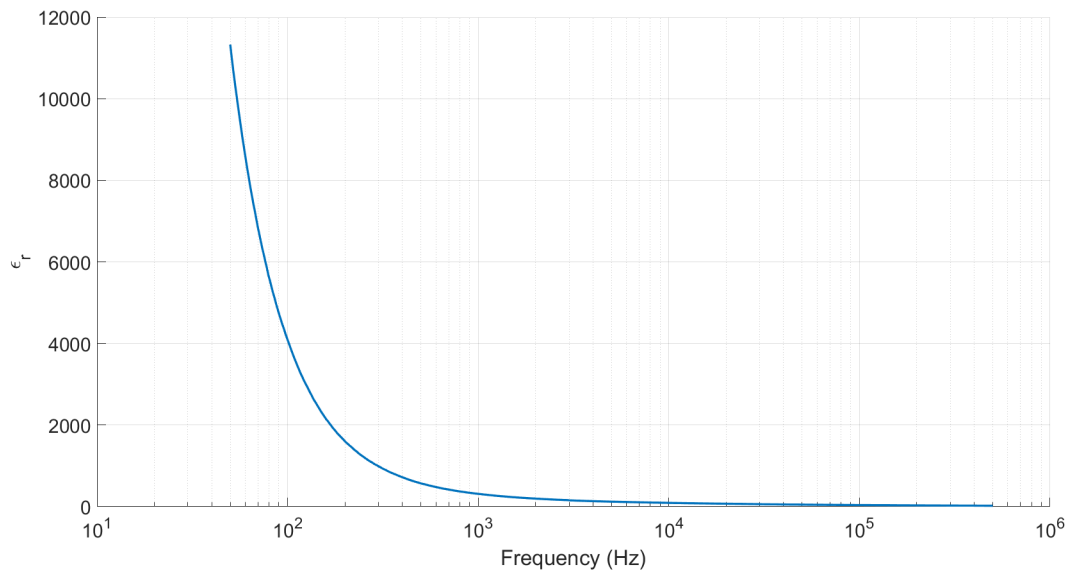


Figure 4.11: Relative permittivity ϵ_r .

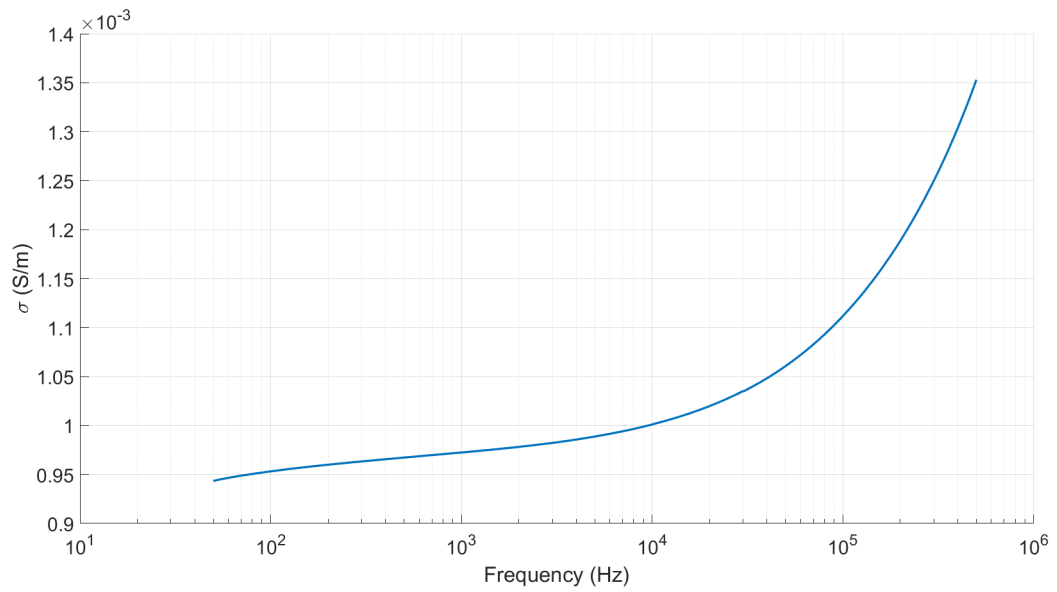
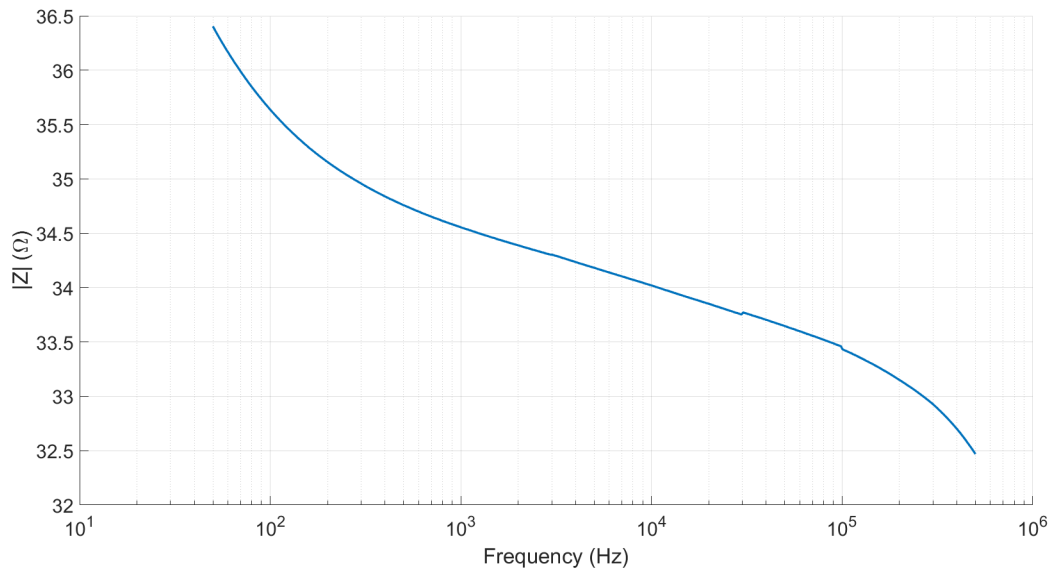


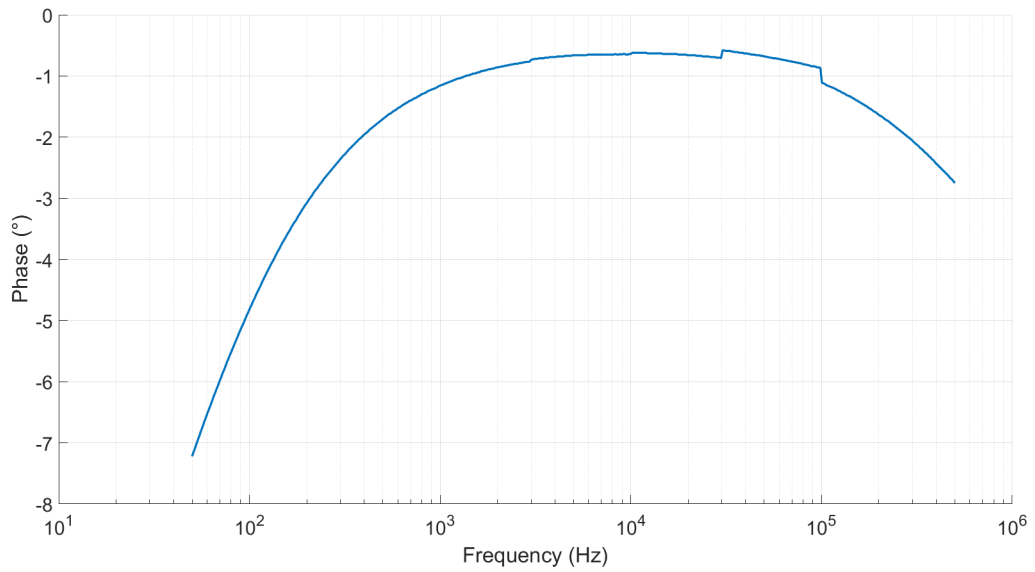
Figure 4.12: Conductivity σ (S/m).

4.5 Cement 2

In this section of the chapter, we will report and analyze the main results of the cement material called Cement 2, which is a type of normal-drying cement. The following graphs are related as usual to the module of the impedance $|Z|$, the phase of the impedance θ , the capacity C_p and resistance R_p measured:

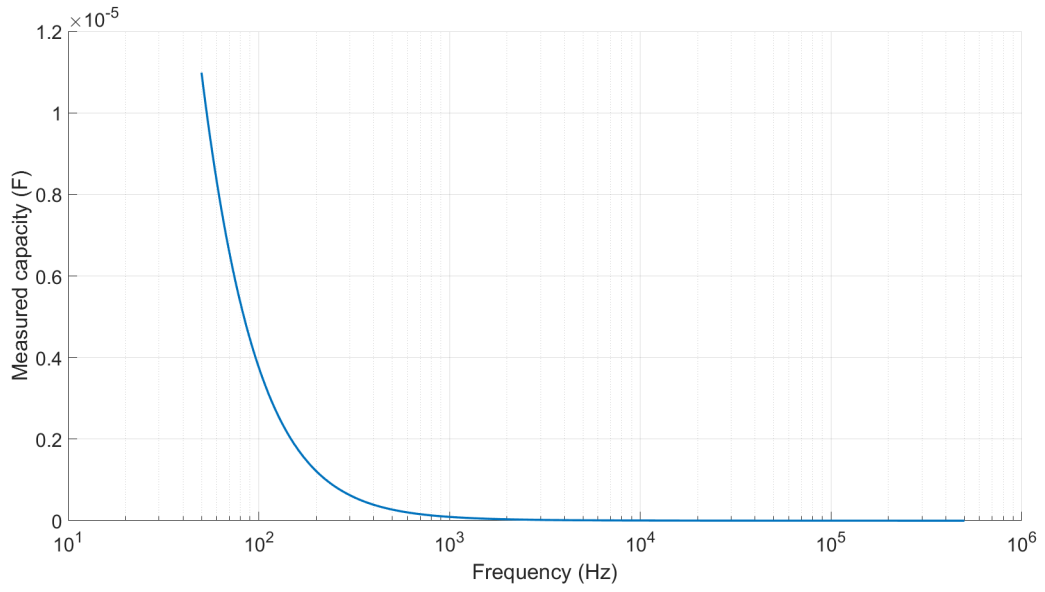


(a)

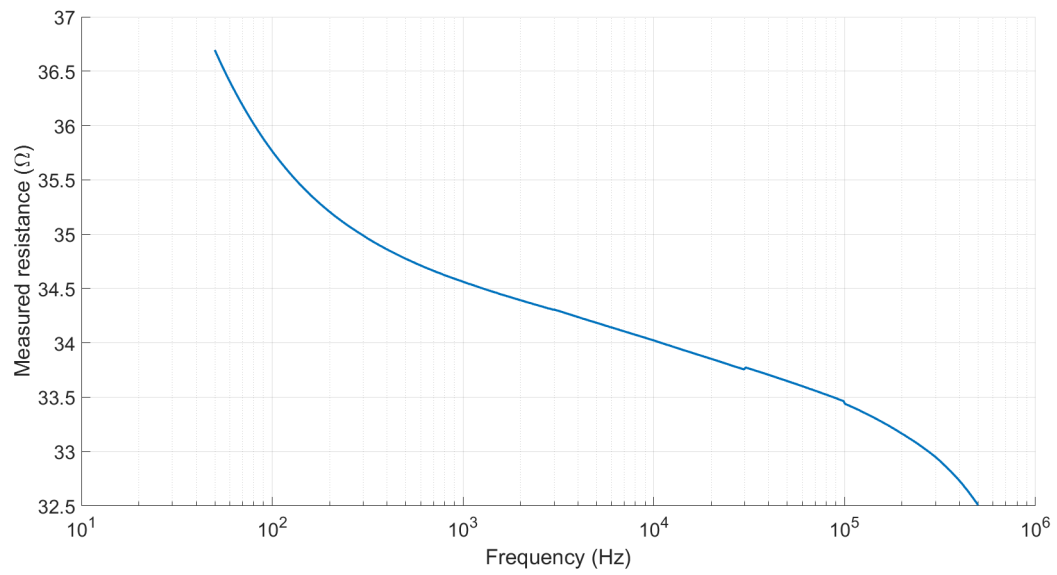


(b)

Figure 4.13: Impedance $|Z|$ (Ω) of the prototype with Cement 2 (a). Phase θ ($^\circ$) of the prototype with Cement 2 (b).



(a)



(b)

Figure 4.14: Measured capacity C_p (F) (a). Measured resistance R_p (Ω) (b).

In order to calculate relative permittivity ϵ_r and conductivity σ , we now report the measured distances and the respective form factors:

- Length electrodes in air $h_{air} = 37.6$ mm

- Length electrodes in Cement 2 $h_{Cement2} = 147.95$ mm
- Length electrodes in resin $h_{resin} = 15.3$ mm

therefore:

- $k_{C_{air}} = 0.4197$ m
- $k_{C_{Cement2}} = 1.6507$ m
- $k_{C_{resin}} = 0.1707$ m
- $k_{R_{air}} = 2.3827$ m⁻¹
- $k_{R_{Cement2}} = 0.6058$ m⁻¹
- $k_{R_{resin}} = 5.8582$ m⁻¹

The relative permittivity and the conductivity of the Cement 2 are calculated with the equations (4.19), (4.20), that we can resume in the following graphs:

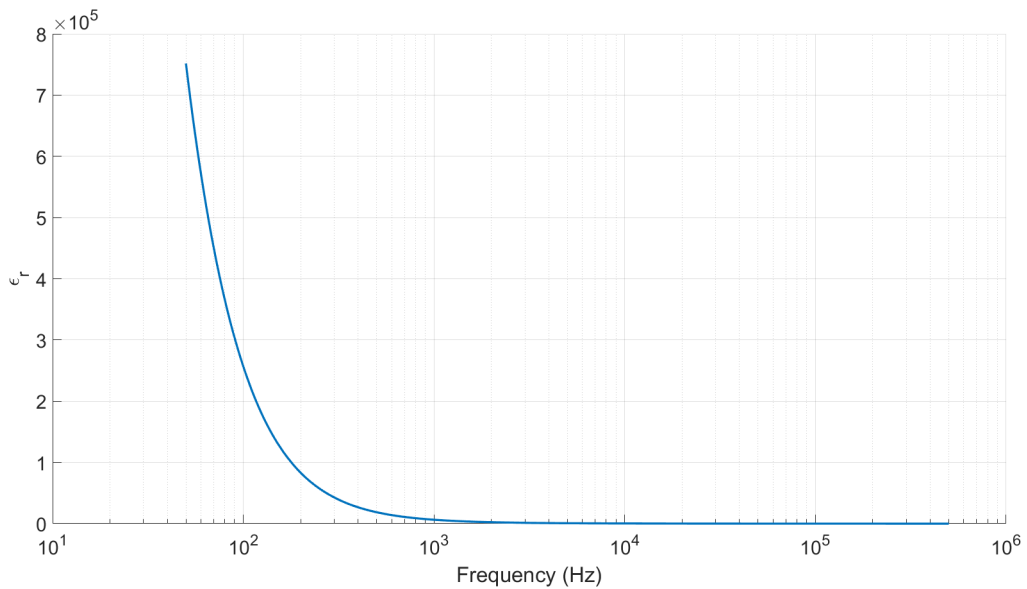


Figure 4.15: Relative permittivity ϵ_r .

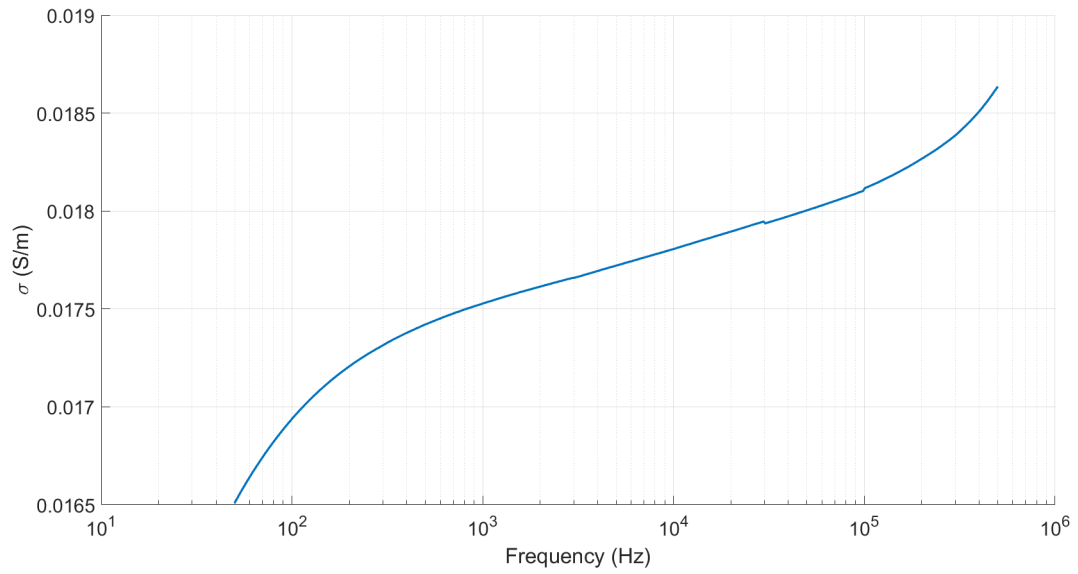
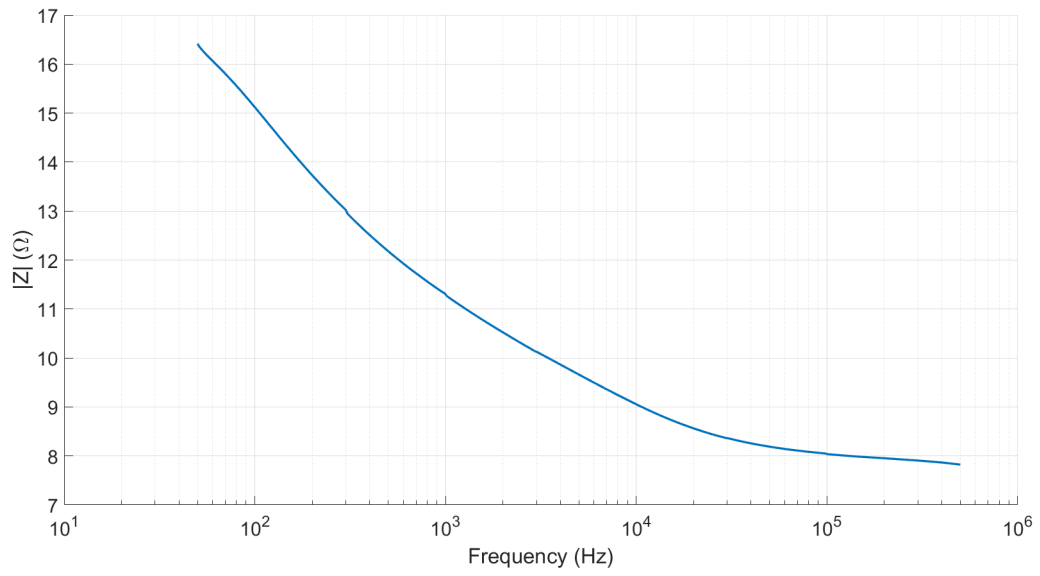


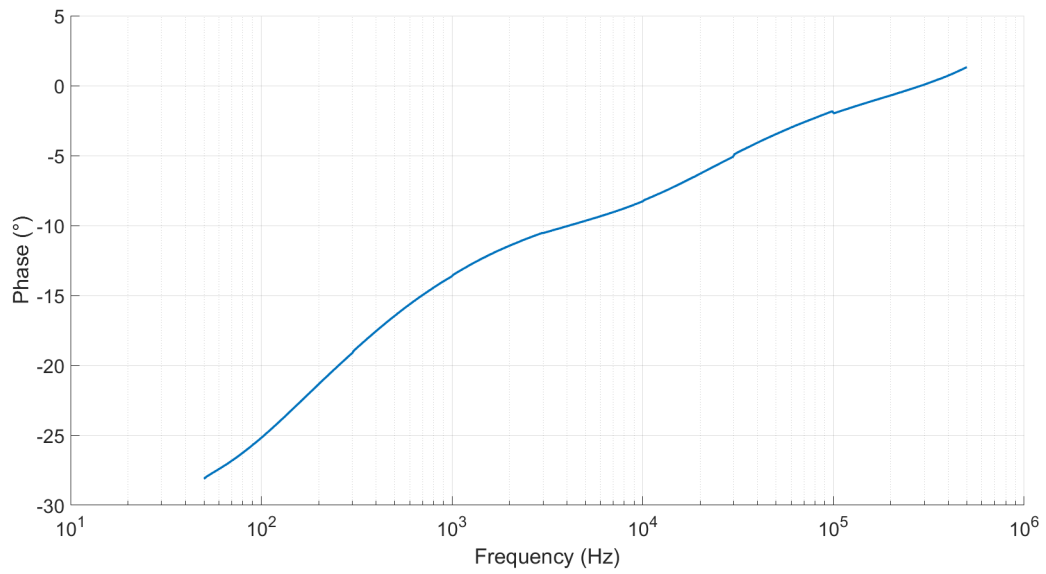
Figure 4.16: Conductivity σ (S/m).

4.6 Unolastic

In this section of the chapter, we will report and analyze the main results of the material called Unolastic. This one is a hybrid material because it has both cement and bituminous chemical characteristics. The following graphs are related as usual to the module of the impedance $|Z|$, the phase of the impedance θ , the capacity C_p and resistance R_p measured:

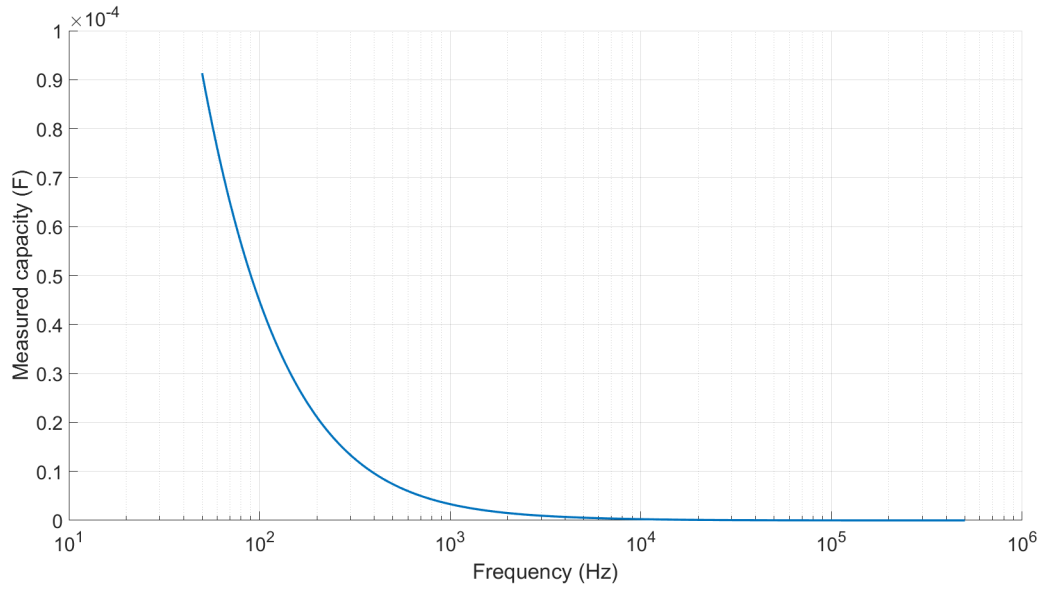


(a)

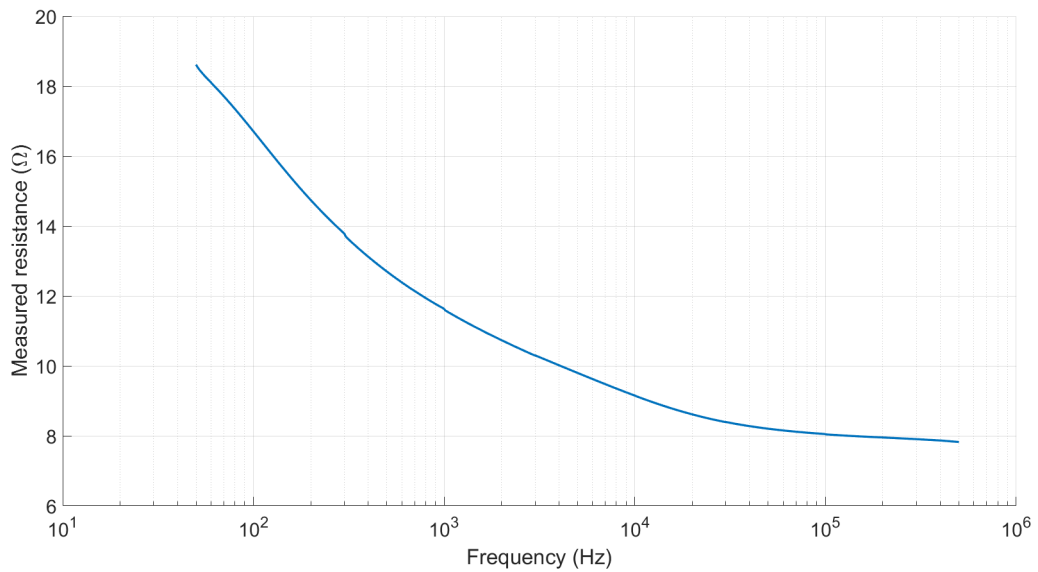


(b)

Figure 4.17: Impedance $|Z|$ (Ω) of the prototype with Unolastic (a). Phase θ (°) of the prototype with Unolastic (b).



(a)



(b)

Figure 4.18: Measured capacity C_p (F) (a). Measured resistance R_p (Ω) (b).

In order to calculate relative permittivity ϵ_r and conductivity σ , we now report the measured distances and the respective form factors:

- Length electrodes in air $h_{air} = 154$ mm

- Length electrodes in Unolastic $h_{unolastic} = 44.81$ mm
- Length electrodes in resin $h_{resin} = 15.19$ mm

therefore:

- $k_{C_{air}} = 1.7182$ m
- $k_{C_{unolastic}} = 0.4999$ m
- $k_{C_{resin}} = 0.1695$ m
- $k_{R_{air}} = 0.5820$ m⁻¹
- $k_{R_{unolastic}} = 2.0004$ m⁻¹
- $k_{R_{resin}} = 5.8997$ m⁻¹

The relative permittivity and the conductivity of the Unolastic are calculated with the equations (4.19), (4.20), that we can resume in the following graphs:

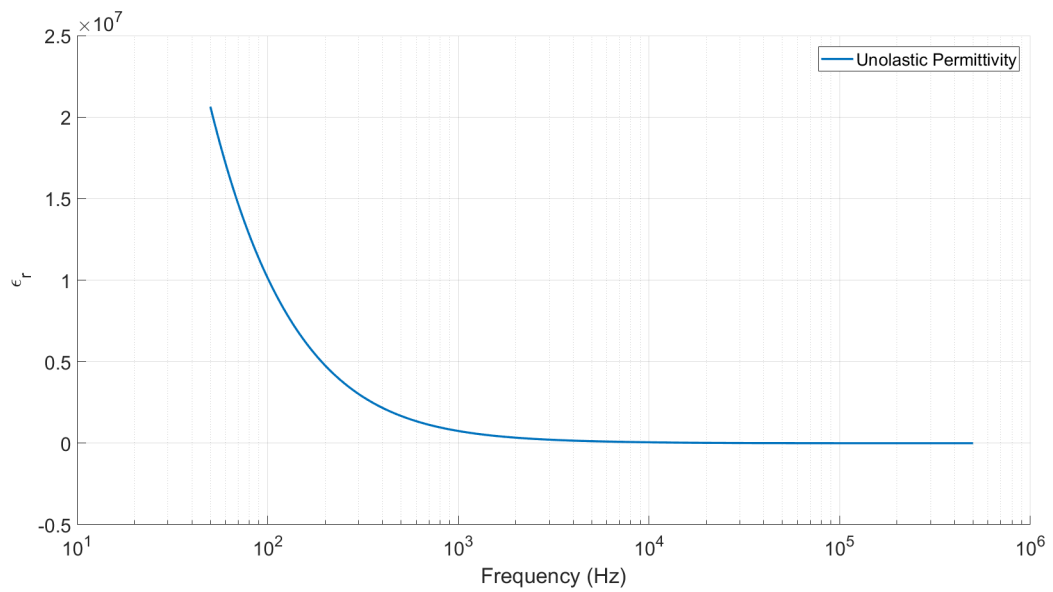


Figure 4.19: Relative permittivity ϵ_r .

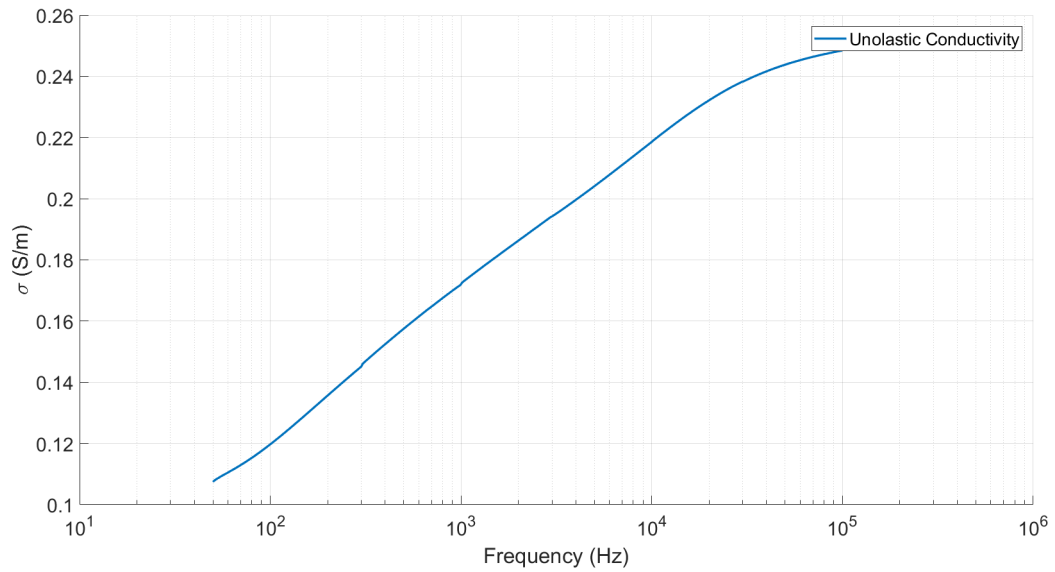
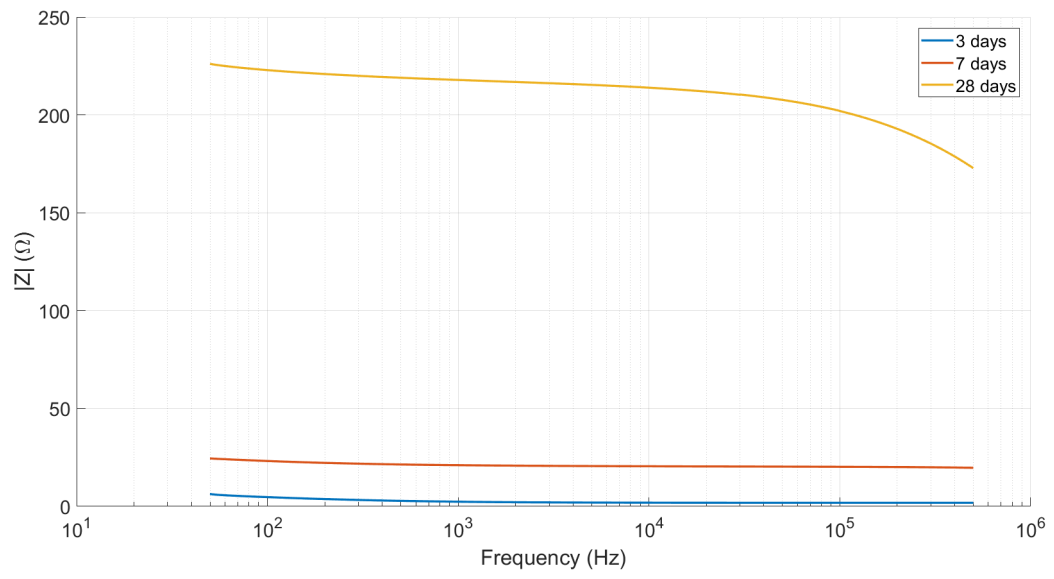


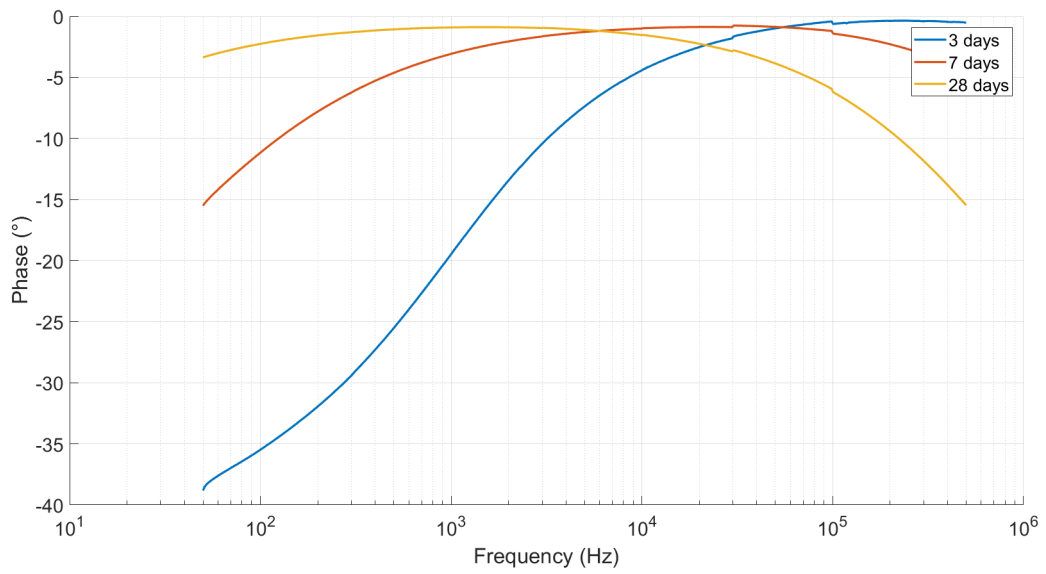
Figure 4.20: Conductivity σ (S/m).

4.7 Variation of impedance and phase of concretes over time

For the cements various measurements were made during the days following the casting. So it is interesting to show now what were the differences in terms of module and phase over the different days. In fact, Figures 4.21 and 4.22 show the variations undergone by the two cements at different days from their casting in order to highlight the variations in measurements according to the quantity of water present inside the cements:

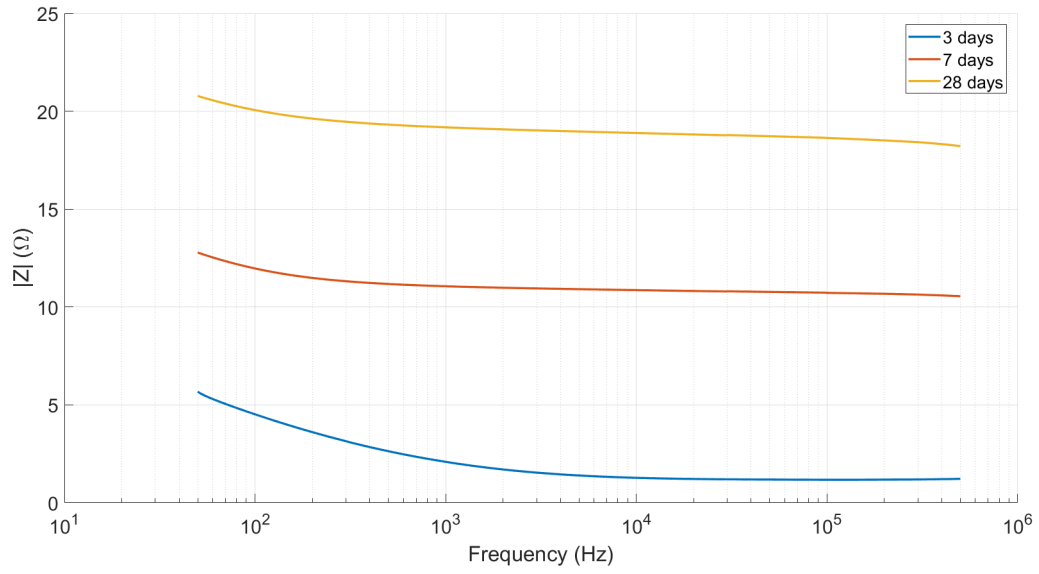


(a)

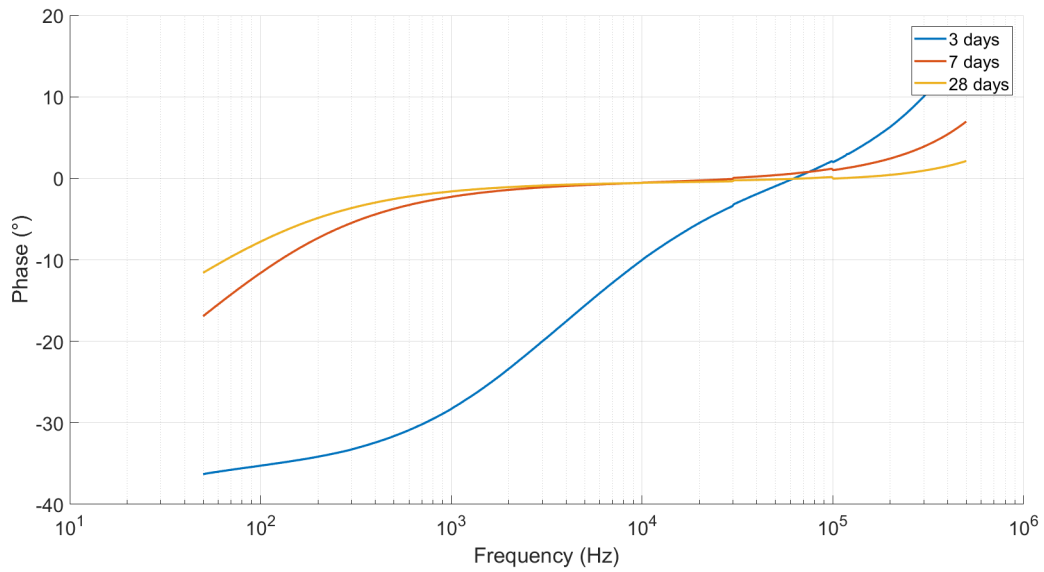


(b)

Figure 4.21: Module $|Z|$ (a) and phase θ (b) of Cement 1 over time.



(a)



(b)

Figure 4.22: Module $|Z|$ (a) and phase θ (b) of Cement 2 over time.

These measures at different days from the casting were carried out for two main reasons. The first is to highlight the variation undergone by the module and the phase during the drying process of the cements. The second reason is to try to simulate the effect of rain or other sources of humidity in the Cement 1 and Cement 2 cements, and

how these affect permittivity ϵ and σ . It is clear that a variation of module and phase causes a variation in the estimation of permittivity ϵ and conductivity σ according to (4.17), (4.18). Thus the final results, previously presented in Figure 4.9, 4.13 are to be considered calculate after 28 days, when therefore there were not appreciable variations in the module and in the phase.

Chapter 5

MAGNETIC RESULTS

In this chapter we will analyze the results of the magnetic tests carried out on the materials. For these measurements, we developed a toroid by using PVC pipes. In first instance the inductor shown in Figure 5.1 has been built by wounding the coil without any material inside the toroid (i.e. air core). Then the same measurement has been repeated by putting the material under test:



Figure 5.1: Air core toroid.

Thanks to the LCR meter it was possible to calculate both the series resistance R_s and

the equivalent inductance L_s of such toroid, according with the real model of an inductor:

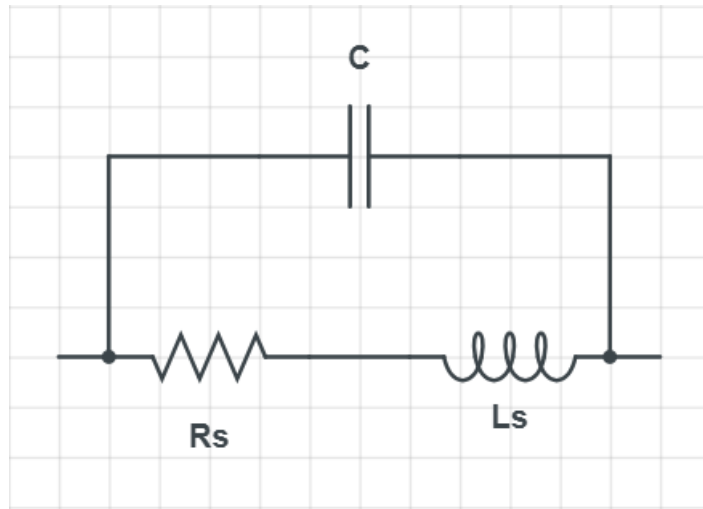


Figure 5.2: Equivalent circuit of a real inductor.

where L_s represent the equivalent inductance of the real inductor, R_s is the series resistance of the windings and C is equivalent capacity of the coils of the winding. In our case capacity C is neglected so the model we use is the inductance with series resistance. So according to table 3.1, the LCR meter has been setted in order to provide us R_s and L_s . The measurements also calculated in the usual frequency range 50 Hz – 500 kHz of the air core inductor toroid is shown in Figures 5.3, 5.4:

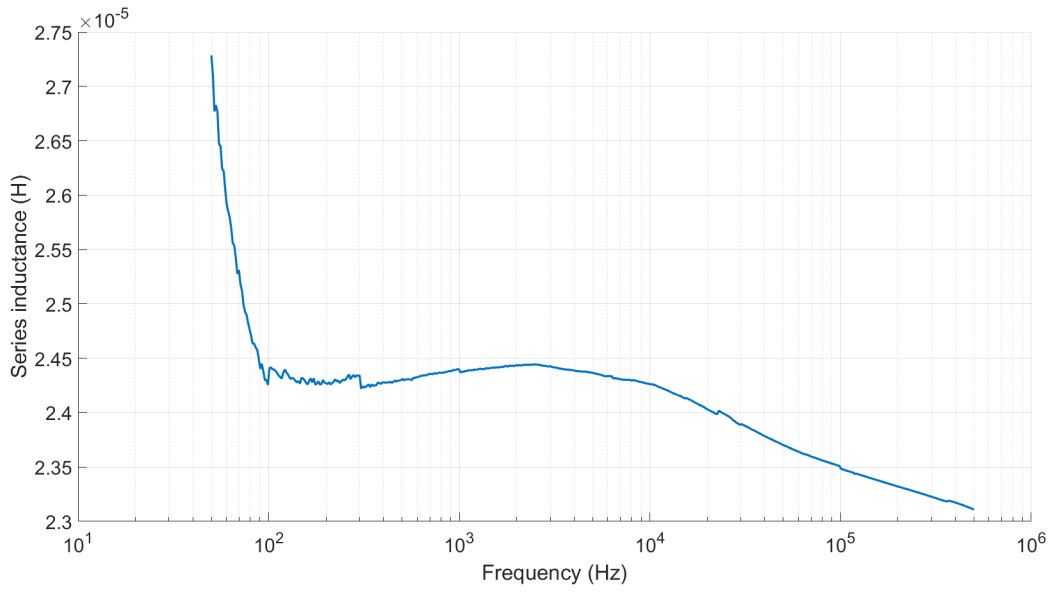


Figure 5.3: Air core inductor series inductance L_s .

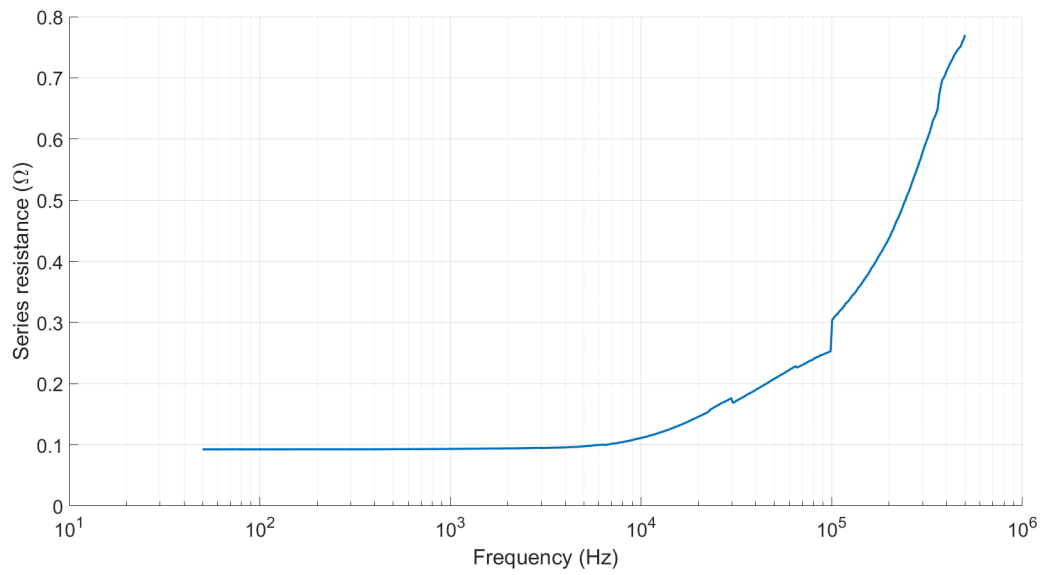


Figure 5.4: Air core inductor series resistance R_s .

In Figures 5.5, 5.6 both the equivalent impedance module $|Z|$ and the phase θ have been reported:

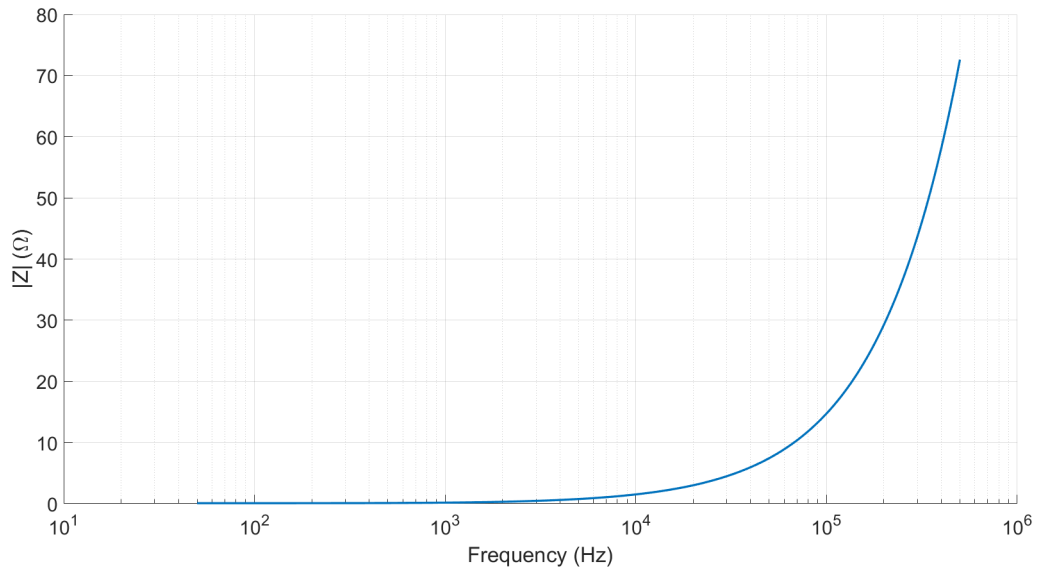


Figure 5.5: Air core inductor impedance $|Z|$.

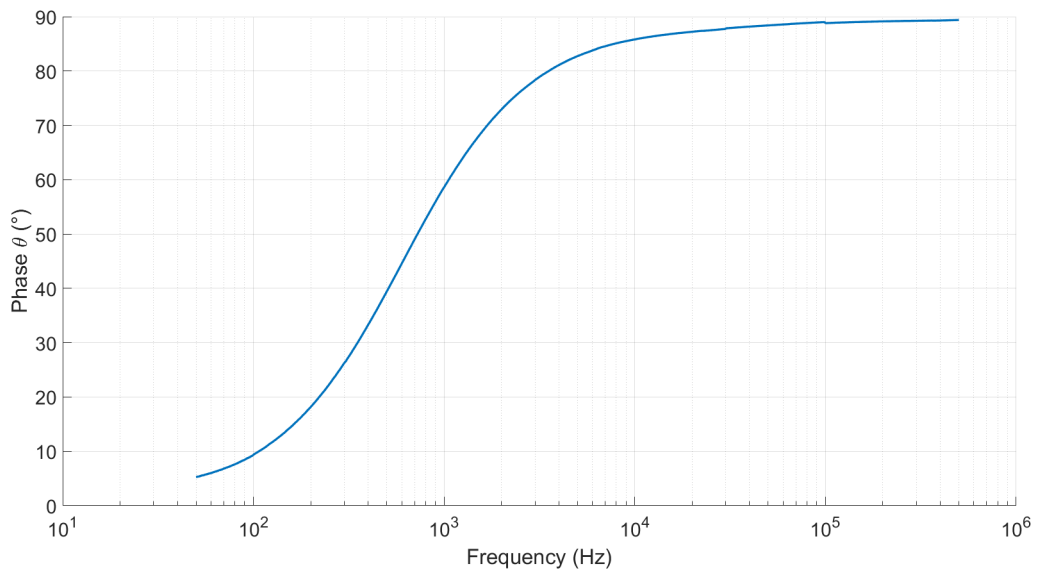


Figure 5.6: Air core inductor phase θ .

As can be seen from the figure 5.6 we can see that at high frequencies the phase θ is close to 90° , so the system is inductive. The same parameters were calculated for the other materials. In particular, once the two series L_s air and material inductances have

been known, the relative magnetic permeability μ_r of the material has been calculated as follows:

$$\frac{\mu_{material}}{\mu_{air}} = \mu_{material} = \frac{L_{s,material}}{L_{s,air}} \quad (5.1)$$

being $\mu_{air} = 1$. All the realized toroids always have the same number of turns, equal to 77, in order to validate equation (5.1).

5.1 Black Catramina



Figure 5.7: Black Catramina toroid.

With this logic the relative magnetic permeability μ_r of the different materials have been calculated. Let's now analyze the results concerning the Black Catramina:

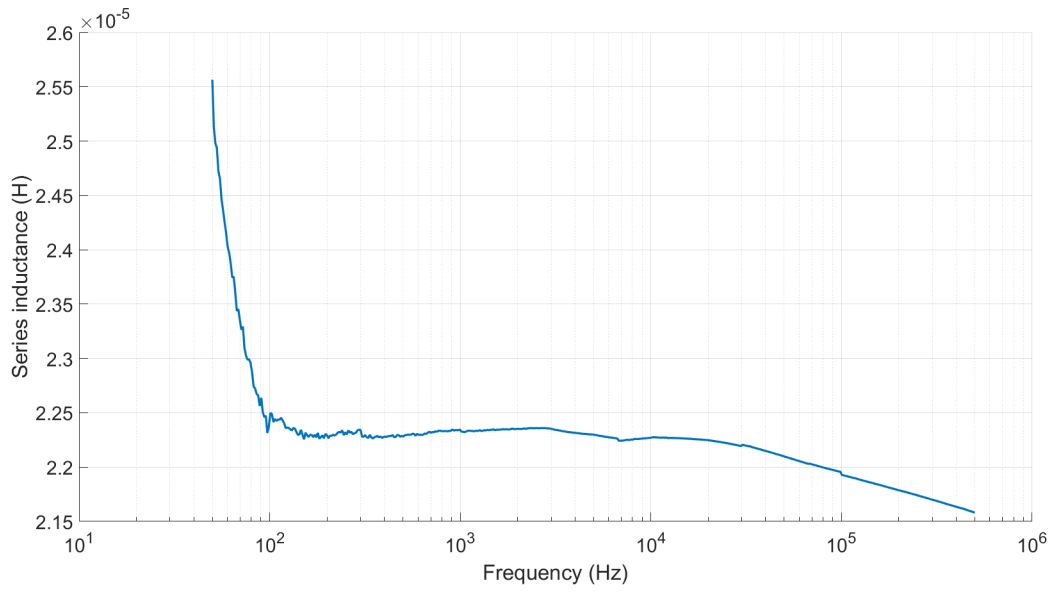


Figure 5.8: Black Catramina core series inductance L_s .

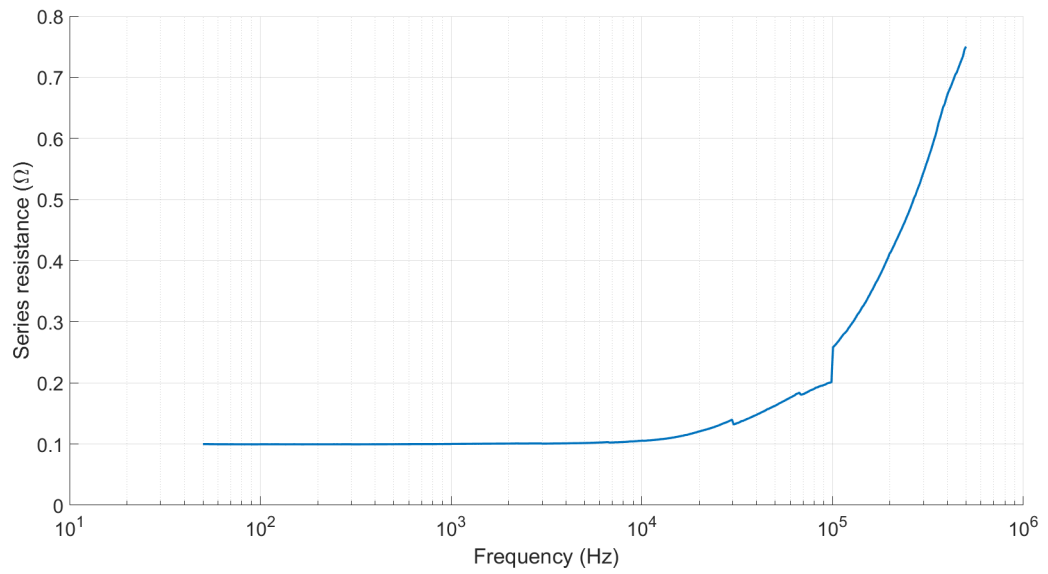


Figure 5.9: Black Catramina core series resistance R_s .

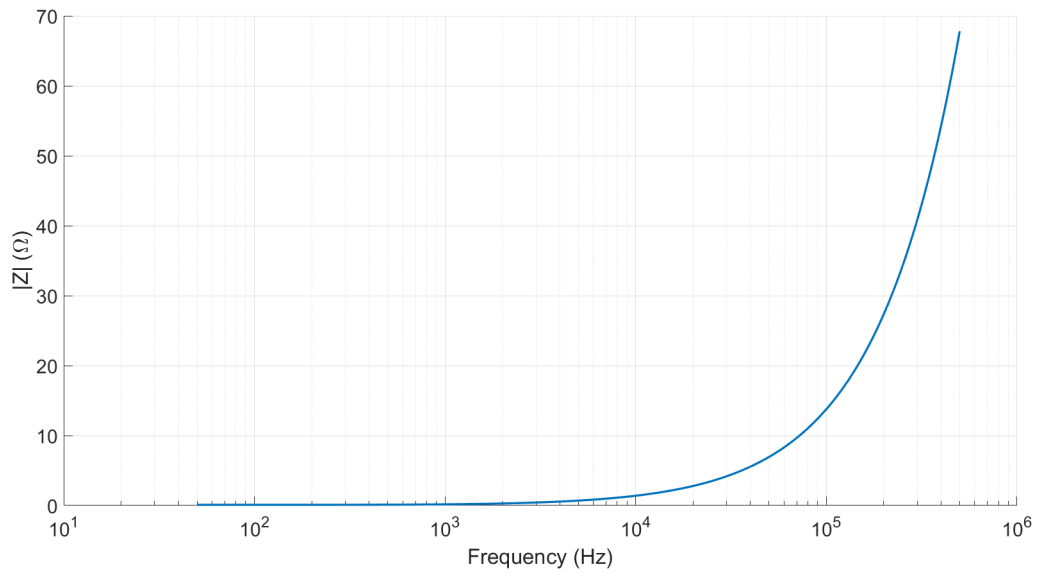


Figure 5.10: Black Catramina core impedance $|Z|$.

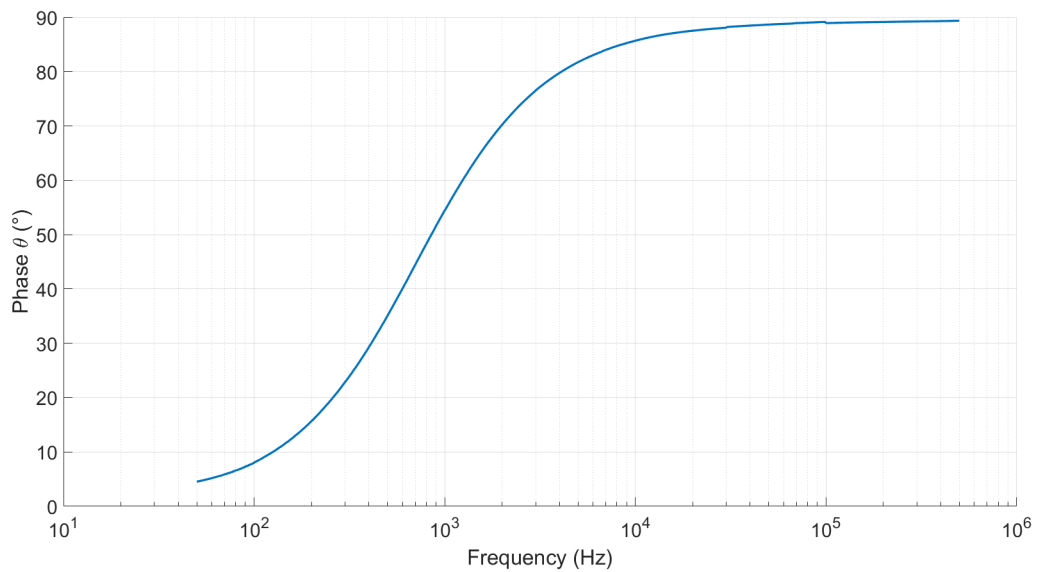


Figure 5.11: Black Catramina core phase θ .

Even for Black Catramina we can see how at high frequencies the system tends to be inductive. The following figure, on the other hand, represents the trend of the relative magnetic permeability of Black Catramina as a function of frequency:

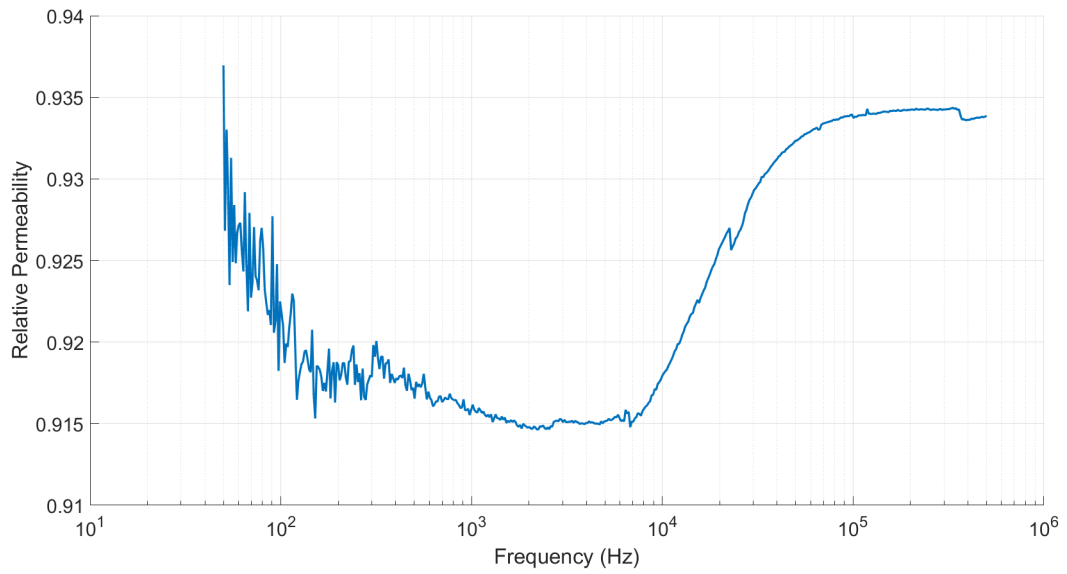


Figure 5.12: Black Catramina core relative permeability μ_r .

As can be seen from the figure 5.12, the Black Catramina has a relative magnetic permeability μ_r always lower than unit, therefore this material can be considered, in the analyzed frequency range, a diamagnetic material.

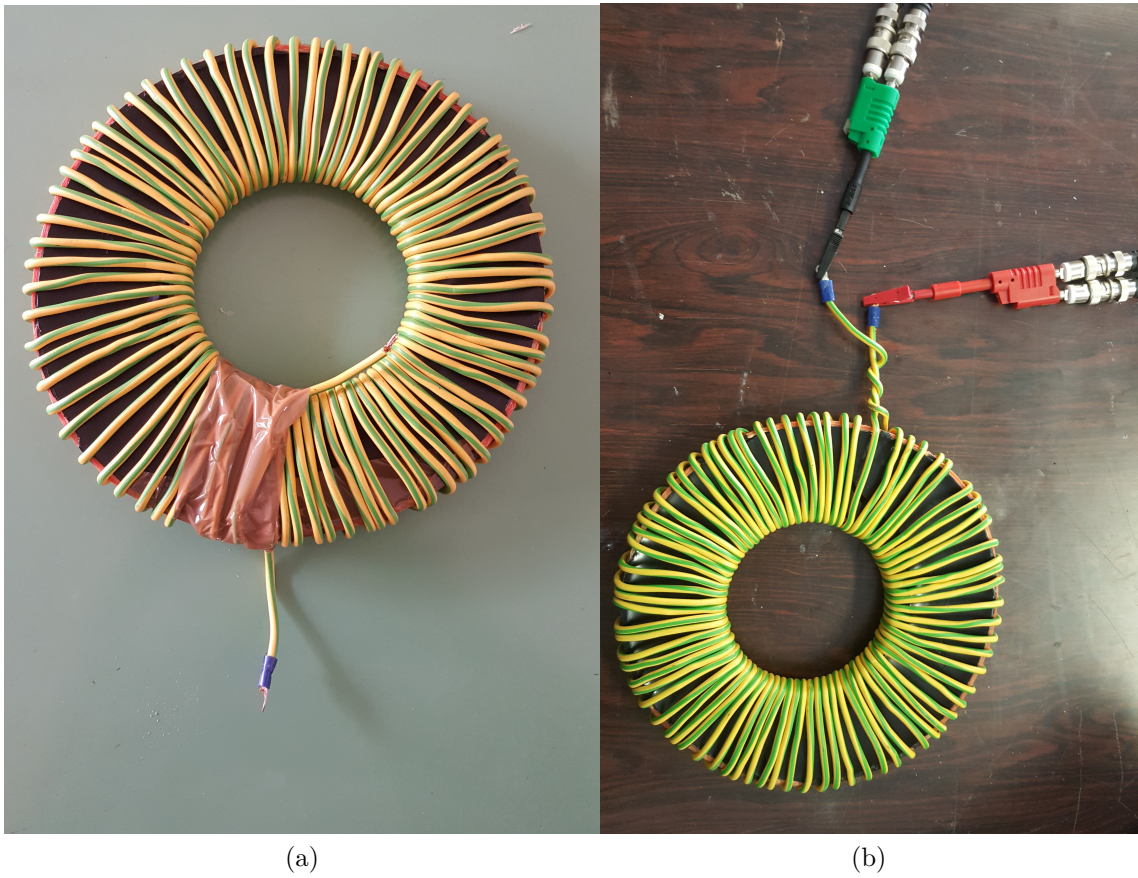


Figure 5.13: Black Catramina core wounded toroid (a). Black Catramina core toroid measure (b).

5.2 Catramix

Let's now analyze the results concerning another material, the Catramix:

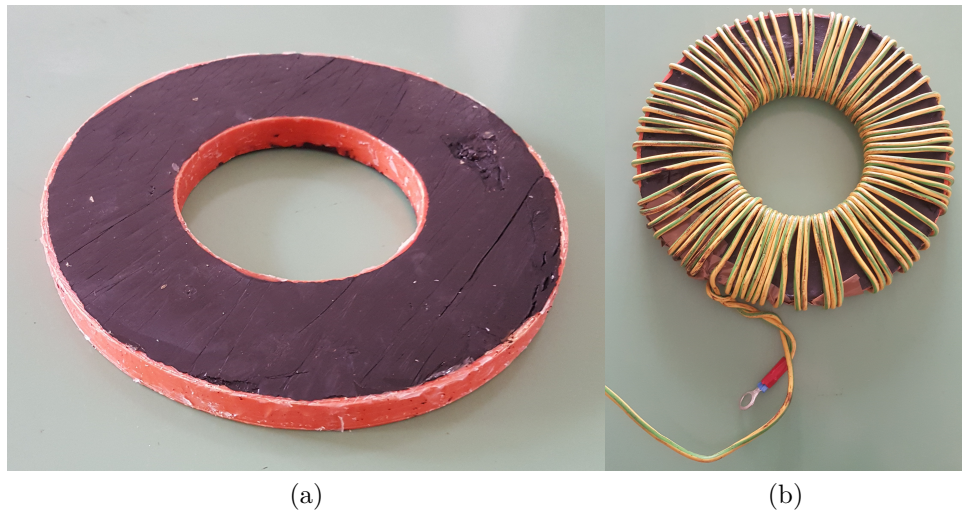


Figure 5.14: Catramix core toroid (a). Catramix core wounded toroid (b).

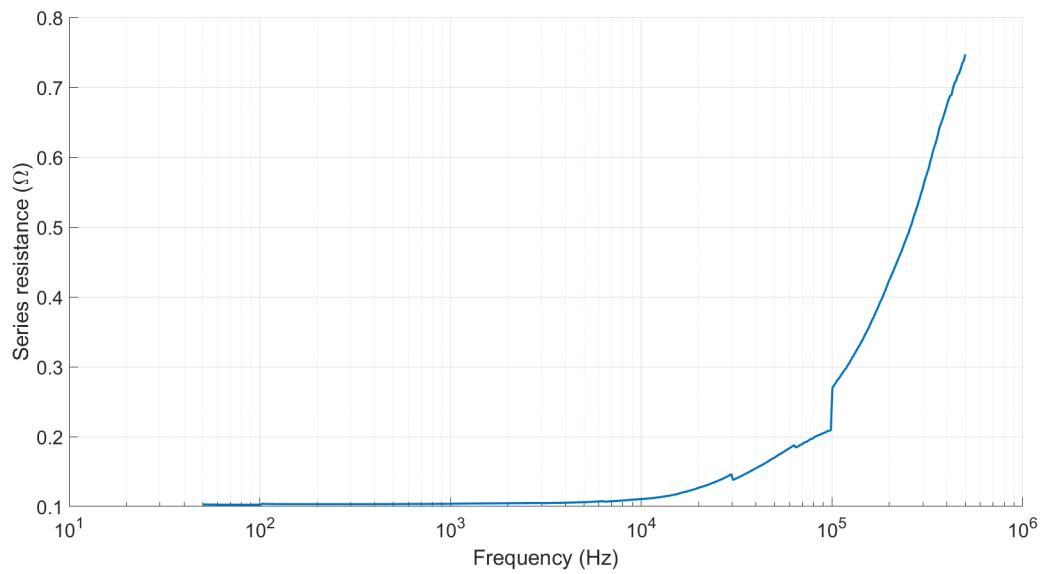


Figure 5.15: Catramix core series resistance R_s .

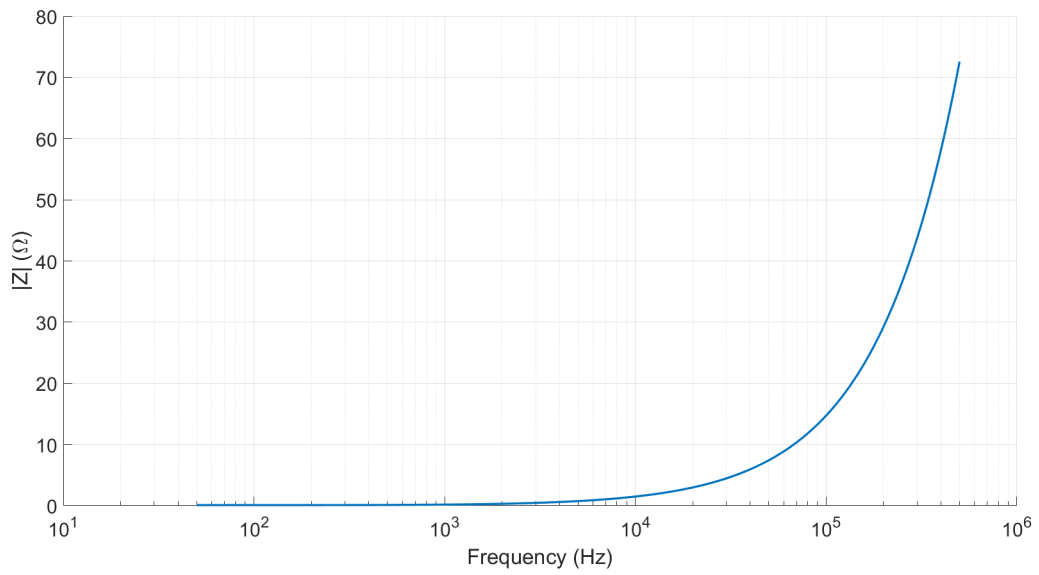


Figure 5.16: Catramix core impedance $|Z|$.

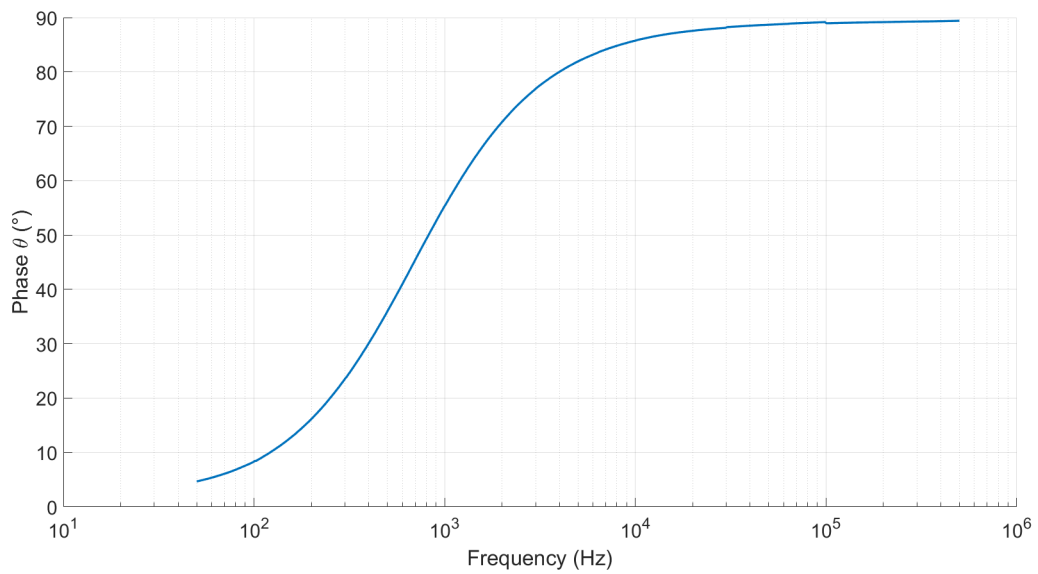


Figure 5.17: Catramix core phase θ .

Even for Catramix we can see how at high frequencies the system tends to be inductive. The following figure, on the other hand, represents the trend of the relative magnetic permeability of Catramix as a function of frequency:

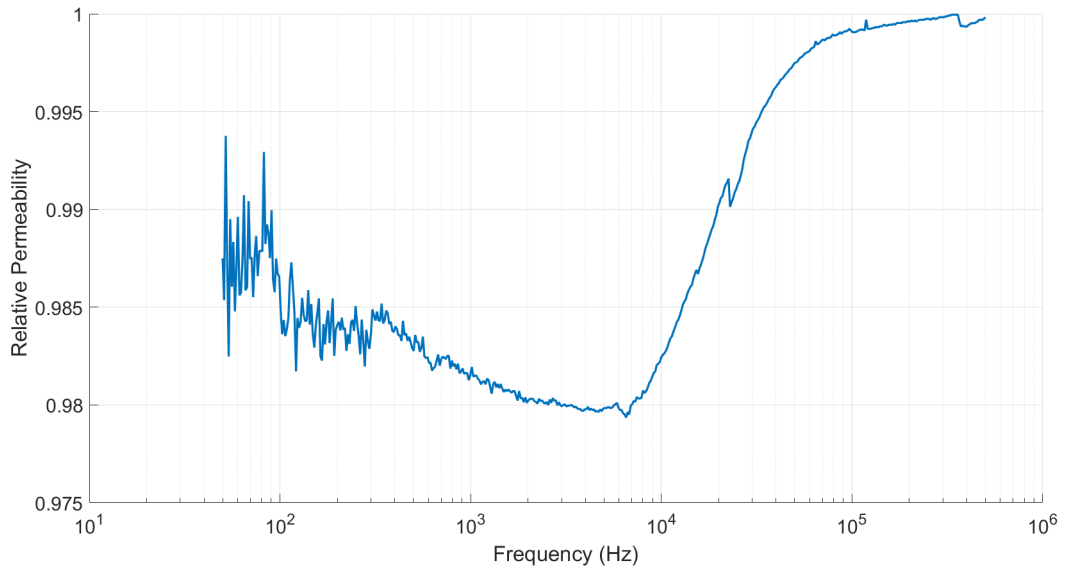


Figure 5.18: Catramix core relative permeability μ_r .

As can be seen from the figure 5.18, the Catramix has a relative magnetic permeability μ_r always lower than unit, therefore this material can be considered, in the analyzed frequency range, a diamagnetic material.

5.3 Cement 1

Let's now analyze the results concerning another material, the Cement 1:

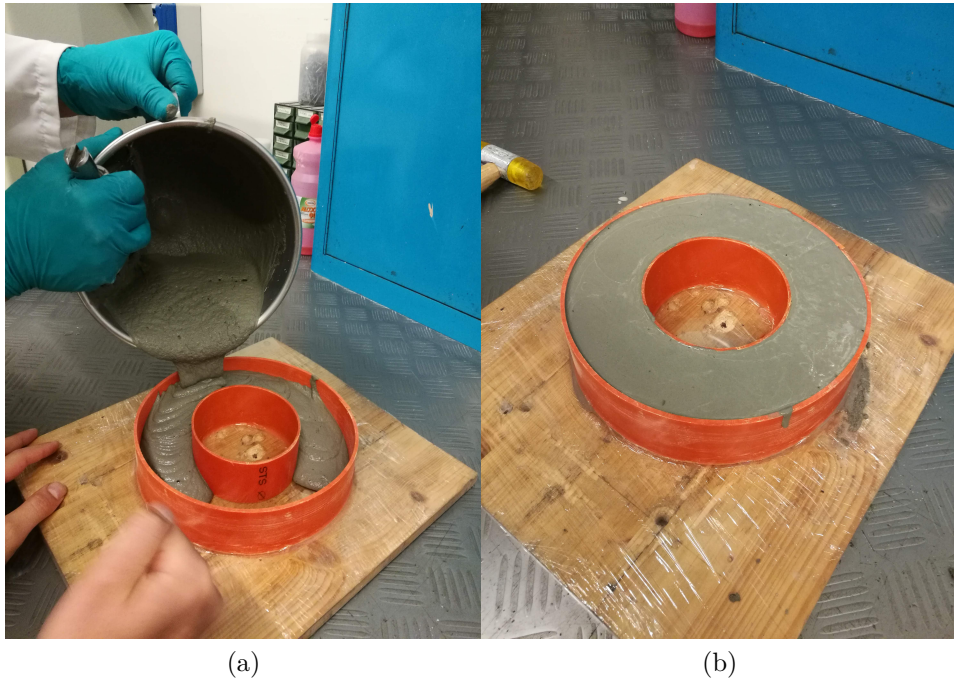


Figure 5.19: Cement 2 core toroid filling (a). Cement 2 core toroid filled (b).

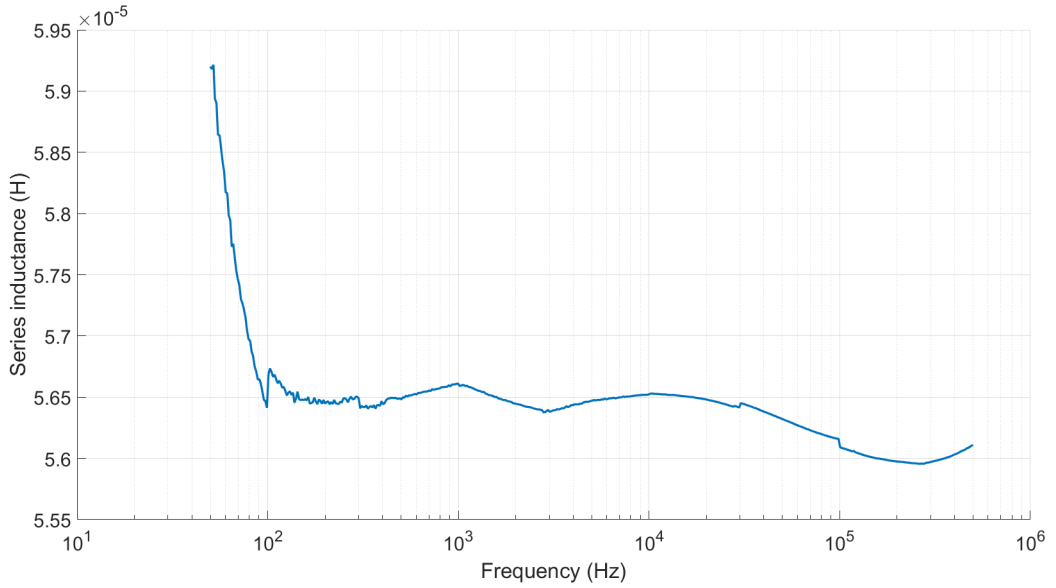


Figure 5.20: Cement 1 core series inductance L_s .

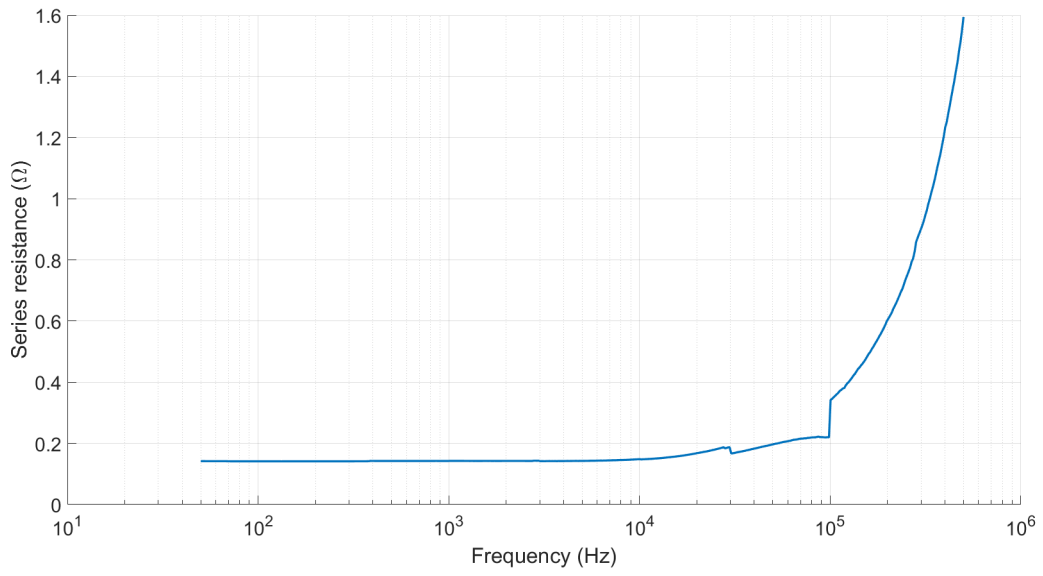


Figure 5.21: Cement 1 core series resistance R_s .

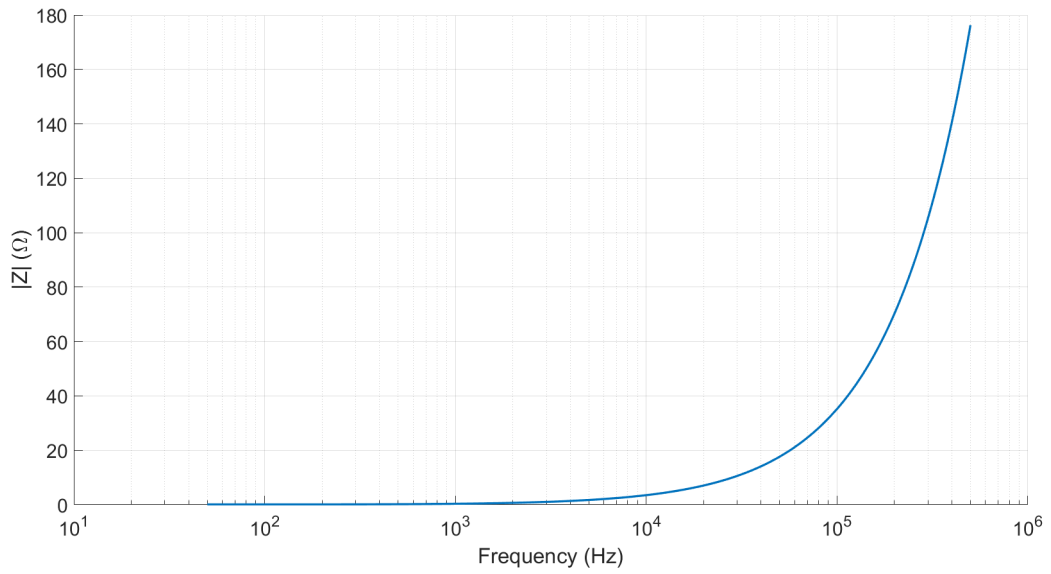


Figure 5.22: Cement 1 core impedance $|Z|$.

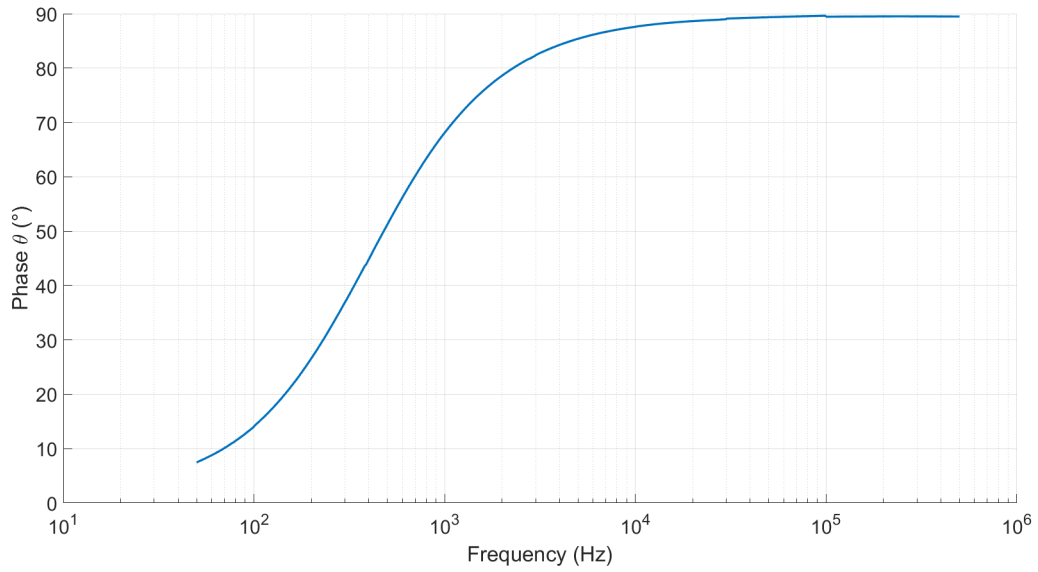


Figure 5.23: Cement 1 core phase θ .

Even for Cement 1 we can see how at high frequencies the system tends to be inductive. The following figure, on the other hand, represents the trend of the relative magnetic permeability of Cement 1 as a function of frequency:

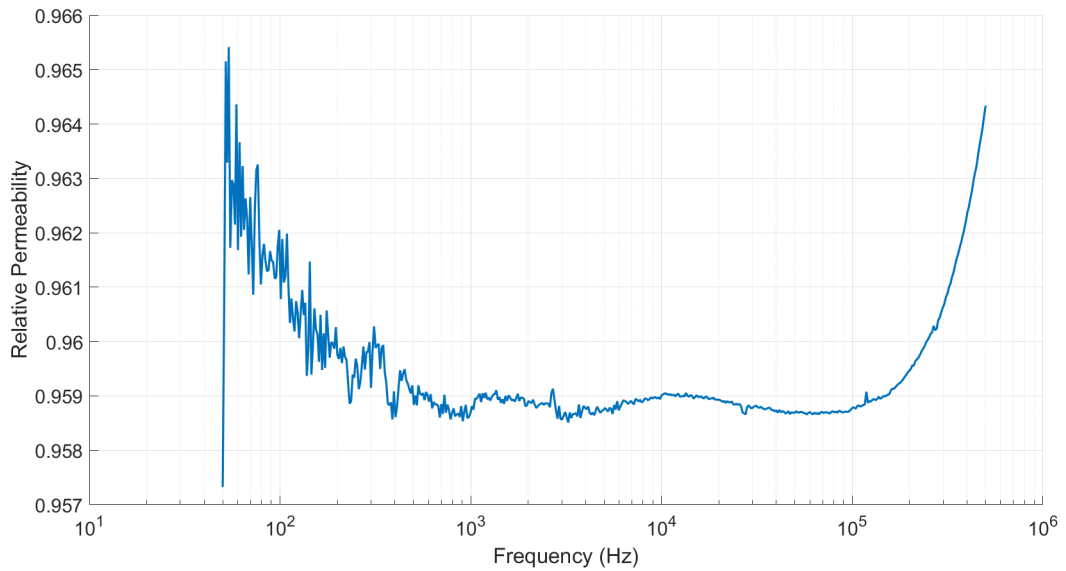


Figure 5.24: Cement 1 core relative permeability μ_r .

As can be seen from the figure 5.24, the Cement 1 has a relative magnetic permeability μ_r always lower than unit, therefore this material can be considered, in the analyzed frequency range, a diamagnetic material.

5.4 Cement 2

Let's now analyze the results concerning another material, the Cement 2:

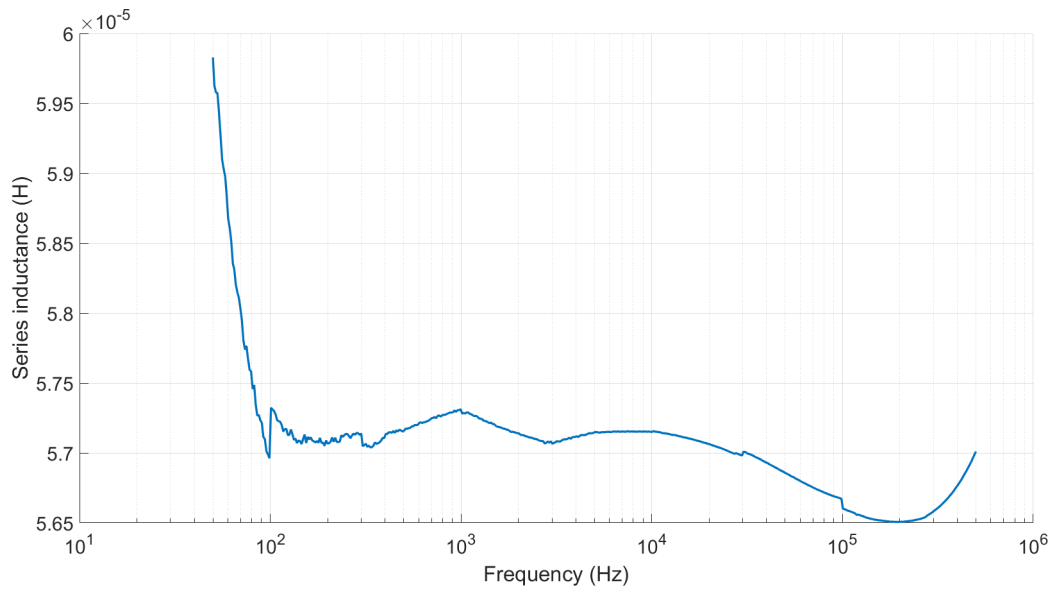


Figure 5.25: Cement 2 core series inductance L_s .

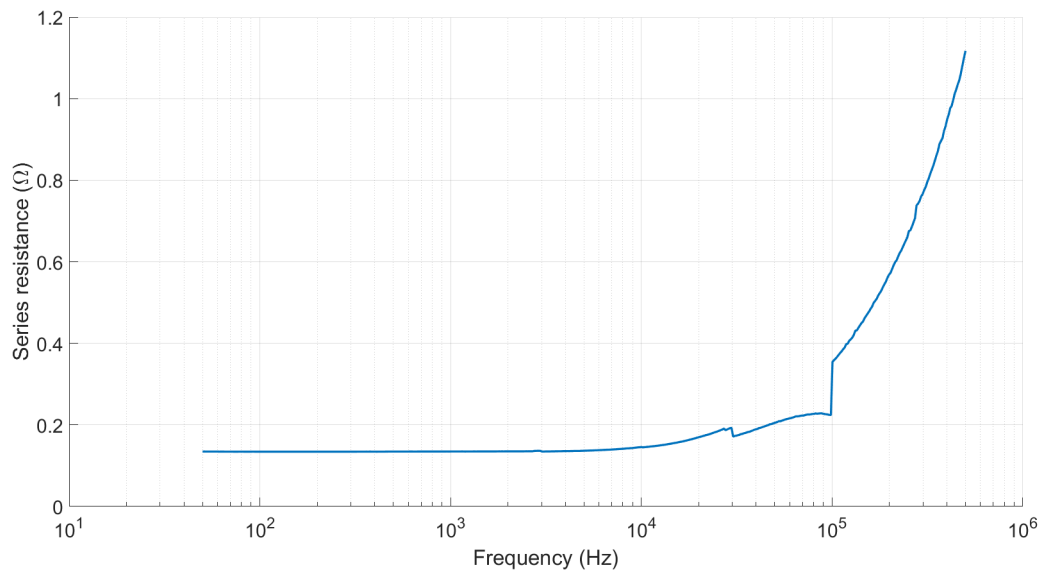


Figure 5.26: Cement 2 core series resistance R_s .

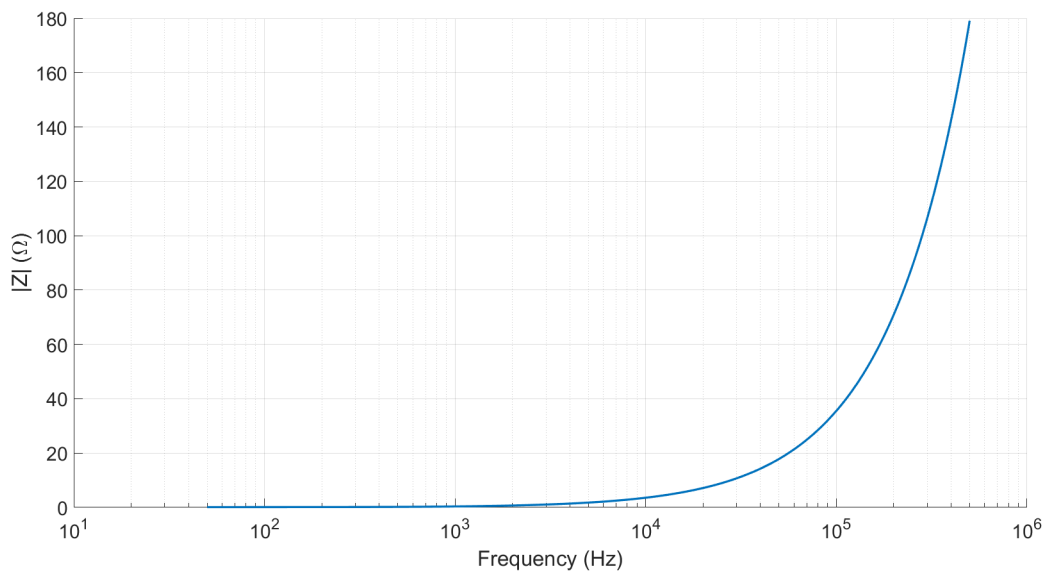


Figure 5.27: Cement 2 core impedance $|Z|$.

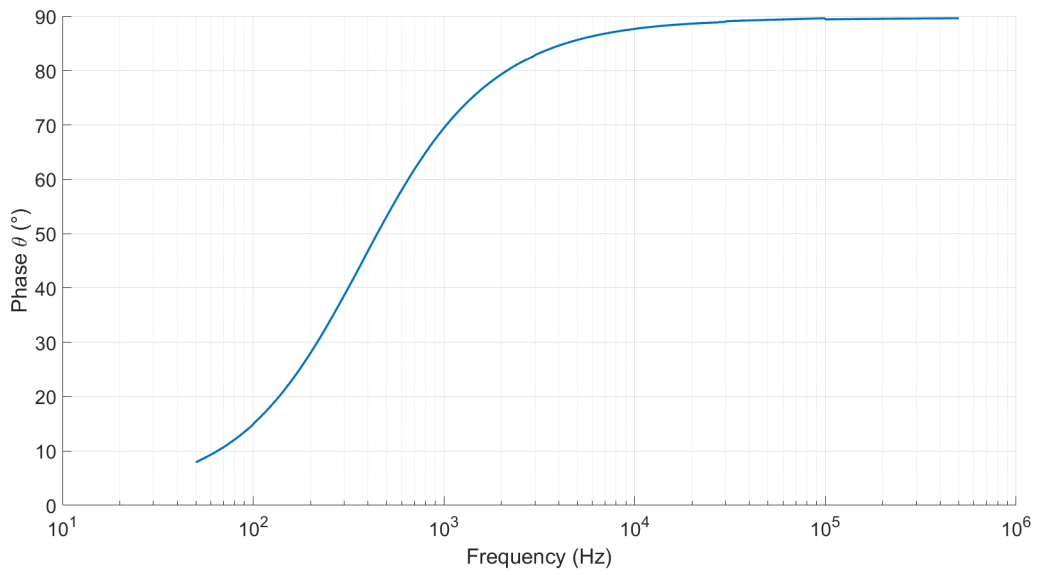


Figure 5.28: Cement 2 core phase θ .

Even for Cement 2 we can see how at high frequencies the system tends to be inductive. The following figure, on the other hand, represents the trend of the relative magnetic permeability of Cement 2 as a function of frequency:

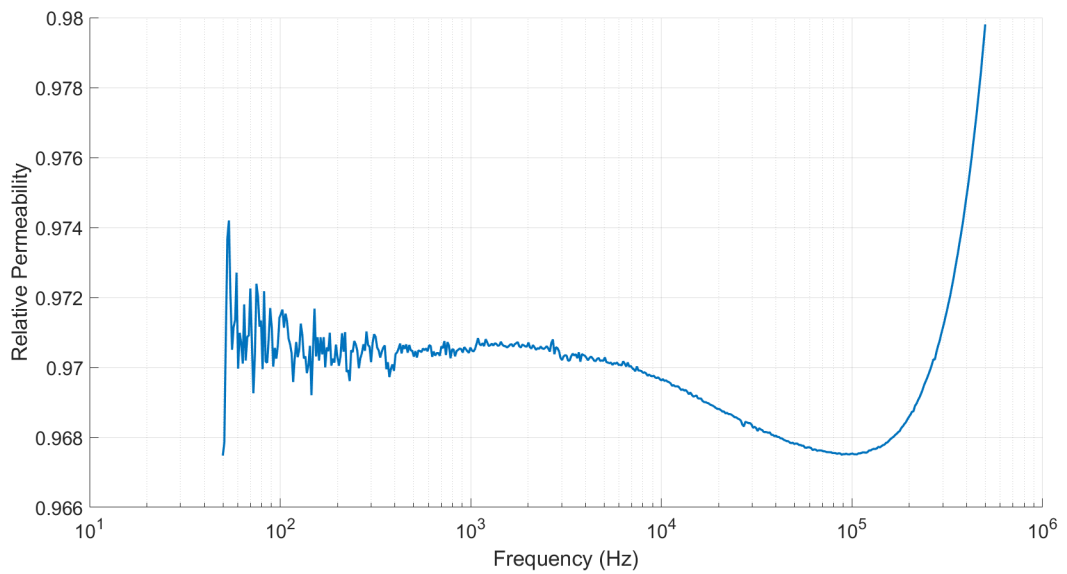


Figure 5.29: Cement 2 core relative permeability μ_r .

As can be seen from the figure 5.29, the Cement 2 has a relative magnetic permeability μ_r always lower than unit, therefore this material can be considered, in the analyzed frequency range, a diamagnetic material.

5.5 Unolastic

Let's now analyze the results concerning another material, the Unolastic:

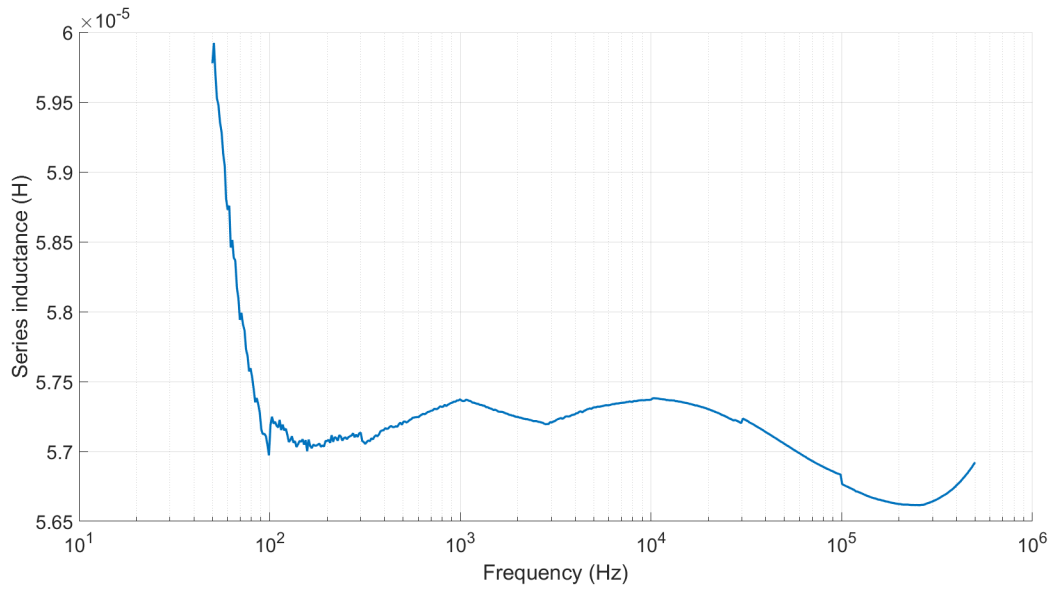


Figure 5.30: Unolastic core series inductance L_s .

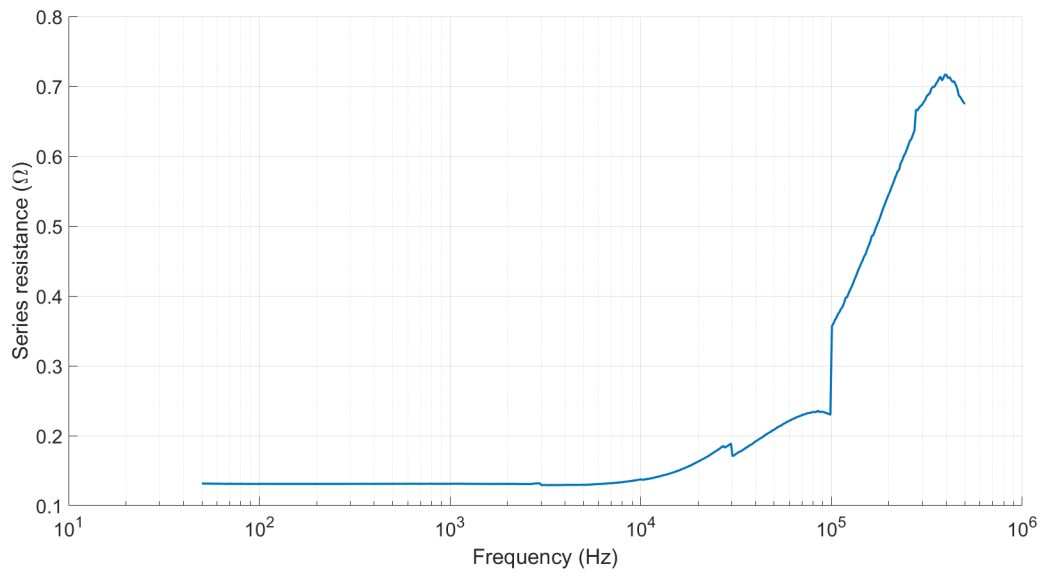


Figure 5.31: Unolastic core series resistance R_s .

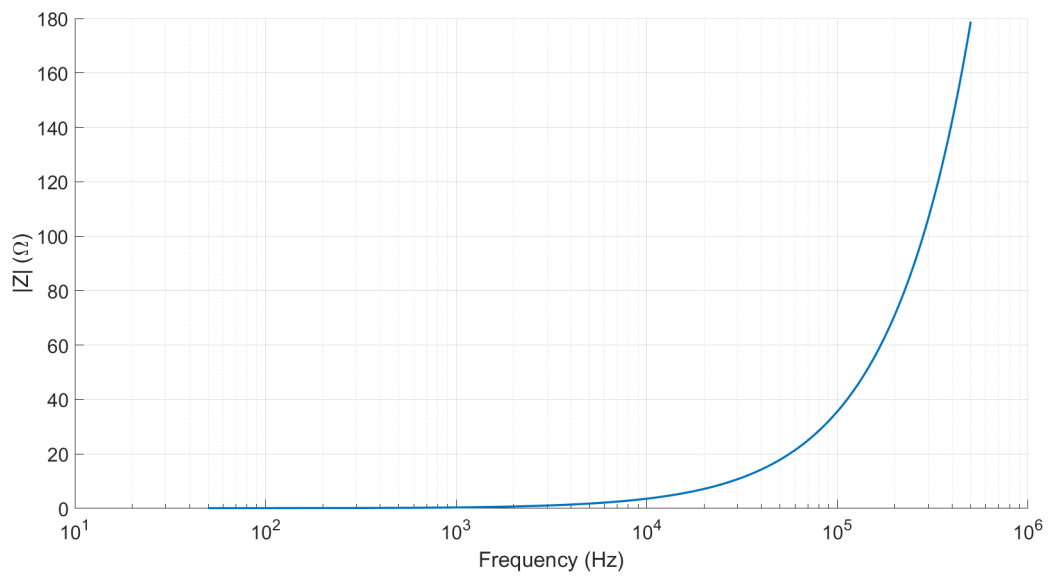


Figure 5.32: Unolastic core impedance $|Z|$.

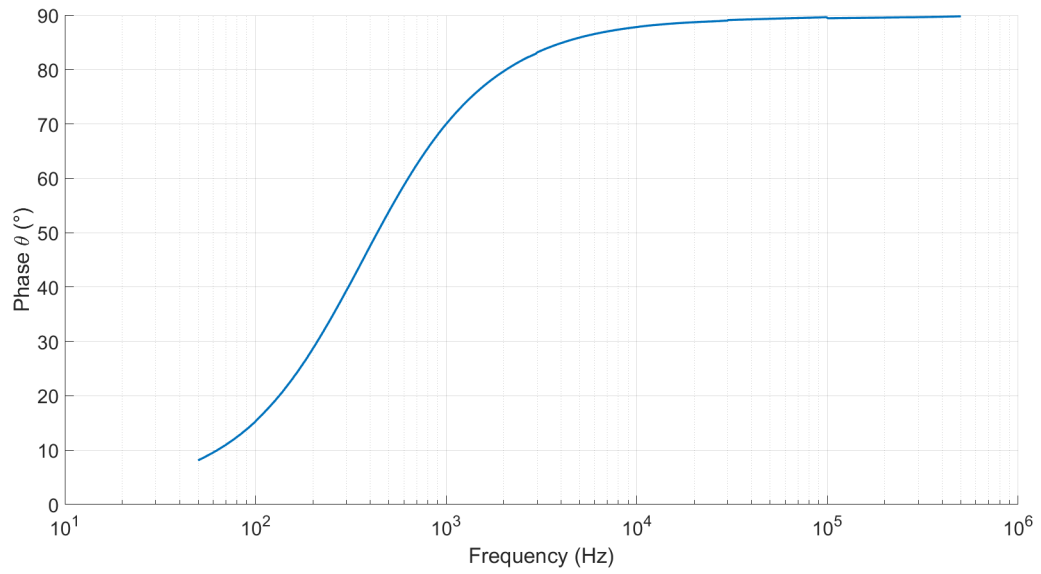


Figure 5.33: Unolastic core phase θ .

Even for Unolastic we can see how at high frequencies the system tends to be inductive. The following figure, on the other hand, represents the trend of the relative magnetic permeability of Unolastic as a function of frequency:

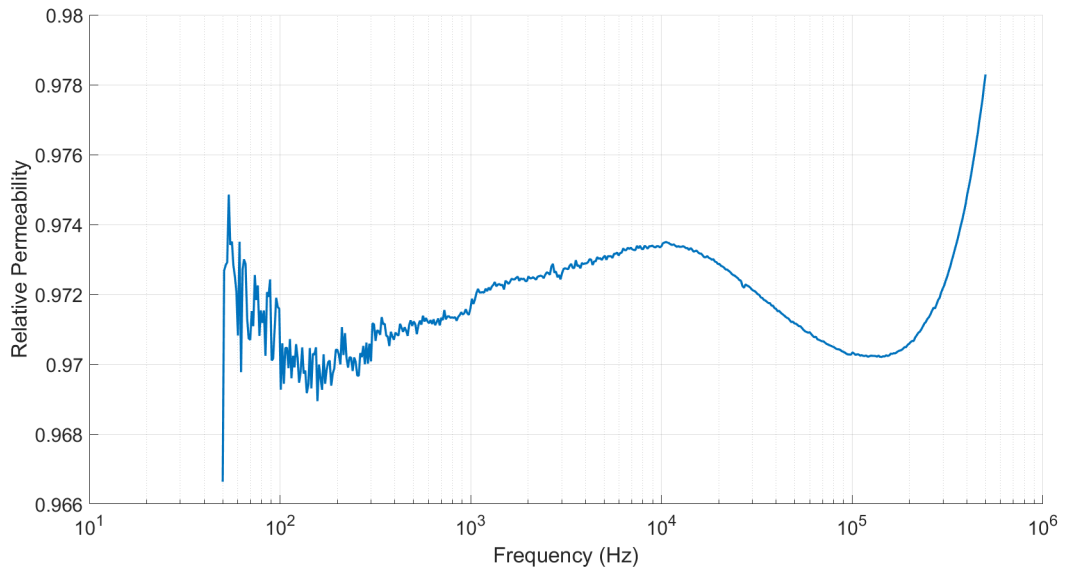


Figure 5.34: Unolastic core relative permeability μ_r .

As can be seen from the figure 5.34, the Unolastic has a relative magnetic permeability μ_r always lower than unit, therefore this material can be considered, in the analyzed frequency range, a diamagnetic material.

Chapter 6

PEEC MODEL OF WPT

The results of the measurements have been finally used in order to built a model for the electromagnetic simulation of the embedded coil in order to investigate the physical phenomena that caused the deviation from the behaviour of an inductor. A Partial element equivalent circuit (PEEC) model [6] of the coil of Figure 6.1 has been developed. Partial element equivalent circuit method is partial inductance calculation used for interconnect problems which is used for numerical modeling of electromagnetic (EM) properties. Using the PEEC method, the problem will be transferred from the electromagnetic domain to the circuit domain where conventional circuit solvers can be employed to analyze the equivalent circuit.



Figure 6.1: Road embeddment of the 9 turns WPT in dry concrete.

The model consist in the transmitter and a layer, cross section 0.05 m x 0.05 m, of dry concrete which completely embeds the coil.

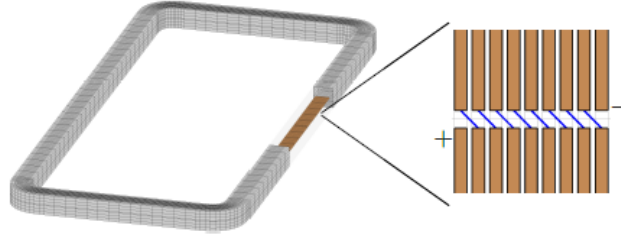


Figure 6.2: PEEC model of the embedded WPT with lumped short circuits detail.

In order to reduce the complexity of the mesh, 9 turns of the WPT have been modelled as 9 independent open turns which are connected with lumped short circuits as shown in Figure 6.2. The coil is fed by a lumped voltage source connected to the terminals of the most internal and external turns. Since the litz wires guarantee an almost uniform current distribution at the frequency range of interest, the 9 turns have been modelled with only one mesh element in the cross section adopting a conductivity $\sigma = 57 \times 10^6$ S/m. The model has been simulated in the range from 10 kHz to 150 kHz and the results in terms of the simulated amplitude and phase of Z_{eq} are shown in Figure 6.3 together with the measured ones, showing the accuracy of the model for the embedded WPT device.

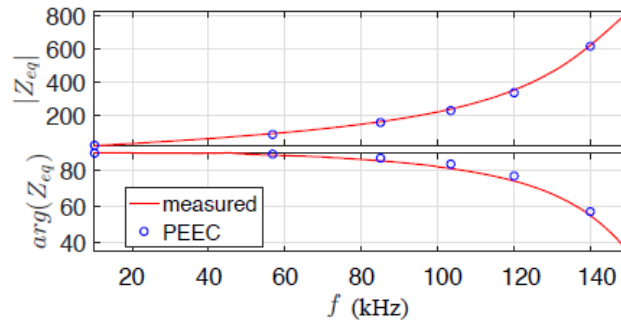


Figure 6.3: Amplitude (Ω) and phase ($^\circ$) of the embedded coil impedance Z_{eq} in the frequency range 10 Hz – 150 kHz. Measurements vs simulations.

The conductivity and the permittivity of the dry concrete are two parameters not commonly known and, moreover, they can widely vary with the change of environmental conditions. Measured values $\sigma = 0.05$ S/m and $\epsilon_r = 10$ have been used in the simulations, according to the values obtained in this thesis for cement materials. The results obtained from the numerical model have allowed to identify two effects. First, only the concrete close to the turns (particularly the one between the turns) actually influences the behavior of the coil. Thus, the PEEC model of the dry concrete can be reduced and only the material in close proximity to the copper turns must be discretized.

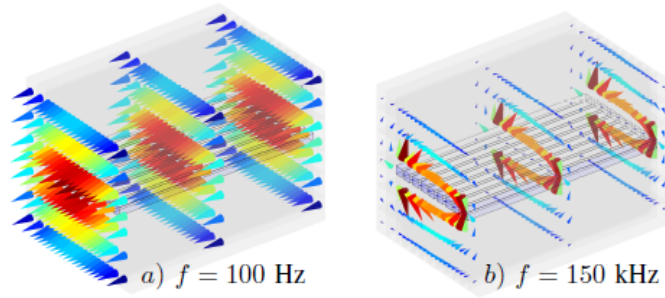


Figure 6.4: PEEC model simulation: distribution of J_e in the concrete. a) Inductive component predominant. b) Capacitive component predominant. a) and b) not in the same scale.

Moreover, when different types of concrete need to be tested in the context of laboratory experiments, a reduced amount of material can be used. Secondly, it has been noticed that the current density in the concrete J_e ($J_e = J + j\omega P_e$, where J is the conduction current density and P_e is the polarization vector) has two main components: one which flows parallel to the current inside the winding (inductive component) and a second one which flows from the external turn to the internal one (capacitive component), accumulating charge on the interfaces between the concrete and the turns. As shown in Figure 6.4, when the frequency is low, the inductive component is predominant while, with the increase of the frequency, the capacitive component becomes more relevant, significantly affecting the overall coil behavior.

Indeed, the current can jump from one turn to the others through the parasitic resistive–capacitive impedance emphasized by the presence of the conductive dry concrete between the turns. This suggests that the issues emerging with the road embedment of WPTs can be probably avoided by placing the litz turns inside a plastic duct filled with a non–conductive material; this would limit the value of the parasitic impedance between the turns of the WPT, moving the resonance frequency far away from the working frequency. The simulation results suggest that the different behavior arising from embedment depends on the geometrical parameters of the transmitter and the electromagnetic characteristics of concrete. Clearly, both properties can have a wide range of variation depending on the production and the embedment process. In the full paper, the sensitivity of the problem with respect to the values of σ , ϵ_r , and geometric parameters will be investigated.

The details about the problem and model formulation (that were not the objects of this thesis) will be presented at the Compumag 2019 conference that will be held in Paris next July.

Chapter 7

CONCLUSION

The results obtained from the tests are summarized in tables 7.1, 7.2, 7.3. Moreover, this tables brief conducibility, relative permittivity and relative permeability of the tested materials:

Conductivity error %	Black Catramina	Catramix	Cement 1	Cement 2	Unolastic
$\sigma_{5\%}$	2.3×10^{-7}	4.1×10^{-7}	—	—	—
$\sigma_{10\%}$	1.21×10^{-6}	1.98×10^{-6}	0.001245	—	—
$\sigma_{20\%}$	1.33×10^{-6}	2.05×10^{-6}	0.001105	0.0171	0.1727

Table 7.1: Values of conductivity σ (S/m) with respect to different relative measurement errors.

Permittivity error %	Black Catramina	Catramix	Cement 1	Cement 2	Unolastic
$\epsilon_{5\%}$	3.15	7.87	—	—	—
$\epsilon_{10\%}$	2.87	7.51	28.54	—	—
$\epsilon_{20\%}$	2.89	7.54	59.21	1.4121×10^5	3.1432×10^6

Table 7.2: Values of relative permittivity ϵ_r with respect to different relative measurement errors.

Permeability error %	Black Catramina	Catramix	Cement 1	Cement 2	Unolastic
$\mu_{5\%}$	0.929	0.9939	0.9593	0.9695	0.9723
$\mu_{10\%}$	0.9285	0.9933	0.9593	0.9696	0.9723
$\mu_{20\%}$	0.9265	0.9913	0.9592	0.9697	0.9723

Table 7.3: Values of relative magnetic permeability μ with respect to different relative measurement errors.

All of these values are reported with a percentage of error committed. In fact we report only the values with an error less than 5%, 10% and 20%. For example, each single value of each row of the tables is obtained from the values that have an error less than the respectively row, and calculating from these the mean value. Therefore, in each box we put the mean value.

It is also important to note that some values are missing. To explain this, we have to use the equation (2.9) that link permittivity ϵ and conductivity σ . In fact, we note that it is not possible to extract a value of permittivity for materials that have an high value of conductivity σ or for DC tests with the approximate formula of (2.9) for which $\epsilon = \epsilon_0 \epsilon_r$. Our cement materials have a much higher conductivity with respect to the bituminous ones so, in other words, they are less resistive. Then the previous approximation is no longer acceptable and this prevent us from extrapolating permittivity values that have a physical meaning.

Moreover, thanks to the equation (2.9), it is possible to explain why, as frequency increases, permittivity ϵ can be interpreted as $\epsilon_0 \epsilon_r$. In fact, the presence of the frequency in the denominator of (2.9) means that at high frequencies the real part of permittivity tends to be much higher than the imaginary part and therefore ϵ is interpreted as $\epsilon_r \epsilon_0$.

As a further confirmation of the results obtained, other tests were carried out. One of these was to perform a power-test of materials within the frequency range of 5 Hz-20 kHz, limit of the power amplifier available to us. For each measure and each prototypes, it was created a screen in order to minimize the environmental effects. These power-test further confirmed the results obtained with the HIOKI 3532-50 LCR HiTESTER, then has further confirmed what we said previously.

Bibliography

- [1] IEEE Std. 80-2000. Ieee guide for safety in ac substation grounding. 2000.
- [2] Feng Chen, Nathaniel Taylor, Nicole Kringos, and Bjorn Birgisson. A study on dielectric response of bitumen in the low-frequency range. *Road Materials and Pavement Design*, 16(sup1):153–169, 2015.
- [3] Vincenzo Cirimele. *Design and integration of a dynamic IPT system for automotive applications*. PhD thesis, Paris Saclay, 2017.
- [4] EC Hioki. Hioki 3532–50 lcr hitester instruction manual. *JAPAN. HIOKI EE CORPORATION*, 2001.
- [5] S. International. Surface vehicle information report, tech.rep. *SAE International*, November 2017.
- [6] Arthur R Von Hippel. *Dielectrics and Waves*. John Wiley and Sons, 1954.